NONLINEAR DYNAMIC RESPONSE OF FLEXIBLE MEMBRANE STRUCTURES TO BLAST LOAD

by

Hitesh Kapoor

A Thesis submitted to the Faculty of
Virginia Polytechnic Institute and State University
in partial fulfillment of the requirements for the degree of

MASTER OF SCIENCE

in

Aerospace Engineering

APPROVED

Rakesh K. Kapania, Chair

Raymond H. Plaut

Eric R. Johnson

February 10, 2005

Blacksburg, Virginia

Keywords: Flexible structures, Shelters, Blast loads, membranes, shells, finite element modeling, structural dynamics, nonlinear finite element analysis

NONLINEAR DYNAMIC RESPONSE OF FLEXIBLE MEMBRANE STRUCTURES TO BLAST LOADS

Hitesh Kapoor

(ABSTRACT)

The present work describes the finite element (FE) modeling and dynamic response of lightweight, deployable shelters (tent) to large external blast loads. Flexible shelters have been used as temporary storage places for housing equipments, vehicles etc. TEMPER Tents, Small Shelter System have been widely used by Air Force and Army, for various field applications. These shelters have pressurized Collective Protection System (CPS), liner, fitted to the frame structure, which can provide protection against explosives and other harmful agents. Presently, these shelter systems are being tested for the force protection standards against the explosions like air-blast. In the field tests carried out by Air Force Research Laboratory, it was revealed that the liner fitted inside the tent was damaged due to the air blast explosion at some distant from the structure, with major damage being on the back side of the tent. The damage comprised of tearing of liner and separation of zip seals. To investigate the failure, a computational approach, due to its simplicity and ability to solve the complex problems, is used.

The response of any structural form to dynamic loading condition is very difficult to predict due to its dependence on multiple factors like the duration of the loading, peak load, shape of the pulse, the impulse energy, boundary conditions and material properties etc. And dynamic analysis of shell structures pose even much greater challenge. Obtaining solution analytically presents a very difficult preposition when nonlinearity is considered. Therefore, the numerical approach is

sought which provide simplicity and comparable accuracy.

A 3D finite element model has been developed, consisting of fabric skin supported over the frames based on two approaches. ANSYS has been used for obtaining the dynamic response of shelter against the blast loads. In the first approach, the shell is considered as a membrane away from its boundaries, in which the stress couple is neglected in its interior region. In the second approach, stress coupling is neglected over the whole region. Three models were developed using *Shell 63*, *Shell 181* and *Shell 41*. *Shell 63* element supports both the membrane only and membrane-bending combined options and include stress stiffening and large deflection capabilities. *Shell 181* include all these options as *Shell 63* does and also, accounts for the follower loads. *Shell 41* is a membrane element and does not include any bending stiffness. This element also include stress stiffening and large deflection capabilities.

A nonlinear static analysis is performed for a simple plate model using the elements, *Shell 41* and *Shell 63*. The membrane dominated behavior is observed for the shell model as the pressure load is increased. It is also observed that the higher value of Young's modulus (E) increases the stresses significantly.

Transient analysis is a method of determining the structural response due to time dependent loading conditions. The full method has been used for performing the nonlinear transient analysis. Its more expensive in terms of computation involved but it takes into account all types of nonlinearities such as plasticity, large deflection and large strain etc. Implicit approach has been used where Newmark method along with the Newton-Raphson method has been used for the nonlinear analysis. Dynamic response comprising of displacement-time history and dynamic

stresses has been obtained. From the displacement response, it is observed that the first movement of the back wall is out of the tent in contrast to the other sides whose first movement is into the tent. Dynamic stresses showed fluctuations in the region when the blast is acting on the structure and in the initial free vibration zone.

A parametric study is performed to provide insight into the design criteria. It is observed that the mass could be an effective means of reducing the peak responses. As the value of the Young's Modulus (E) is increased, the peak displacements are reduced resulting from the increase in stiffness. The increased stiffness lead to reduced transmitted peak pressure and reduced value of maximum strain. But a disproportionate increase lead to higher stresses which could result in failure. Therefore, a high modulus value should be avoided.

ACKNOWLEDGEMENT

I would like to thank Prof. Rakesh K. Kapania, for his professional guidance and giving me the opportunity to work on the project. He met me on the regular basis and helped me structure my research. Prof. Kapania and Prof. Raymond H. Plaut were the part of regular project meetings for over more than a year and discussion held during the meeting were invaluable. I would like to thank Prof. Plaut and Prof. Eric Johnson for serving on the committee.

This research project was sponsored by Air Force Research Laboratory. I would like to thank Mr. John Hawk for providing the financial support for that.

I would like to thank Dr. Sangeon Chun and Michael R. Motley for the cooperation during the research project. I would like to acknowledge the valuable discussions with Dr. Sangeon Chun during the project. Also, I would like to thank the $Structure\ Group$ and the computing staff in AOE department for their support.

In the end, I would like to thank my grandfather, parents and sister for their support and encouragement. Over the years they have been a source of motivation and keep me moving in the right direction.

Contents

List of Figures

Chapter 1

INTRODUCTION

1.1 Flexible Structure

The application of flexible structures began with the birth of the human race. The human organs like the heart, veins, and skin are examples of flexible membrane structures. Due to being lightweight, having multifunctional capabilities, low cost, etc; these structures are widely used in the engineering field and find numerous applications in the aerospace industry. Some space structures are categorized as thin structures and have very large span. Due to the limitations of the size of the launch vehicle and zero gravity conditions, hingeless, mechanism-free deployable structures are widely sought. Communication antennas, solar thermal propulsion systems, space solar power, and solar sails are examples of flexible structures, characterized as lightweight, inflatable, easily deployable structures. Gossamer spacecrafts are large apertured, highly-integrated and thin-walled

structures with multiple functional capabilities and are modeled as flexible membrane structures [1] . The extra retractable control surfaces in advanced aircrafts are also flexible structures. Large wings and turbine and rotor blades may also come under the same category.

In civil applications, exhibition pavilions, storage facilities, tents, and domes are all classical examples of flexible structures. These structures fall into two categories: firstly, the inflated membrane structures which drive their integrity from the internal pressure used to inflate them, known as pneumatic structures, and secondly, the pre-stressed structures stretched over the frames to form enclosed tents. These flexible membrane structures (with little or no bending) are characterized by large-displacement behavior. Inflated dams and inflated cylindrical tubes, used for offshore and underwater applications such as submarine detection, oceanographic surveying and offshore exploration, are air-supported flexible structures. Fabrics are also categorised as flexible structures. The automotive air bags, hot-air baloons, airships, large sandbags for flood protection, flexible tanks, and storage vessels are, all built from high strength fabrics. Fabrics with heat-resistant quality can be used in protective clothing. Pressurized fabric tubes are also flexible membrane structures. In marine conditions, membrane structures find usage as breakwaters, fluid-filled airbags, sea balloons, and flexible membrane dams. Figure 1.1 shows the application of flexible structures in various fields like solar sail and inflated torus in aerospace industry, membrane roof in civil industry and rotor blades in helicopter dynamics.

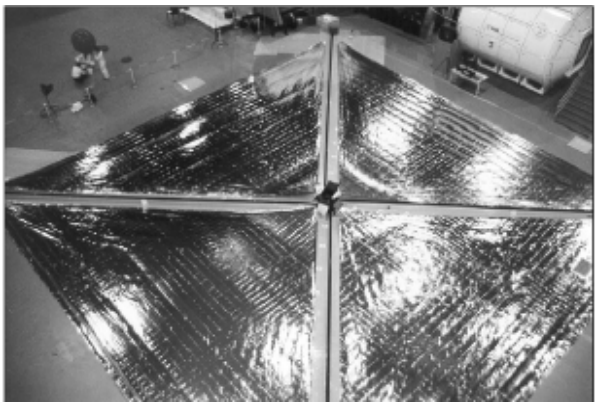

Solar sail

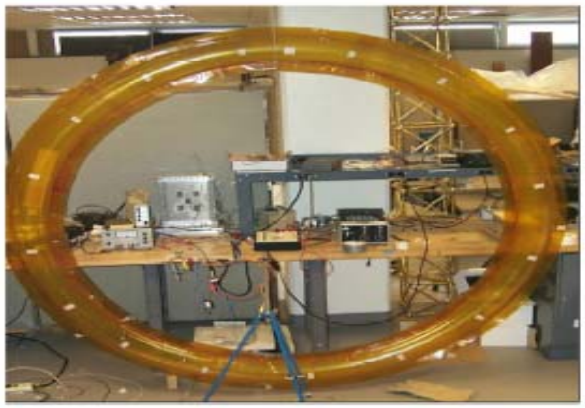

Kapton Torus

Membranous Roof

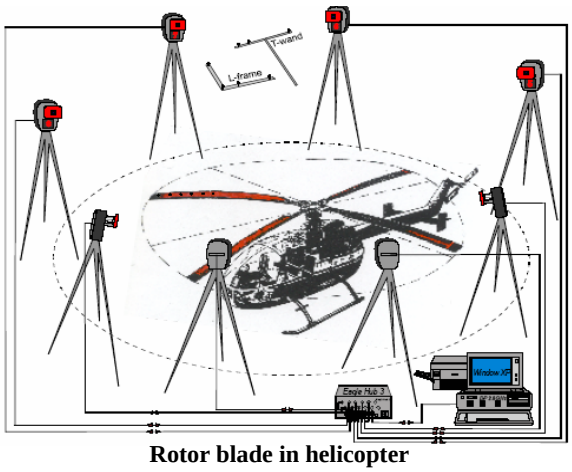

Rotor blade in helicopter

Figure 1.1: Applications / Flexible structures

1.2 Shelters

Fabric structures are often used as temporary storage places for equipments, vehicles and temporary housing for personnels. The collective protection systems have generated interest due to their applicability against chemical and biological agents. A collective protection system consists of a soft-wall shelter and control system which include blower to overpressurize and a filter system to clean the contaminated air. Through the years, several advances have been made in barrier material to improve the protective capability of these systems. Some of the applications of such systems for military purposes are as follows: Expeditionary shelters such as Tent Extendable Modular Personnel (TEMPER) tents [2] and Small Shelter Systems (SSS) [2], Army Chemical Protection Medical System, Chemical-biological Protection system, the Marine Corps Portable Collective Protection System, Army's Expandable Light Air Mobility Shelters (ELAMS) [3], and AES Rapid Development Shelters. A Medical Unit Self-Contained Transportable (MUST) shelter was developed in the 1960's and 1970's. Hypalon and neoprene coated polyester were used for the skin fabric. The collective protection systems like TEMPER Tents fitted with M28 liner were developed to provide protection against the chemical and biological agents [4]. Civil applications include temporary housing for people, maintenance hangers in aviation, emergency shelters, mobile field hospitals and aesthetic tents. Inflated shelters like Small Air Force Shelters (SAFS), AIIMS (Aviation Inflated Maintenance Shelters) and STAT (Small Tactical Air Beam Tent) provide greater flexibility in construction and require less time.

Figure 1.2: Various types of shelters

1.3 Previous Research - Shelters

The U.S Army has been involved in the development of lightweight shelters consisting of a fabric skin supported by pressurized arches. The pressurized arches are made of thin flexible material and take a very stiff structural form when inflated, providing the framework for the shelter systems. Mohan [16] and Goh [5] studied the behavior of these arches under snow and wind loads. The equations for the pressurized arches using shell theory were used and the numerical solution was obtained using the Rayleigh-Ritz method under different loading conditions. Mohan [16] used the finite element method, with a flat shell element formulation, to study the behavior of these arches under pressure loading conditions. The tents, consisting of arches with the skin connected to arches and held in tension, are thin flexible structures which can be folded and compressed when deflated. Thus, they are categorized as soft shelters. The static analysis of these soft shelters under snow and wind loads and the computation of linear vibration modes and frequencies, have been studied in the past. Carradine [6] performed an experimental study on arch-supported membrane structures under snow and wind loads, using scaled models. It was concluded from the tests that the failure mode for the membrane was the tearing occurring near where the skin was connected to the frames. Mohan [16] performed a numerical analysis of large tents consisting of a membrane skin connected to inflated arches under wind and snow loads. The large-deformation behavior was analyzed numerically using the finite element method with a three-node, flat, triangular element obtained by combining the Discrete Kirchhoff Theory plate bending element and a membrane element similar to the Allman element. The follower effects of the pressure load were included in the formulation.

The response of these and similar soft structures to blast and impact loads has generated much interest with the idea of their utilization in combat zones, subjected to projectiles and exploding bombs. In order to investigate the force protection standards of such shelters, the Air Force Research Laboratory conducted field tests [2]. The tests were designed to demonstrate the structural response of expeditionary and Temper Tents to large bomb blasts (generating high pressure and impulse). Structural damage in the form of liner failure was observed. The experimental tests could not dwell deep into the causes of failure of the liner system on the side opposite to the blast due to limitations on the experimental measurements. Thus, the computational modeling and analysis of such structural systems was proposed.

The finite element method provides the most flexible approach to such kind of complex problems. The present research deals with the complete finite element model development of TEMPER Tents and investigate their structural response under highly dynamic conditions generated due to blast loads.

1.4 Problem Formulation

1.4.1 Problem description

Temper tents consist of fabric material stretched over metal frames fitted with the Collective Protection System (CPS) liner M28 [7]. The liner consists of 16-foot center sections, end sections and the entry vestibules that are joined by air-tight zip seals. Plastic strays with arrowhead type

Figure 1.3: Temper Tent overview and liner (collective protection system)

connectors are riveted to the outside of the M28 liner and are attached to the tent frame to hold the liner up when not inflated. A ventilation system provides clean air to the liner and maintains a positive pressure slightly above the surrounding atmospheric pressure inside the liner. This positive pressure ensures that the flow of the air is outward from the liner, thus not allowing contaminated air to enter.

The Air Force Research Laboratory conducted experimental tests on the Temper tents with a liner system (CPS) installed, exposed to a surface air blast (generating high impulses as well as pressure), in order to validate their survivability against blast conditions and identify potential structural failure. Tests were conducted for various TNT weights and stand-off distances. These tests revealed the failure of the CPS liner characterized by tears in the liner and failure of zip-seals over a large area which allowed the outside air to enter in, causing the complete loss of positive pressure inside. Most zip seals failed in separation and the liner was riped at places on the back side, the side opposite to the one facing the blast. The frames experienced minor damage and, in general, were able to withstand the significant load. Figure 1.4 shows the post-blast pictures of the liner system, damaged due to separation of zip seals and tearing of the liner.

1.4.2 Physics of the problem

An air blast creates a compression wave that moves outward in all directions, initially faster than the speed of sound. As this compression wave propagates, it is weakened as it spreads over a larger area. As this pressure wave hits an obstacle in its path, part of the pressure wave is transmitted and

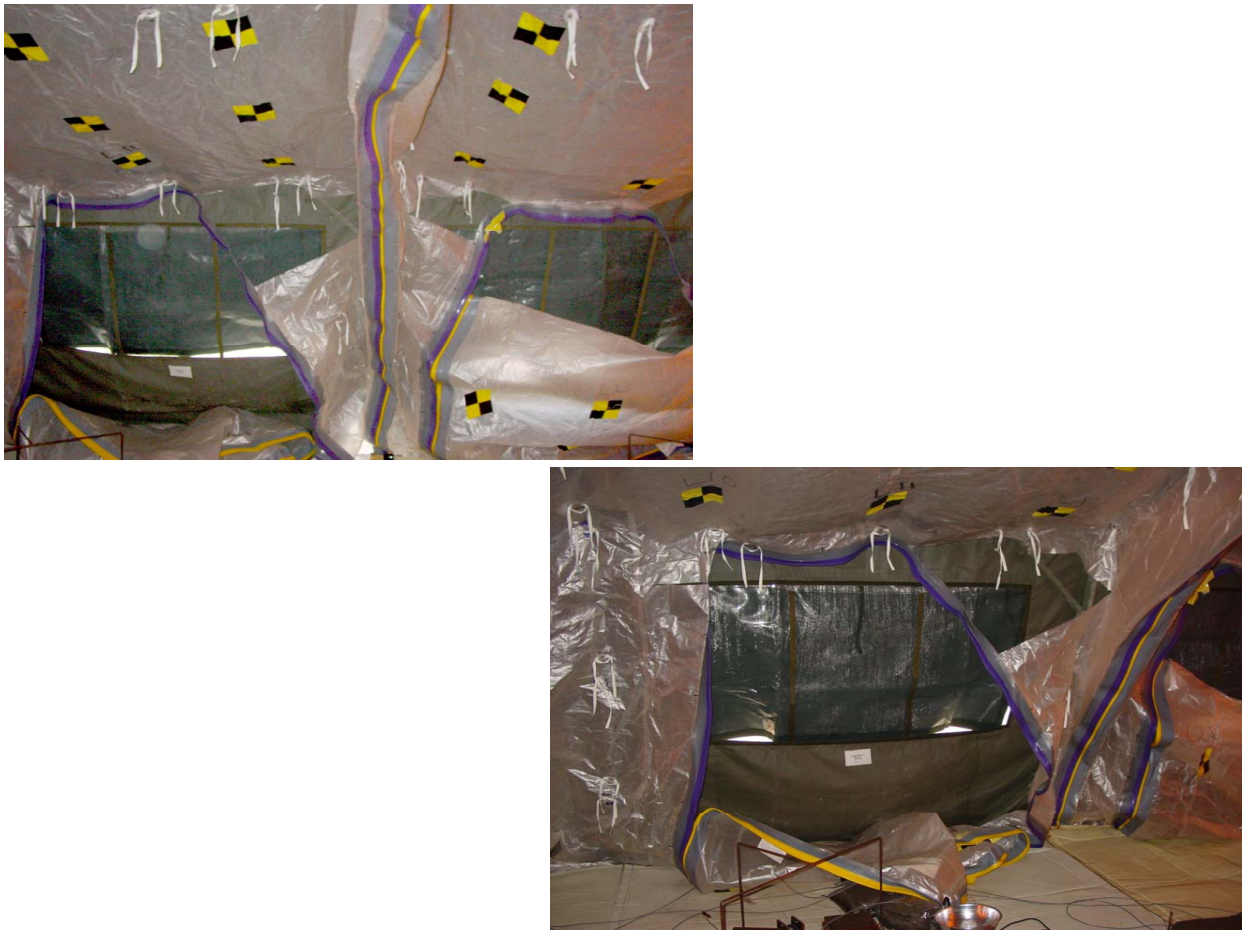

Figure 1.4: Post Blast figure for TEMPER Tent showing back side damage with tearing

part is reflected back, being a function of the rigidity of the reflecting surface and orientation of the surface to the wave. The reflected pressure is the pressure imposed on the structure immediately after the reflection of the pressure wave and is greater than the incident pressure. The blast load is modeled as the time dependent function of exponentially decaying pressure. The pressure profile consists of positive and negative phases where the positive phase is characterized by an initial sudden rise in the pressure and then decays exponentially with time till reaching the reference pressure. The negative phase is characterized by an under-pressure i.e. a pressure which is lower

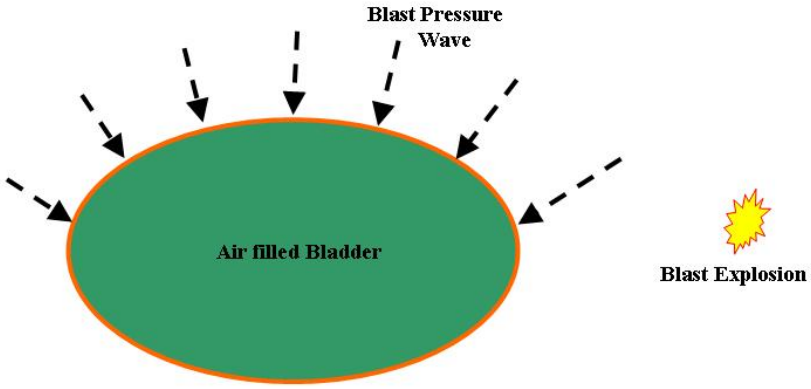

Figure 1.5: An Air-filled bladder surrounded by the blast pressure

than the reference pressure, increasing again to the reference pressure. The overpressure generated by an air blast surrounds the whole tent-liner system with time delays over the other surfaces relative to the surface facing the blast. Here, the liner system can be considered analogous to an air-filled bladder with surrounding pressure pushing in from all sides, with time delay relative to the front side where the blast reaches first. Due to high overpressure, structural movement is very sudden. This fast movement generates a shock wave or high-speed transmitted pressure wave inside the closed structural system, thus opposing the structural movement. The resulting profile changes the overall pressure distribution, generating complex reflection and diffraction patterns, thus altering the dynamics of the whole structural system.

1.4.3 Approach

The problem described is a classical fluid-structure interaction problem, where nonlinearity amplifies the complexity of the problem in terms of obtaining the response.

From the structural point of view, understanding the dynamics of the shell structures, among all structural forms, is the most challenging, physically and mathematically. Physically, the shell behavior involves the interaction of the membrane mode with the bending mode, and when large deformations are included, a pure bending state is seldom encountered as membrane stresses are almost generated. Initially, shells carry load in both membrane and bending action, but with increasing deformation, the characteristic of problem changes to being membrane dominated. Obtaining a solution analytically presents a very difficult proposition when nonlinearity (large deformation) plays a significant role. The numerical approach provides a better way to the solve problems of this kind. Therefore, the finite element method is adopted to determine the structural response of the tent due to blast. The finite element code ANSYS is used for studying the response.

A simplified finite element model is used, consisting of fabric skin (shell) supported over the frame. Two approaches are used. In the first approach, the shell is considered as a membrane away from its boundaries, in which the stress couple is neglected in its interior region. In the second approach, stress coupling is neglected over the whole region. Based on these approaches, two basic finite element models are built. In the first model, a shell element (including both bending and membrane action) is used for modeling the fabric skin and a beam element is used for the frames. In second model, the skin is modeled with a membrane-only element and the frames are

modeled with a beam element.

Blast load is modeled as a normal pressure load with loading varying over each side with time. Transient analysis is performed to determine the response of the structure. The response is characterized by large deformations. Newmark's time integration method is used for the dynamic solution while Newton-Raphson method is used for the solution of the nonlinear equations. The response consisting of displacement-time history and the dynamic stresses are computed. A parametric study has been carried out.

Chapter 2

THE BLAST PHENOMENA

2.1 Introduction

Explosion is defined as a large-scale, rapid, and spectacular expansion of air or in a more restricted sense it is a process by which a pressure wave is generated in the air by a rapid release of energy. The failure of a high-pressure gas storage vessel or a steam boiler, or the muzzle blast from the gun, are some of the examples of an explosion. With this definition, an explosion could be categorized as a physical, a nuclear or a chemical event.An example of physical explosion is a violent mixing of two liquids at different temperatures. Here explosion results from a rapid conversion to vapor of the cooler fluid, resulting in generation of a shock wave. In nuclear explosion, the energy released arise from the formation of different nuclei by the redistribution of the protons and neutrons within the interacting nuclei.

Blast, in general, refers to the fluctuation of air pressure due to the explosion or to the vibrations induced on the ground. Due to this initial finite pressure disturbance, the properties of air as a compressible gas causes the front of the disturbance to steepen as it passes through the air until it exhibits nearly discontinuous increase in pressure, density, and temperature, resulting in a shock front. This shock front moves supersonically in the air ahead of it. This transmission of the blast wave is a nonlinear process involving nonlinear equations of motion. A sonic boom could be categorized as a blast load.

Before studying the effect of an explosion on the structural system, it is very important to predict the detonation behavior and deduce the mathematical expression for the energy of the explosion and for the propagation and decay of the blast wave. The early work of Earnshaw and Lamb on the theory of sound and sound waves to an extent formed the basis for the mathematical expression for the propagation of the shock wave through air. Rankine and Hugoniot studied the conditions existed related to pressure, density and velocity before and after the passage of the shock wave. Later Chapman and Jouget studied the shock wave propagation. [8]

Many studies have been conducted related to the form of overpressure as a function of the distance of the point of measurement from the center of the explosion and the overpressure duration relationship for a high explosive in the air. Hopkinson introduced the factor $R/w^{1/3}$, an important scaling factor in the relationship between overpressure and the distance from an explosion, which enabled the results to be applied to any detonation as long as the equivalent weight is TNT (Tri-Nitro-Taulene). His scaling law emphasized that similar blast waves are produced at the identical scaled distance when explosions of similar geometry and material but of different size are deto-

nated in the same atmosphere. The behavior of spherical charges of Pentolite was recorded by Goodman from his compilation of the measurements taken from the experiments. While the above work concentrated on a spherical charge in the air, Lindberg and Firth studied the overpressure versus distance form for various shapes with different scaling factors.

Although the physical properties of the explosion source affect the characteristics of air blast waves in many aspects, studies indicate that at a reasonable distance from the center of an explosion, all blast waves, regardless of the source, share a common configuration. The attempts to define the mathematical form of the blast wave versus time have not been easy. Baker [8] has reported overpressure/time functional forms of varying complexities describing the positive phase.

2.2 Types of explosion

Explosion can be categorized into different types, depending on the conditions under which the explosion takes place [9].

2.2.1 Explosion in Air

When the explosive is detonated in air far from the ground or the reflecting surface, the explosion is termed as an Air explosion. When the explosion is initiated, the reaction generates hot gases which can be at pressure between 100 kilobars to 300 kilobars and temperatures ranging from 3000-4000 C^0. A violent expansion of these gases then occurs and the surrounding air is forced out of the

volume it occupies. As a result, a layer of compressed air (Blast wave) is formed in front of these gases, containing most of the energy released by the explosion. With the expansion of the gases, the pressure falls to the atmospheric. Due to continued expansion, the gases cool and their pressure falls little below the atmospheric pressure. This happens because gas molecules have mass, and are moving and it takes a longer distance to travel before the momentum is destroyed. This state is the over-expanded state and results in the reversal of the flow towards the source due to a small pressure difference between the atmospheric pressure and the pressure of the gases. This is called the negative phase. The pressure of the compressed air at the blast also falls with distance.

2.2.2 Above-Ground Explosion

When an explosive is located a set distance above a reflecting surface such as ground, the explosion is termed as Above-Ground Explosion. The reflection process is similar to that shown in the figure 2.1. When the incident wave first touches the flat surface, it is reflected, and this reflected shock front moves at a higher velocity than the incident shock front. When the reflected front overtakes the incident one, the fronts merge to form a single outward-traveling front known as the Mach stem.

2.2.3 Ground Burst Explosion

In ground-burst explosions, the charge detonates in contact with an unyielding surface in perfect conditions. The shock wave has a hemispherical wavefront and therefore the energy of the explo-

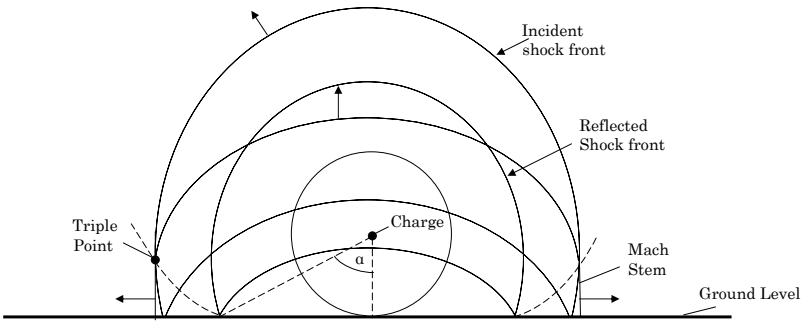

Figure 2.1: Reflection of shock waves from an above ground explosion

sion is concentrated over a smaller total surface area. All the relationships for the free-air burst are valid if a value twice the charge (2W) is substituted for W. However, since the soil on earth is yielding and capable of absorbing part of the energy, the factor on the weight of the charge is taken to be 1.7 instead of 2 with experimental validation. The detonation on the ground will generate much greater stresses due to the enhanced degree of the coupling between the explosion and the ground. Figure 2.2 shows the hemispherical wave front for the ground contact explosion [10].

2.2.4 Underground Explosion

When the explosion is below the ground level, the explosion is termed as below-ground explosion, e.g., mine explosion. The pressure in the earth from the detonation of a charge below the surface

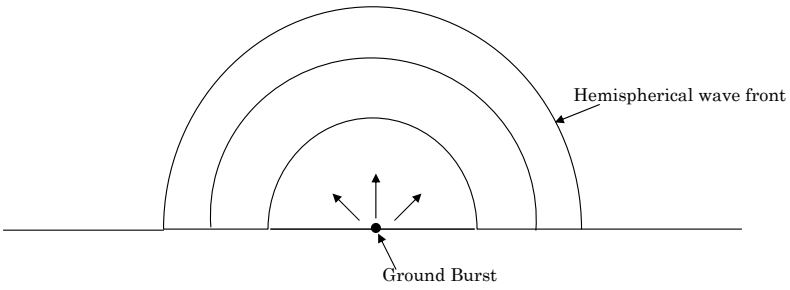

Figure 2.2: Hemispherical wave front from ground contact explosions

is influenced by the distance of the point under consideration from the center of the explosion (R), the weight of the explosive (W), the characteristic of the soil (K), and the depth of burial of the charge (H).

$$p_0 = fK(R/W^{1/3})^{-n} \tag{2.1}$$

2.2.5 Underwater Explosion

In underwater explosions, the development of the explosive wave is similar to that for an air explosion. There is only a small quantitative difference. Due to relatively higher pressure and the weight of the water, particularly at some depth, explosive gases after explosion get violently compressed. Due to the inertia of the water, gases are compressed to such an extent that they exceed the hydrostatic pressure of the water, resulting in a new expansion followed by a repeated com-

pression. A gas sphere rises toward the water surface and at every expansion of the sphere, a new pressure wave separates. Thus, a system of secondary pressure waves is formed, in contrast to the primary wave developed due to the first expansion. These secondary waves have less and less energy consequently. The profile of the shock wave has the same shape as in the air.

2.3 Blast Wave Configuration

For the ideal blast wave, we assume that explosion occurs in a still, homogeneous atmosphere, and the source is spherically symmetric, so the characteristics of the blast wave are a function of the distance from the center of the source, R, and time t [8]. Figure 2.3 shows the pressure/time plot for the ideal blast wave. After an explosion, the ambient pressure p_0 exists for some time. At the arrival time t_a, the pressure rises quite abruptly to a peak value $p_s^+ + p_0$. The pressure then decays to the ambient pressure in total time $t_a + T^+$ and then drops to a partial vacuum of amplitude p_s^-, eventually returning to p_0 in total time $t_a + T^+ + T^-$. The term p_s^+ is called the peak side-on overpressure or peak overpressure. The portion of the time history above the ambient pressure is called positive phase with duration T^+, and the period below the ambient pressure is called the negative phase with duration T^-. The positive and the negative impulses are given in the Fig. 2.3, respectively.

$$I_s^+ = \int_{t_a}^{t_a+T^+} [p(t) - p_0]dt \tag{2.2}$$

$$I_s^- = \int^{t_a+T^++T^-}_{t_a+T^+} [p(0) - p_t]dt \tag{2.3}$$

Under well-controlled experimental conditions, the ideal blast wave characteristics could be ob-

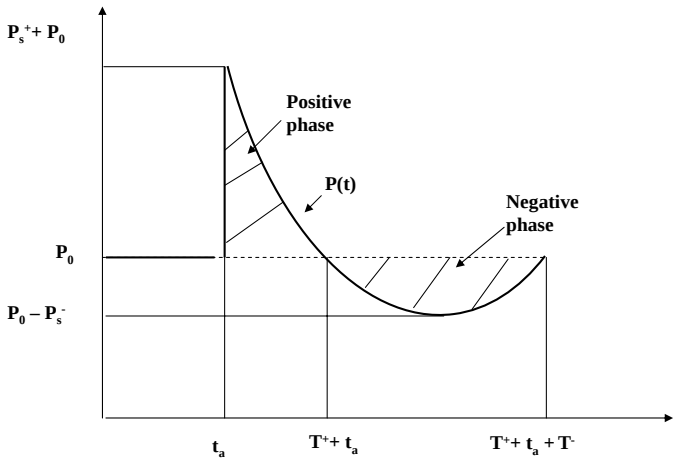

Figure 2.3: The pressure variation as a function of time for an ideal blast wave.

served. Many authors have tried to present some functional form for the pressure-time history of the ideal blast wave by empirical fitting to predict the time histories. The simplest of these blast wave shapes involve only two parameters. Flynn considered a linear decay of pressure, given by

$$p(t) = p_0 + p_s^+(1 - t/T^+), \;\; 0 < t \leq T^+ \tag{2.4}$$

where t is the time after shock arrival. In fitting this form to the data, p_s^+ is preserved while the positive phase duration T^+ is adjusted to maintain the positive impulse I^+.

The next formulation involves three parameters. This form is usually termed as the modified Friedlander equation and is given as

$$p(t) = p_0 + p_s^+(1 - t/T^+)\exp(-bt/T^+) \tag{2.5}$$

where time is measured from the time of arrival. This equation is reasonably simple and allows

more accurate matching with the observed parameters. This form has been widely accepted for its simplicity as well as it allows adjustment to match to the important blast properties.

2.4 Blast Wave Interaction

Blast waves, on encountering any solid surface or more dense object than the transmitting wave, are seriously modified as they reflect from this object and diffract around it. The effect of a shock wave on bodies and structures differs in character on the kind of explosion, distance from the point of explosion, size of the charge, and shape of the body.

2.4.1 Reflection

The simplest case of the reflection is the normal reflection of a plane shock wave from a plane rigid wall. Assume that the incident wave I, before hitting the wall, has velocity U into the still air with ambient conditions, and conditions behind the shock front are for the free-air shock. This shock, on hitting the wall gets reflected normally and immediately after reflection, the front moves away from the wall into the flow compressed relative to the incident wave at velocity U_r. In this reflection process, the incident velocity becomes zero u_s (u=0) and pressure, density and temperature are all increased above the values in the incident wave. This overpressure at the wall surface is termed as reflected overpressure P_r. For very weak shocks, $p_s << p_0$, acoustic approximations are valid and the reflected overpressure is twice the incident overpressure, $P_r = 2p_s$. But for stronger shocks, the enhancement of the reflected pressure is increased. This process is shown in Fig. 2.4. When the

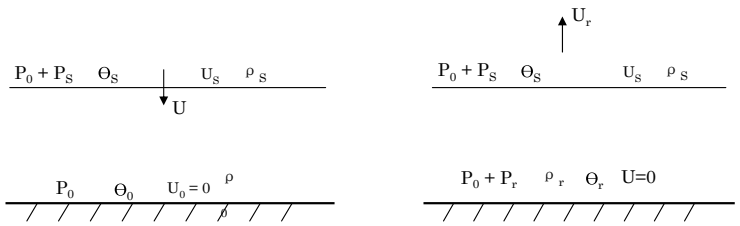

Figure 2.4: Normal reflection of a plane shock from a rigid wall

shock front hits the wall at some angle, the reflection is no more normal and the characteristics of the front change due to this angled incidence, this type of reflection is called oblique reflection. and these reflection processes are very complex. Consider a regular, oblique reflection of a plane shock from the rigid, plane wall. Figure 2.5 shows the phenomenon schematically. Here, the incident shock travels into the still air at some velocity U at an angle of incidence α_i with respect to the wall, with properties behind the shock of free-air shock. After hitting the wall, the flow behind the shock is turned and the shock is reflected at some angle α_r. In determining the quantitative character of the phenomenon, the particle velocity of the incident wave front is resolved into two components, one parallel to the barrier surface and the other normal to the surface. The normal component is reflected normally while the horizontal component causes motion of the compressed

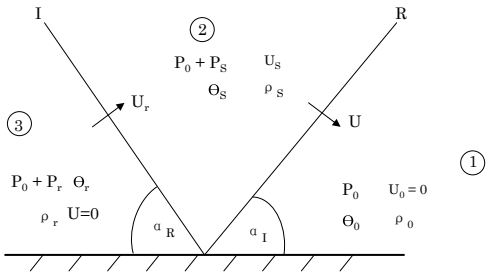

Figure 2.5: Regular oblique reflection of a plane shock from a rigid wall

air along the air barrier, thus shifting the vertical reflected particle to right. This reflected shock front is compressed and therefore has higher velocity, consequently, $\alpha_R > \alpha_I$. It has been observed that for a given strength of incident shock, there is some critical angle of incidence $\alpha_{i_{crit}}$ such that this reflection is not possible for $\alpha i > \alpha_{i_{crit}}$.

The most complex type of reflection is a Mach reflection of a plane shock obliquely incident on a plane, rigid wall. In this case, incident and reflected shocks coalesce to form a third shock. Because of the geometry of shock fronts they are termed as Mach V or Y. A single shock formed by the coalesced incident and reflected shocks is called Mach stem. Figure 2.6 shows the geometry of mach reflection where the incident (I) and reflected shocks (R), Mach stem (M) and junction (T) of the three (which is called the triple point) is shown.

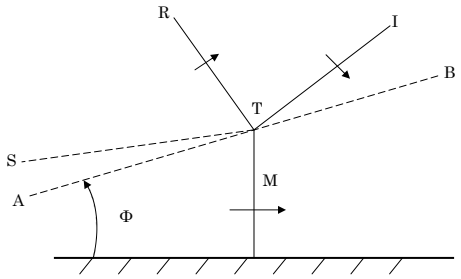

Figure 2.6: Mach reflections from a rigid wall

2.4.2 Reflection Process for Blast Wave

Considering strong blast wave that is generated by a finite source and reflected from a rigid, plane wall, Fig. 2.7 shows three successive stages of the reflection process of a strong shock. The incident wave I_1 impinges upon the reflecting surface S. Due to this incidence, normal reflection occurs. At this point, excess pressure above that of the atmosphere becomes more than twice that of I_1 elsewhere. As the incident wave expands to a greater size I_2, the reflected wave R_2 also expands but not spherically. The angle at which I_2 and R_2 meet the surface S are also not equal. At some distance from charge C, determined by the distance of C from the surface S and from the strength of the incident shock, a new phenomenon occurs, i.e., the intersection of R and I no longer lies on S but lies above it and follow some path ρ. The new shock M, the Mach stem, connects the intersection of R and ρ to the surface. This intersection of R, ρ and M is called the triple point.

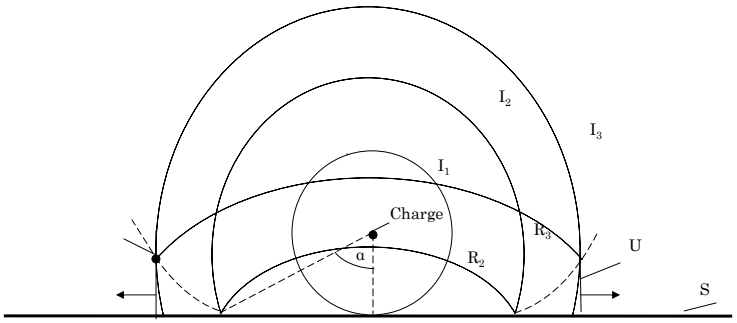

Figure 2.7: Reflection of strong shock waves

As the shock system expands further, the Mach stem grows rapidly, tending to swallow up the two-shock system above it. If C is very close to the surface, the stem is almost formed directly under C and in the short time, this grows so much that most of the shock system is a Mach stem.

For the Weak Shocks, the process of reflection is very different. Considering a point source of C and a plane reflecting surface S at some distance from it, the incident shock I striking the surface gets reflected in such a way that the reflected wave R may be considered to arise from the second source C' on the opposite side of the reflecting surface perpendicularly below the source and equally distant.

2.5 Diffraction Process

When a blast wave encounters a solid object of finite extent, the interaction of the shock front with such an obstacle results in a complicated phenomenon called Diffraction. Figure 2.8(a) shows a plane blast wave traveling over a rigid plane rectangular wall. The blast front is normally incident on the front face of the wall, with pressure on each face being the ambient pressure. As the incident shock hits the front wall, some portion is reflected and the reflected wave R moves to the left and pressure increases to $P_r + p_0$. Above the wall, the incident shock continues to move without any disturbance. As the reflected wave moves back from the wall, a rarefaction front moves down the front wall. A formed vortex is shed from the top corner of the front wall. Figure 2.8(b) shows that the reflected pressure on the lower side of the front wall is $P_r + p_0$ and the pressure on the upper portion of the front wall is that of the incident wave $P_s + p_0$ while the pressure ahead of the front and other walls is still ambient.

As this incident wave passes beyond the rear wall, it diffracts around the wall. Another vortex is formed at the top corner of the rear wall. At this instant the reflected wave from the front wall is completely attenuated by the rarefaction wave and pressure on the front wall attains a new value q + p_0 where q is the dynamic pressure, while the pressure behind the diffracted incident wave on the rear wall is less than $P_r + p_0$ shown in Fig. 2.8(c). As a result of the vortex phenomenon and the time required for the back wall to be fully enveloped by the blast wall, maximum pressure develops slowly on the back wall. When the incident wave has passed over the back wall, the diffraction process is over.

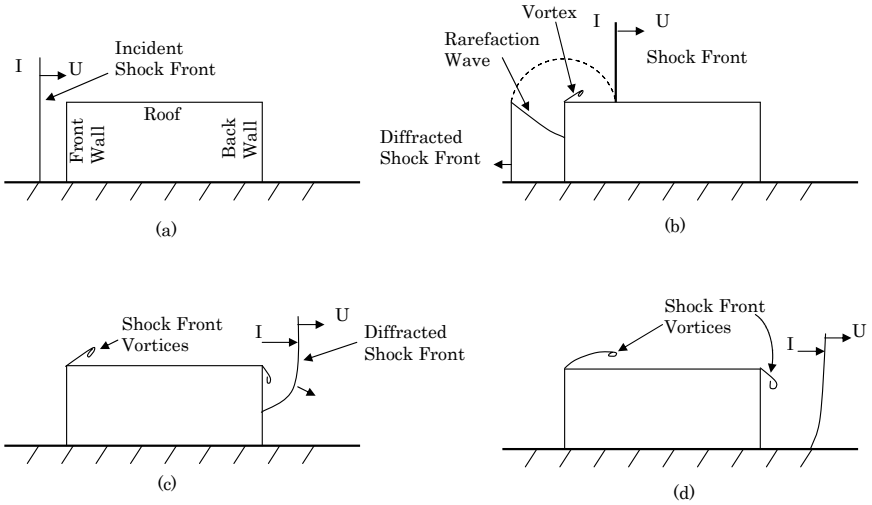

Figure 2.8: Diffraction of shock front over a wall

Chapter 3

SHELL MODEL AND ANALYSIS

3.1 Introduction

Shell structures are abundantly found in nature in the form of sea shells. Although thin and light, these structures have a very effective load carrying capacity, an egg shell is the most common example. This large load carrying ability can be explained as the shell resist the applied load by its curvature. Because of this property, shells find usage in the engineering design applications in various industries. In aeronautical engineering, the bodies of aeroplane and rockets are shell structures. In automobile industry, car bodies are made of shells, while civil applications like roof structures and cooling towers come under this category. Naval applications like ship hulls are predominantly in the form of shells. Their lightweight and large load carrying capacity make them attractive for space structures like satellites, solar sails, and inflated structures, like gossamer

spacecraft. Structural applications with smaller thickness can be categorized as future structures, with the objective being the use of minimum material while still having a safe design.

A shell is a three dimensional structure, with thickness being small compared to the other two dimensions and have high load carrying capacity. These are much stiffer and stronger than other structural forms and are also referred as " $form\ resistant\ structures$ ". Their characteristics like reduced thickness, high load carrying capacity etc. make them a challenging problem from the design and analysis point of view. Shell structures show remarkable change in behavior as the thickness is reduced, and solutions become very difficult to predict, as the rate of convergence goes down in the nonlinear analysis.

This chapter discusses the finite element model for the tent structure. With difficulties associated with the formulation of the curved shell element, a flat shell element provides a simpler and effective mechanism for the shell analysis. General flat shell formulation [12] is discussed and some literature is reviewed related to the development of the shell element formulation and shell analysis. Issues related to shell analysis, like the role of drilling degree of freedom and asymptotic behavior are described briefly.

3.2 General Flat Shell Element Formulation

A shell is basically a structure that can be derived from a plate by initially forming the middle surface as a singly or doubly curved surface. But the way a shell supports external loads is very different from that of the flat plate. The stress resultants acting on the middle surface of the shell

have both tangential and normal components which carry a major part of the load, explains the load carrying capacity of shells.

The analysis of general shells is mathematically very complicated. As a consequence, there is a dearth of analytical solutions of the governing differential equations of shell theory except for cylinders and shells. The derivation of governing equations for the curved shell element poses many difficulties, e.g., the derivation of the force-displacement relationship, which has led to alternative formulation with physical approximations in the form of polyhedral shells composed of flat facet finite elements. It is assumed that the behavior of a continuously curved surface can be adequately represented by the behavior of a surface made from flat facet elements. The only reservation that whether the flat facet elements with the independent membrane and bending actions would properly be able to present the true behavior of the curved shells especially in common situations where the actions are coupled together in shell response, was put to rest with theoretical development and the evidence of the numerical examples. With the decrease of the size of the mesh, convergence of solution to exact value increases.

A typical polygonal flat element in its local co-ordinate system consists of in-plane and bending actions. Considering in-plane action (plane stress), the state of the strain is uniquely described in terms of the displacements u and v at node i. The minimization of potential energy lead to the stiffness matrices and gives nodal forces f_i^p due to the displacement parameters Δ_i^p

$$f_i^p = (K^e)^p \, \Delta^p \tag{3.1}$$

Considering the bending action, the strain is uniquely defined in terms of the nodal displacement

w (z-direction) and two rotational components, θ_x and θ_y. The stiffness matrices $(K^e)^b$ is defined

$$f_i^b = (K^e)^b \, \Delta^b \tag{3.2}$$

with

$$\Delta_i^b = \left\{ \begin{array}{c} w_i \\ \theta_x \\ \theta_y \end{array} \right\}, \qquad f_i^b = \left\{ \begin{array}{c} F_{zi} \\ M_{xi} \\ M_{yi} \end{array} \right\}$$

There are two important facts to remember at this stage. First, the deformation prescribed by both actions are uncoupled with respect to each other. Second, the rotation θ_z is not included as a nodal deformation parameter. But while assembling, this rotation is taken into account and associated with the fictitious couple M_z. Since this does not enter the minimization process, it is accounted for in the stiffness matrix by adding an appropriate number of zeros.

Combining the nodal displacement, we have

$$\{\Delta_i\} = \left\{ \begin{array}{c} u_i \\ v_i \\ w_i \\ \theta_{xi} \\ \theta_{yi} \\ \theta_{zi} \end{array} \right\}, \qquad \{f\}_i^e = \left\{ \begin{array}{c} F_{xi} \\ F_{yi} \\ F_{zi} \\ M_{xi} \\ M_{yi} \\ M_{zi} \end{array} \right\}$$

We can write the complete form as

$$K^e \Delta = f^e \tag{3.3}$$

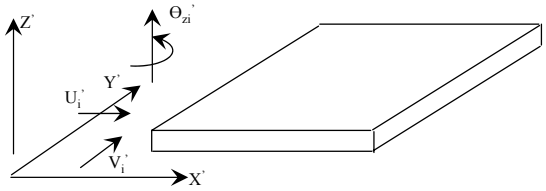

In - Plane Deformation

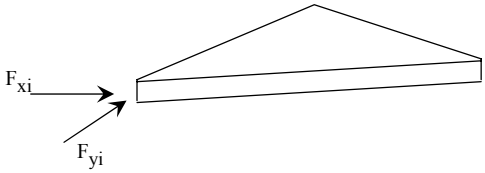

In - Plane forces

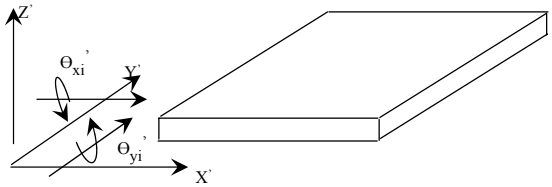

Bending Deformation

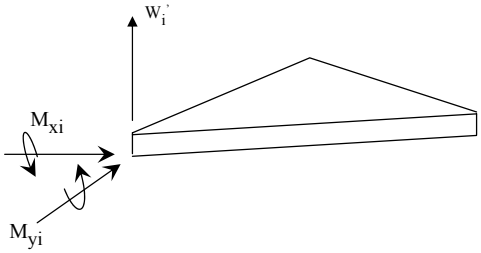

Bending Moments

Figure 3.1: Flat Shell Element Formulation

The above formulation is valid for any shape of the polygonal element especially, for the rectangular and triangular elements. The stiffness matrix corresponds to the element's local co-ordinate system. The transformation of each element stiffness matrix to the common global system is necessary in order to form the assembled system and to write the appropriate equilibrium equations. This is accomplished using the transformation matrix, T:

$$\{\Delta_i'\} = [T]\,\{\Delta\} \tag{3.4}$$

$$\{f_i'\} = [T]\,\{f_i\} \tag{3.5}$$

These equations transform the nodal displacements and forces from the global to local system. The transformation matrix is composed of cosines of angles between the particular axis in the local and the global co-ordinate system. After the assemblage of the stiffness matrix, forces are assembled in the same pattern. The displacements obtained are referred to in the global system, but the stresses are computed in the local co-ordinate system for each element.

In this formulation, a problem arises if all the elements meeting at a node are co-planar. This situation arises for folded plate segments and at the straight boundaries of developable surfaces (e.g., cylinders or cones). The problem lies in the zero stiffness in the θ_{zi} direction and from the fact that classical shell equations do not produce equations associated with the rotational parameters. Inclusion of rotation in the z-direction, and the associated force F_{zi}, has its benefits in that the rotations and displacements at nodes can be treated in a simple manner using the transformations.

Drill Stiffness

Drilling degree of freedom [13] is defined as the rotational degree of freedom normal to the plane of the element and is denote by θ_z, assuming that the surface normal is the local z direction. In most of the formulations, this does not form the part of the membrane kinematics of the shell. The absence of this drill freedom causes rank deficiency.

Two basic approaches are implemented. Firstly, an artificial drill stiffness parameter is used to remove the rank deficiency for those elements without drill freedom. This artificial stiffness parameter acts as a spring stiffness for the 6th degree of freedom. An inappropriate value of this parameter can affect the solution dramatically. One way is to give a large value for this parameter, this acts as a penalty parameter and causes the computed solution for the drill freedom to be nearly zero. Therefore, it is important to determine the nodal points that need to be penalty imposed ,e.g., at the stiffener skin interaction, the drill freedom of the stiffener element is the bending rotation, therefore, there is no need to impose the penalty. However, if all the elements meeting at a node are co-planar, there is a need to add a penalty in order to avoid the singularity. This situation arises for folded plate segments and at the straight boundaries of developable surfaces (e.g., cylinders or cones).

Alternatively, a small value may be specified and thus, its contribution to the strain energy will be nearly zero regardless of the solution obtained for the drill freedom. This approach deals with the removal of rank deficiency or singularity without influencing the finite element approximation for the element, and leads to a perfectly well-behaved set of equations from which all the displace-

ments can be obtained. The coordinate, θ_z, does not affect the stresses and is uncoupled from all the equilibrium equations. Application of this approach brings the programming complexities, therefore, modifications are required so that the rotational parameters arise more naturally and have real physical meaning. This can be accomplished by introducing rotational degree of freedom in the membrane kinematics. Element formulations have been built which inherently possess the drill freedom and thus do not exhibit rank deficiency or singularity.

Surface Normals

A separate nodal coordinate system or nodal triad is introduced at the element nodal level in order to restrain the computational degrees of freedom. For the flat shell elements, this corresponds to the original nodal triad in the global systems. In the flat shell formulation for the curved structures, each element generates the nodal surface normals at the shared nodes. These surface normals [13] are used to define the averaged surface normal vectors. If coplanarity exists between the elements, these normals are identical, resulting in rank deficiency in the assembled matrix. The drill freedom is not resisted here, thus resulting in the singularity in the global matrix. This problem can be taken care of by suppressing the drill freedom using one of the techniques described above.

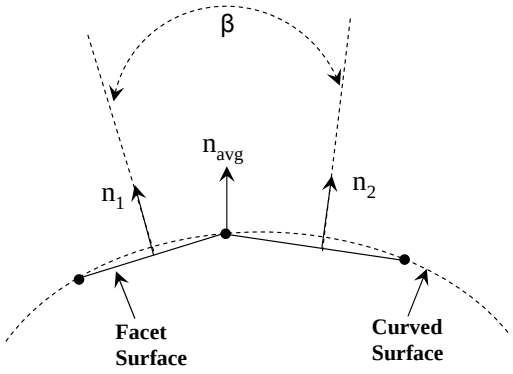

Figure 3.2: Surface Normals for two adjacent flat shell elements

3.3 Literature Review

3.3.1 Shell Element Development

The CST (Constant Strain Triangle) element formulation is the common formulation used for the membrane kinematics. The CST element consists of three corner nodes with two inplane displacements, with displacements varying linearly within the element. But this element formulation shows limitations for folded plate structures due to the absence of drill freedom resulting in rank deficiency. A better approximation for the membrane kinematics was derived with LST (Linear strain), with displacement field varying quadratically within the element. This element is most popular for estimating the plane stress and more accurate as compared to the CST element but

suffers from the drill singularity. Another element named OST, a quadratic strain triangle, having displacement and its derivative at each corner as degrees of freedom, provides high precision but lacks generality when required for problems having different regions having different material properties and other isoparametric elements.

The idea of finite element modeling using vertex rotation for the quadrilateral and triangular elements of various degrees has been researched in order to find the simplified membrane kinematics for thin-walled structures. A triangular element with added drill rotation was derived by Allman [14], known as Allman triangle. The displacement field was represented by a cubic polynomial including the vertex rotational freedom, denoting the most simplified form for membrane action of thin-walled structures and folded-plate structures. Combination of this element with the appropriate plate bending element provides the complete element formulation. There are several approaches used for the construction of the flat shell element: based on the Kirchhoff hypothesis, degenerated element formulation, and discrete Kirchoff element where a condition is imposed on discrete points. Allman [15] used the Kirchhoff hypothesis for the formulation of a triangular flat shell element with 6 degree of freedom at each node. It consists of a nine node membrane element, having drilling degree of freedom combined with the nine-noded plate bending element, resulting in a reasonably accurate flat element for the shell analysis. A triangular flat shell element with CST membrane element and DKT plate bending element shows limitation in nonlinear analysis. Mohan [16], developed a flat shell element by combining the Discrete Kirchhof Theory (DKT) plate bending element and a membrane element similar to the Allman triangle, but derived from the Linear Strain Trianglar (LST) element.

Better approaches have been derived for more accurate nonlinear shell analysis. The DQT shell element, a combination of DKT and QST elements, presents one such approximation. But due to lack of generality on the part of the QST element, find limited usage. Dhatt et al. [17] formulated a new triangular element with 6 degrees-of-freedoms at each corner node and three degrees of freedom at the mid-nodes. The formulation consists of LST membrane formulation and DKTP plate bending formulation (based on the discrete Kirchhoff model). A fictitious rotational diagonal matrix of small terms corresponding to θ_z (driliing degree-of-freedom) was added to avoid any singularity for the flat plate assemblage. This element provides good membrane behavior for the nonlinear analysis.

3.3.2 Shell/Membrane Analysis

Membrane structure usage includes solar sails, tents, balloons, radar domes, inflated structures to modern era protection standard forms like air blast barriers. Membrane behavior is denoted by large deformations and these large deflections are termed geometric nonlinear behavior. Jenkins et al. [18] reviewed the dynamic response associated with membrane structures. They described static analysis as the subcase of the dynamic response of membranes and generally, a step toward complete dynamic analysis. Modeling membrane structures presents a challenge due to being a lightweight system and having large slender ratio. Smalley et al. [19] studied the structural modeling of a five-meter thin-film inflatable structures. They observed that there are modeling issues related to inflatable structures and convergence becomes a major issue in nonlinear static analysis due to the thinness of the structure. Approaches generally used to obtain the stabilized

solution for such cases is either by adding the arbitrary stiffness term or by using an artificial constraint to aid convergence. Marco Quadrelli et al. [20] studied modeling issues related to tensioned, inflated membrane structures, including follower loads. A displacement-based finite element model based on the virtual work principle was derived for the membrane kinematics. Due to the thickness being very small as compared to the other dimensions, response was localized to the membrane plane with bending being negligible as rotations due to bending were extremely small. The pressure stiffness and follower load (representing actuator forces) matrices were added to the tangent stiffness matrix, in addition to the geometric nonlinear terms.

Besides large deformations, another feature of the membrane behavior is the formation of a crease, termed as localized post-buckling behavior or more commonly wrinkling patterns. Bonet et al.[21] analysed such inflated pneumatic structures. These structures are characterized by high internal pressure, capable of supporting large external loads. The finite element analysis was performed considering conservation of mass inside the enclosed structure upon the application of external load. It was observed that due to nonlinear behavior, application of pressure becomes deformation dependent which adds to the tangent stiffness matrix. Wrinkling developed during the membrane kinematics is regarded as a destabilizing factor.

Stanuszek [22] argues that wrinkling is a consequence of lack of compressive and bending rigidity resulting in formation of one or two directional wrinkles, causing instability. It was observed that the necessary and sufficient conditions for the wrinkle formation are, firstly, the distance between two current material points should decrease and secondly, one of the principle stresses should become negative. Thus, in order to avoid this state of stress, element starts to wrinkle in one

or more directions. Modeling of wrinkling can be done following two approaches. One process sees the formation of wrinkling due to the ill-conditioning of the second derivative of the strain energy , and thus tries to eliminate the compressive stresses in each stage due to incremental loading by an iterative algorithm, a finite element approach. The second school uses the concept of relaxed strain energy i.e., the problem is formulated in such a way that strain energy takes different forms in different regions corresponding to the wrinkled regions, thus compressive stresses are automatically excluded.

3.4 Finite Element Model - Tent

TEMPER tents are constructed of synthetic fabric on an aluminum frame with liner installed inside. The finite element model consists of fabric skin supported over three frame structures connected to each other by aluminum rods. Each frame structure is separated from each other by 8 ft. The thickness of the outer skin is 0.65 mm. Figure 3.3 shows the model for the tent. The tent consists of four sides named as the front wall, front roof, back wall and back roof where the front denotes the blast-facing side. The aluminum frames are modeled with the *Beam 4* element and the fabric is modeled with a shell element. Two approaches are used. In the first approach, the shell is considered as a membrane away from its boundaries so that the stress couple is neglected in its interior region. In the second approach, stress coupling is neglected over the whole region. The elastic, isotropic material behavior behavior is assumed.

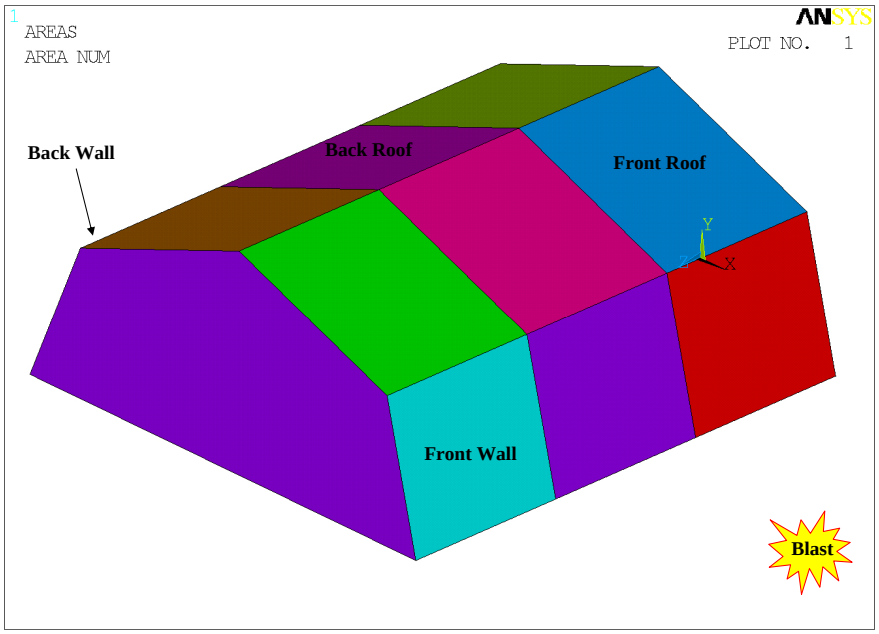

Figure 3.3: Tent model showing front and back sides

The *Beam 4* Element

For all the three finite element models, the *Beam 4* element is used for modeling the frames. *Beam 4* is a uniaxial element with tension, compression, torsion, and bending capabilities. The element has six degrees of freedom at each node: translations in the nodal x, y, and z, and rotations about the nodal x, y, and z directions. Stress stiffening and large deflection capabilities are included. A consistent tangent stiffness matrix option is available for use in large deflection (finite-rotation) analysis.

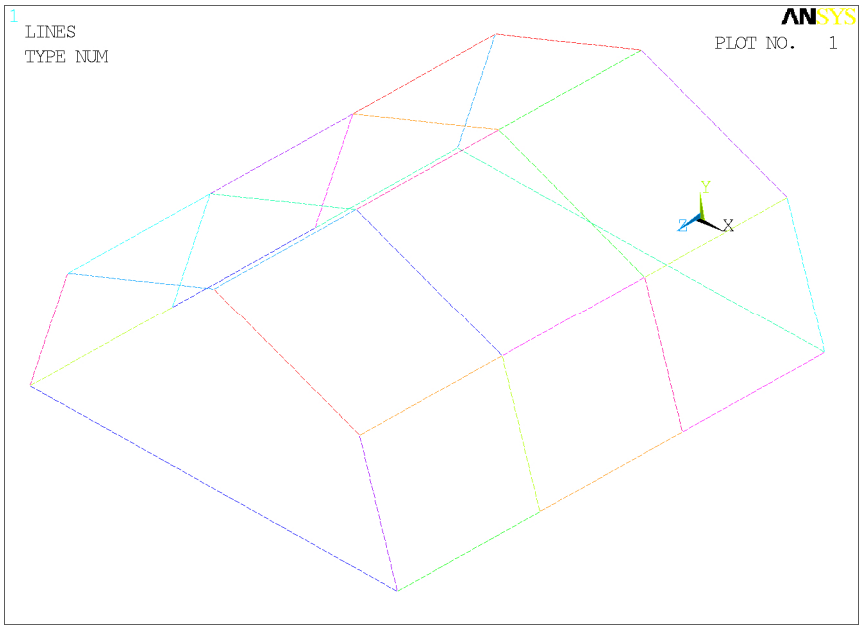

Figure 3.4: Finite element model for frames using Beam 4 element

3.4.1 Model 1

Using the first approach, the skin is considered as membrane away from the boundary, thus neglecting any stress couple in the interior. Using this approach, the skin is modeled using *Shell 63* and the frames using Beam4 elements.

***Shell 63* - Elastic Shell Element**

The formulation of the *Shell 63* (flat shell) element [23] consists of a CST membrane element and a DKT plate bending element without shear deformation, with arbitrary drill stiffness added through the elastic foundation stiffness. It has both bending and membrane capabilities, and both in-plane

and normal loads are permitted. This element has six degrees of freedom at each node: translations in the nodal x, y, and z directions, and rotations about the nodal x, y, and z axes. It also allows for the membrane only option, neglecting bending stiffness. Stress stiffening and large deflection capabilities are included. A consistent tangent stiffness matrix option is available for use in large deflection (finite rotation) analysis. This element type has the option for choosing the type of in-plane rotational stiffness. Allman rotational stiffness is used as the in-plane rotational stiffness. It enhances the convergence behavior in large deflection (finite rotation) analysis of planar shell structures (flat shells or flat regions of shells).

The use of a consistent tangent stiffness in a nonlinear analysis speeds up the rate of convergence greatly. It normally results in a quadratic rate of convergence. This consistent tangent stiffness matrix is derived from the discretized finite element equilibrium equations without the introduction of various approximations.

Figure 3.5 shows the finite element model for the shelter. Triangular elements are used for the modeling. The triangular element is an obvious choice as it can be used to model arbitrary geometry. Also, an element with corner nodes is desired as the data preparation becomes tedious in the case of an element with the nodes at the mid-sides and interior.

3.4.2 Model 2

Applying the same theory as for the first model, the skin is considered as a membrane away from the boundary and thus any stress couple is neglected in the interior. The fabric skin is modeled

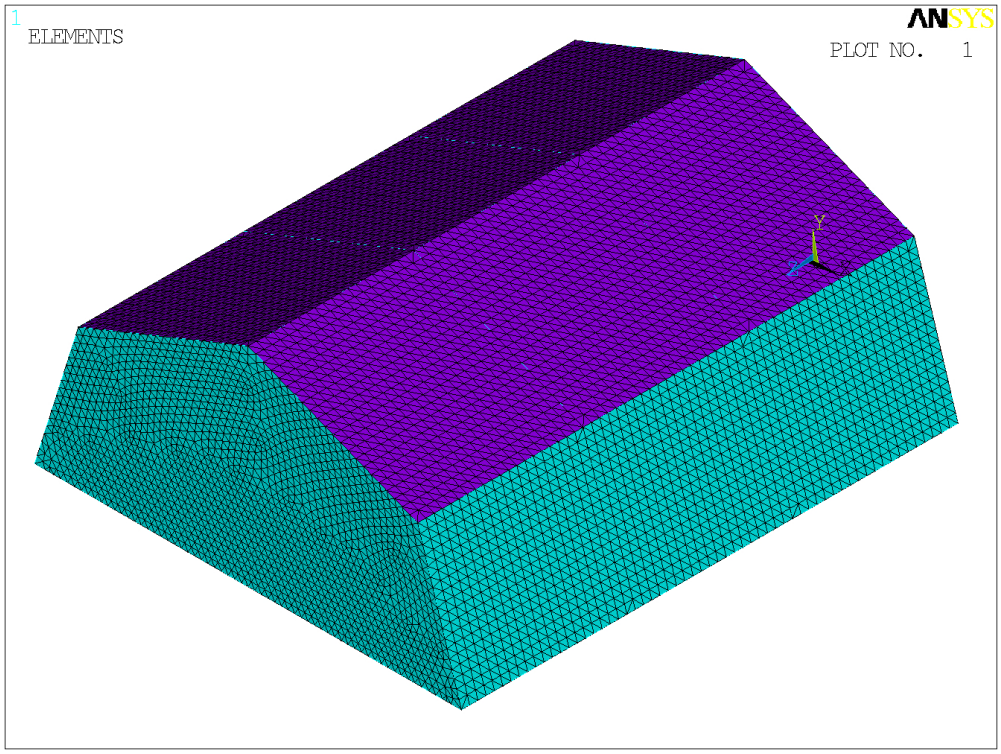

Figure 3.5: Finite element Model / Shell 63

using *Shell 181* and the frames with *Beam 4* elements.

The *Shell 181* Element

Shell 181 [23] is suitable for analyzing thin to moderately-thick *Shell* structures. It is a 4-node element with six degrees of freedom at each node: translations in the x, y, and z directions, and rotations about the x, y, and z-axes. (If the membrane option is used, the element has translational degrees of freedom only). The degenerate triangular option should only be used as filler elements in mesh generation. It allows for the membrane only option, neglecting bending stiffness. *Shell 181* is well-suited for nonlinear applications. Change in thickness is taken into account in the nonlinear analysis. In the element domain, both full and reduced integration schemes are supported. *Shell 181* accounts for follower (load stiffness) effects of distributed pressures. This features help in accelerating the convergence of the solution. *Shell 181* uses a penalty method to relate the independent rotational degrees of freedom about the normal (to the shell surface) with the in-plane components of displacements. The ANSYS program chooses an appropriate penalty stiffness by default. User input is allowed through the real constant input.

Figure 3.6 shows the finite element model for the shelter using *Shell 181* elements. The rectangular element formulation is used as the triangular form is not recommended for this element.

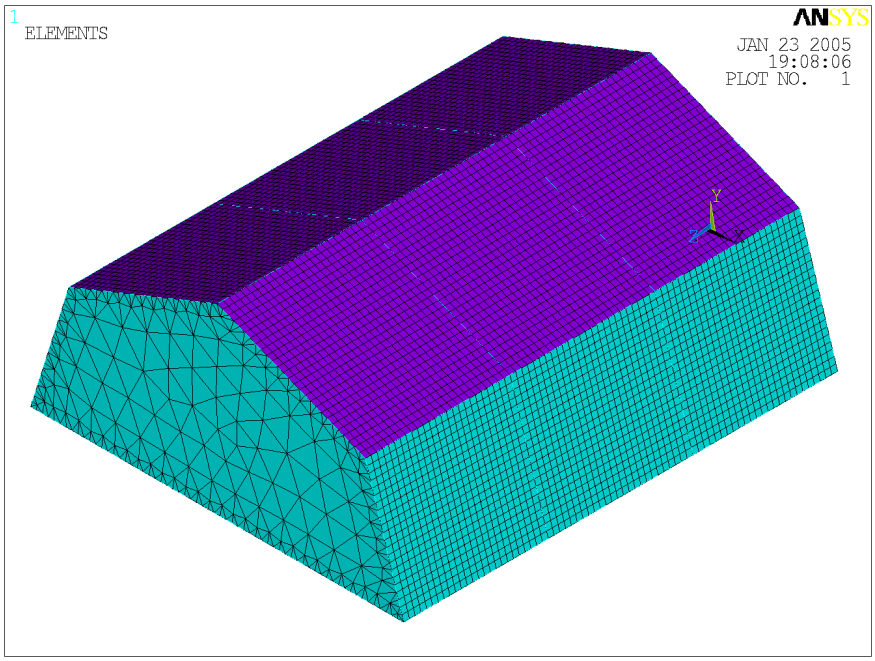

Figure 3.6: Finite element model / Shell 181

3.4.3 Model 3

Using the theory that stress couple is neglected over the whole region, the skin is modeled with *Shell 41* (membrane only) element and the frames are modeled with beam elements.

***Shell 41*- Membrane Element**

Shell 41 is a 3-D element [23] having membrane (in-plane) stiffness but no bending (out-of-plane) stiffness. It is intended for shell structures where bending of the elements is of secondary importance. The element has three degrees of freedom at each node: translations in the nodal x, y, and z directions. The element has variable thickness, stress stiffening and large deflection option. Out-of-planeness within the element or roundoff error in nodal locations may cause instability in the

displacement solution. So to counteract this, the element has the option of adding a slight normal stiffness with the elastic foundation stiffness (EFS) parameter.

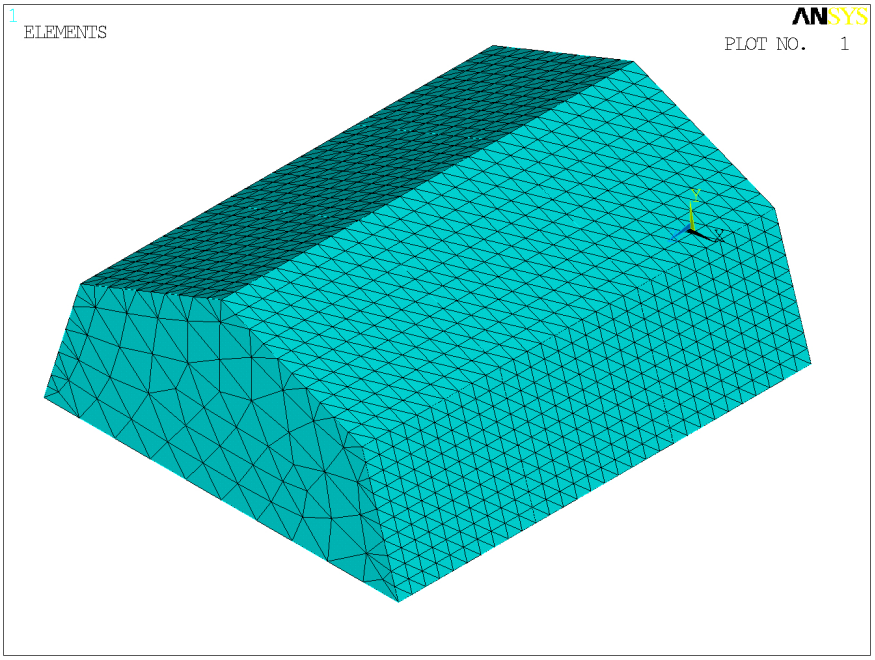

Figure 3.7: Finite Element Model / Shell 41

3.5 Shell - Asymptotic behavior

It is very unusual to think of a structure with thickness smaller by several order as compared to the other dimensions. It has been observed that it is difficult to comprehend shell behavior as thickness is reduced and therefore, it is essential to determine sensitivity of the structure to variation in thickness. This discussion is based on the investigation done by Lee and Bathe [25] on the asymptotic behavior [24] of shell structures. They found that the behavior of a shell converges to a specific limit state (zero displacement state) as the thickness approaches zero. This phenomenon

is called the asymptotic behavior of shells.

Shell kinematics consists of bending, membrane, and shearing actions as the basic loading mechanisms. These states correspond to the bending, membrane, and shear strain energy states. Since the thickness is very small, the shear energy state is negligible. Shell problems are therefore referred to as bending dominated, membrane dominated or mixed. Bending dominated state is referred to when the shell carries load in the bending action, while in membrane dominated form, the load is carried by the membrane action. The mixed action is referred to where the bending and membrane actions act in combination to describe the behavior of the shell. When large deformations are included, pure bending state is seldom encountered as membrane stressed are generated. Due to these large deformations, initially, shell carry load in both membrane and bending action, but with time, characteristic of problem changes purely to membrane dominated. An important aspect of the structural analysis of the membranes, regardless of the membrane thickness, is that the significant bending develops near the restraint. And the presence of these bending terms could result in the numerical problems if appropriate care is not taken in numerical simulation.

Chapter 4

NONLINEAR FINITE ELEMENT FORMULATION AND ANALYSIS

4.1 Introduction

A problem based on the assumption of smallness of some quantities in the formulation, is a linear problem. For a linearized model, small displacements and linear elastic material behavior are considered. Additionally, the equilibrium equations are derived using the undeformed configuration. Linear solutions involve less computation, are easily obtainable and, form a great tool in solving complex problems.

But in many practical applications, limitation of linear elasticity or linear behavior preclude obtaining an accurate solution. Nonlinear analysis is the only suitable approach in these types of

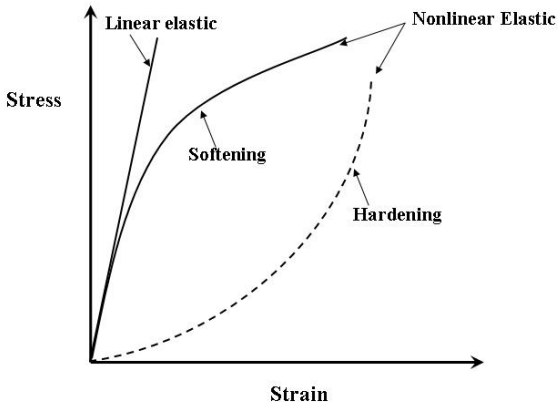

Figure 4.1: Material elastic stress-strain curve

problems. Nonlinear analysis finds wide application in the aerospace industry, e.g., in designing space structures and in automobile industry e.g in crash analysis, failure mechanisms, etc. It can be said that it is a path toward understanding the physical phenomenon realistically.

The most basic characteristic of structural nonlinearity is its changing structural stiffness. The nonlinear behavior can be categorized as material and geometric. Material nonlinearity comes from the nonlinear relationship between the kinetic and kinematic variables, e.g., stress-strain relations, heat flux-temperature gradient relation, etc. There are many factors which influence the material stress strain properties e.g load history (as as elastic plastic response), environmental conditions (temperature) and the amount of time a load is applied (creep). Figure 4.1 shows the material nonlinear elastic behavior, characterized by stress being a nonlinear function of strain with elastic deformation resulting in no energy loss when the load is removed.

If the structure experiences the large deformation, its changing geometric configuration corre-

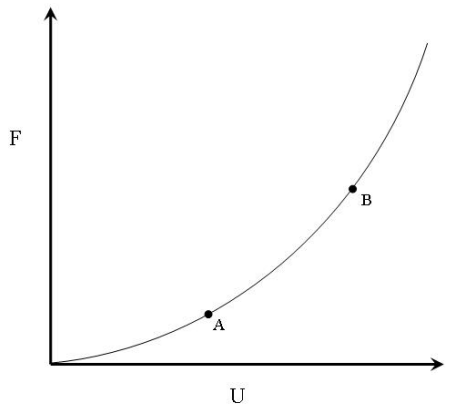

Figure 4.2: Force versus Displacement curve

sponds to the nonlinear behavior of the structure and is termed as geometric nonlinearity. In structural mechanics, the nonlinearity comes from large strain or large displacement and is added in the formulation through the strain-displacement relation. Figure 4.2 shows the nonlinear geometric behavior through the force-displacement plot.

4.2 Principle of Virtual Displacement

The static field variables consist of stress components (τ_{ij}), body forces acting per unit volume (B_j), and traction forces (T_j) acting externally on the surface of the body. The kinematically admissible field consists of displacements and strain in the domain V and the prescribed displacements in the domain S. The static field is said to be statically admissible if it satisfies

$$\partial\tau_{ij}/\partial x_i + B_j = 0 \quad in \;\; V \tag{4.1}$$

$$\tau_{ij}\ \nu_i = T^{(\nu)_j} \quad on\ \ S_1 \tag{4.2}$$

and the kinematically field is said to be kinematically admissible if it satisfies the following conditions:

$$\epsilon_{ij} = (\partial u_j/\partial x_i + \partial u_i/\partial x_j)\ \ on\ \ V \tag{4.3}$$

$$u_i = U_i\ \ on\ \ S_2 \tag{4.4}$$

These fields, static and kinematic, are related to each other through the principle of virtual work, independent of the constitutive behavior.

The principle of virtual displacement states that the static field in the deformable body is statically admissible only if the total external virtual work is equal to the total internal virtual work for every kinematically admissible field. The principle of virtual displacement is an equilibrium requirement and is independent of the material behavior.

$$\delta(W)_{ext} = \delta(W)_{int} \tag{4.5}$$

$$\delta(W)_{ext} = \int_V B_j \delta(U)_i dV + \int_S T_j \delta U_i^s dS \tag{4.6}$$

where the externally applied forces are the surface tractions, T_i, and body forces, B_i. $U_i(x_j)$ and $\delta(U)_i(x_j)$ are actual and virtual displacements where $\delta(U)_i(x_j)$ are kinematically admissible, i.e., continuous and satisfy the geometric boundary conditions.

$$\delta(W)_{int} = \int_V \tau_{ij}\ \delta\epsilon_{ij}\ dV \tag{4.7}$$

where $\delta\epsilon$ is the virtual strain corresponding to the imposed body and surface virtual displacements.

4.3 Nonlinear Continuum Mechanics

The principle of virtual displacements is used in deriving the governing equations for a body undergoing large deformation (large displacement and rotation), large strain, and nonlinear constitutive response [26]. The basic problem in general nonlinear analysis is to find the state of equilibrium of the body corresponding to the applied loads. Since, the configuration of the body is changing continuously, it is necessary to use the incremental formulation. The Lagrangian incremental formulation is used for obtaining the solution for the equilibrium position. The equilibrium of the body using the principle of virtual displacements is written as

$$\int_{V^2} \tau_{ij}^2 \, \delta e_{ij} \, d^2V = R^2 \tag{4.8}$$

and

$$R^2 = \int_{V^2} f_i^2 \, \delta u_i \, d^2V + \int_{S^2} T_i^2 \, \delta u_i^s \, d^2V \tag{4.9}$$

where τ_{ij}^2 and δe_{ij} are the components of Cauchy's stress and finite strain tensor, respectively. The $f_{B_i}^2$ and the $f_{s_i}^2$ are the externally applied body and surface force vectors with superscript 2 denoting the current load state.

Consider the three configurations of the body at three different loads where the first is the initial undeformed state S_0, the second is the deformed state S_1 where the response of the body is known, and the final state S_2 corresponds to the deformed state where displacement, strain and stresses are unknown. It is assumed that the deformation of the body $1-2$ is small since the increment in the load is small while the accumulated deformation from $0-1$ is large but continuous.

A rectangular cartesian system is used to formulate the governing equation of motion. The equi-

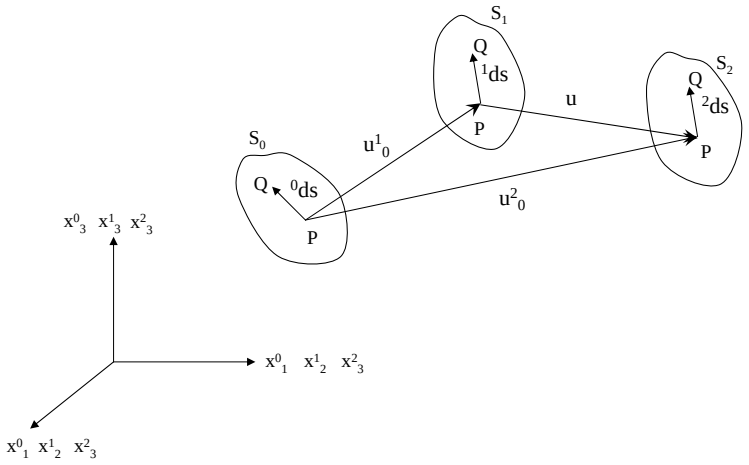

Figure 4.3: Initial and two consecutive configurations of a body

librium equations for the complete body system are obtained using an incremental Lagrangian formulation where static and kinematic variables for the deformed state S_1 are known and the solution for the equilibrium at state S_2 is sought. Figure 4.1 shows the initial and other two configurations of a body. the position and displacement co-ordinates corresponding to these configurations are as follows.

From Fig. 4.3, the coordinates of point P in the states S_0, S_1, S_2 are (x_1^0, x_2^0, x_3^0); (x_1^1, x_2^1, x_3^1) and (x_1^2, x_2^2, x_3^2) respectively. And the total displacement of point P in these states are

$$u_i^1 = x_i^1 - x_i^0 \tag{4.10}$$

$$u_i^2 = x_i^2 - x_i^1 \tag{4.11}$$

and the incremental displacement from state S_1 to S_2 is

$$u = u_0^2 - u_0^1 \tag{4.12}$$

4.3.1 Total Lagrangian Formulation

In the Total Lagrangian formulation, all the kinematically and statically admissible variables are referred to the reference configuration/initial configuration and take all the effects due to nonlinear (geometric and material) behavior into account. Using this formulation, equations 4.8 and 4.9 can be written as

$$R_0^2 = \int_{V^0} S_{0\,ij}^2 \; \delta\epsilon_{0ij}^2 \; d^0V \tag{4.13}$$

$$R_0^2 = \int_{V^0} f_{0\,i}^2 \; \delta u_i \; d^0V + \int_{S^0} T_{0\,i}^2 \; \delta u_i \; d^0S \tag{4.14}$$

where the following transformations are used.

$$\int_{V^2} \tau_{ij}^2 \; \delta e_{ij} \; d^2V = \int_{V^2} {S^2}_{ij} \; \delta(e_{0ij}^2) \; d^0V \tag{4.15}$$

$$\int_{V^2} f_i^2 \; \delta u_i \; d^2V = \int_{V^0} f_{0\,i}^2 \; \delta u_i \; d^0V \tag{4.16}$$

$$\int_{S^2} T_i^2 \; \delta u_i \; d^2S = \int_{S^0} T_{0\,i}^2 \; \delta u_i \; d^2S \tag{4.17}$$

Here, $f_{0\,i}^2$ and $T_{0\,i}^2$ are the body and surface forces in state S_2 measured in the initial undeformed state S_0. $S_{0\,ij}^2$ is the second Piola-Kirchhoff stress tensor and gives the transformed current force per undeformed area.

$$S_{0\,ij}^2 = J \; F^{-1}.\tau.F^{-T} \tag{4.18}$$

where F is the deformation gradient and J is its determinant, commonly known as the Jacobian. After obtaining the deformation gradient, with Cauchy stresses known, the second Piola stress tensor can be calculated using the kinematic transformations. Since the Cauchy stresses are symmetric, the second Piola stress tensor is also symmetric. The strain tensor used with the 2nd Piola-Kirchhoff stress tensor is the Green-Lagrangian strain as these form the energetically conjugate pair. The Green-Lagrange strain tensor is measured with reference to the initial configuration and is given as

$$\delta\epsilon^2_{0ij} = 1/2(u^2_{0i,j} + u^2_{0j,i} + u^2_{0k,j}u^2_{0k,j}) \tag{4.19}$$

where $u^2_{0i,j} = \frac{\partial^2 u_i}{\partial^0 x_j}$

Simplifying the virtual work equation by incrementally decomposing the stresses and strains, we get the following relationships.

$$S^2_{0ij} = S^1_{0ij} + S_{0ij} \tag{4.20}$$

$$\epsilon_{0ij} = e_{0ij} + \eta_{0ij} \tag{4.21}$$

$$e_{0ij} = 1/2(u_{0i,j} + u_{0j,i} + u^1_{0k,i}u_{0k,j} + u_{0k,i}u^1_{0k,j}) \tag{4.22}$$

$$\eta_{0ij} = 1/2u_{0k,i}u_{0k,j} \tag{4.23}$$

Where e_{0ij} and η_{0ij} are the linear and nonlinear parts of the strain tensor and S^2_{0ij}, S^1_{0ij} are second Piola stress tensor components in the corresponding states and S_{0ij} are the components of the Kirchhoff stress tensor. Using these relations, we get the following form.

$$\int_{V^0} S_{0ij}\delta\epsilon_{0ij}d^0V + \int_{V^0} S^1_{0ij}\delta\eta_{0ij}d^0V + \int_{V^0} S^1_{0ij}\delta e_{0ij}d^0V - \delta(R^2_0) = 0 \tag{4.24}$$

First term in this equation gives the change in the virtual strain energy due to the change in the virtual incremental displacement between S_1 and S_2. The second term shows the virtual work done by the forces due to the initial stresses while the other two terms are change in virtual work due to the externally applied body and traction forces, resulting in the change in geometry between the two states. In deriving the finite element model for the nonlinear analysis, it is necessary to specify the stress-strain relations in the incremental form. In the total Lagrangian form, this relation is written in terms of Green-Lagrangian strain tensor and Kirchhoff stress increment tensor.

$$S_{0ij} = C_{0ijkl}\delta e_{0ij} \tag{4.25}$$

$$\delta\epsilon_{0ij} = \delta e_{0ij} \tag{4.26}$$

Using the constitutive approximation, the above equation is linearized and takes the following form.

$$\int_{V^0} C_{0ijkl}\ e_{0kl}\delta e_{0ij} d^0V + \int_{V^0} S^1_{0ij}\delta\eta_{0ij} d^0V + \int_{V^0} S^1_{0ij}\delta e_{0ij} d^0V - \delta(R^2_0) = 0 \tag{4.27}$$

This equation represents the weak form.

4.3.2 Updated Lagrangian Formulation

In this formulation, all the static and kinematic variables are referred to the last load step or the previous known configuration. All the quantities in the formulation are updated at each load step. The same approach is followed for driving the weak form as used in the Total Lagrangian formulation.

$$\int_{V^1} S^2_{1ij}\ \delta\epsilon^2_{1ij}\ d^1V = R^2_1 \tag{4.28}$$

$$R_1^2 = \int_{V^1} f_{1\,i}^2\, \delta u_i\, d^1V + \int_{S^1} T_{1\,i}^2\, \delta u_i\, d^1S \tag{4.29}$$

Simplifying the virtual work equation by incrementally decomposing the stresses and strains, we get the following relationships:

$$S_{0\,ij}^2 = \tau_{ij}^1 + S_{0ij} \tag{4.30}$$

$$\epsilon_{1ij} = e_{1ij} + \eta_{1ij} \tag{4.31}$$

$$e_{1ij} = 1/2(u_{1i,j} + u_{1j,i}) \tag{4.32}$$

$$\eta_{0ij} = 1/2 u_{1k,i} u_{1k,j} \tag{4.33}$$

Using these equations, we get the following form:

$$\int_{V^1} S_{1ij} \delta\epsilon_{1ij}^2 d^1V + \int_{V^1} \tau_{ij}^1 \delta\eta_{1ij} d^1V + \int_{V^1} \tau_{ij}^1 \delta e_{1ij} d^1V - \delta(R_1^2) = 0 \tag{4.34}$$

Linearizing the above form with the constitutive relations $S_{1ij} = C_{1ijkl}\delta e_{1kl}$, $\delta\epsilon_{1ij} = \delta e_{1ij}$

we get the approximate equation as follows

$$\int_{V^1} C_{1ijkl}\; e_{1kl} \delta e_{1ij} d^1V + \int_{V^1} \tau^1{}_{ij} \delta\eta_{1ij} d^1V + \int_{V^1} S_{0\,ij}^1 \delta e_{1ij} d^1V - \delta(R_1^2) = 0 \tag{4.35}$$

4.4 Nonlinear Finite Element Form

Using the displacement approach, the continuum is divided into a number of surfaces or lines i.e. spatial discretization into finite elements. The elements are assumed to be interconnected at the discrete number of nodal points situated at the boundaries. For the nonlinear analysis, the Lagrangian approach used for the continuum is extended to the finite element form. Continuing

from the weak form obtained in Eq. 4.27 and Eq. 4.35, the total and updated Lagrangian finite element forms are obtained.

4.4.1 Total Lagrangian Form

The first term in the equation 4.27 can be written as

$$\int_{V^0} C_{0ijkl}\, e_{0kl}\, \delta e_{0ij}\, d^0V = \int_{V^0} \{\delta e_0\}^T [C_0]\ \{e_0\}\ d^0V \tag{4.36}$$

Here, e_0 presents the linear components of the Green-Lagrange strain. Using the incremental displacement components, the above equation becomes

$$= \int_{V^0} \{\delta \overline{u}\}^T \left([D] + [D_u]\right)^T [C_0] \left([D] + [D_u]\right) \{\overline{u}\}\ d^0V \tag{4.37}$$

where

$$\{e_0\} = \left(\begin{bmatrix} \frac{\partial}{\partial x} & 0 \\ 0 & \frac{\partial}{\partial y} \\ \frac{\partial}{\partial x} & \frac{\partial}{\partial y} \end{bmatrix} + \begin{bmatrix} \frac{\partial u}{\partial x}\frac{\partial}{\partial x} & \frac{\partial v}{\partial x}\frac{\partial}{\partial x} \\ \frac{\partial u}{\partial y}\frac{\partial}{\partial y} & \frac{\partial v}{\partial y}\frac{\partial}{\partial y} \\ \frac{\partial u}{\partial y}\frac{\partial}{\partial x} + \frac{\partial u}{\partial x}\frac{\partial}{\partial y} & \frac{\partial v}{\partial y}\frac{\partial}{\partial x} + \frac{\partial v}{\partial x}\frac{\partial}{\partial y} \end{bmatrix} \right) \begin{Bmatrix} \overline{u} \\ \overline{v} \end{Bmatrix}$$

$$= \{[D] + [D_u]\} \{\overline{u}\} \tag{4.38}$$

$$[C_0] = \begin{bmatrix} C_{11} & C_{12} & 0 \\ C_{21} & C_{22} & 0 \\ 0 & 0 & C_{66} \end{bmatrix}$$

The second expression in the equation 4.27 can be written as

$$\int_{V^1} S^1_{0ij}\ \delta(\eta_{ij})\ d^0V = \int_{V^1} \{\delta\eta_0\}^T\ \left\{S^1_0\right\}\ d^0V \tag{4.39}$$

where η_0 is the nonlinear Lagrange strain component and S^1_0 is the total stress component. The incremental displacement components transform Eq. 4.39 into the following form.

$$= \int_{V^0} \{\delta\overline{u}\}^T\ [\overline{D}]^T[C_0]\ [\overline{D}]\ \{\overline{u}\}\ d^0V \tag{4.40}$$

where

$$[S^1] = \begin{bmatrix} S^1_{xx} & S^1_{xy} & 0 & 0 \\ S^1_{xy} & S^1_{yy} & 0 & 0 \\ 0 & 0 & S^1_{xx} & S^1_{xy} \\ 0 & 0 & S^1_{xy} & S^1_{yy} \end{bmatrix}$$

$$[\overline{D}] = \begin{bmatrix} \frac{\partial}{\partial x} & 0 \\ \frac{\partial}{\partial y} & 0 \\ 0 & \frac{\partial}{\partial x} \\ 0 & \frac{\partial}{\partial y} \end{bmatrix}$$

The total and incremental displacement fields are approximated by a set of interpolation functions acting on the nodal displacements. These interpolation functions are usually simple functions of the position within the element and do not depend upon the deformed shape or time:

$$\{u\} = [\Psi]\,\{\Delta\} \tag{4.41}$$

$$\{\overline{u}\} = [\Psi]\left\{\overline{\Delta}\right\} \tag{4.42}$$

Substituting from Eq. 4.42 for the displacement field into Eq. 4.37 and 4.39, we get

$$\int_{V^0} \{\delta e_0\}^T [C_0]\ \{e_0\}\ d^0V = \int_{V_0} \delta\overline{\Delta}^T\ [B_L]^T\ [C_0]\ [B_L]\ \left\{\overline{\Delta}\right\}\ d^0V \tag{4.43}$$

$$\int_{V^0} \{\delta\eta_0\}^T\ \left\{S_0^1\right\}\ d^0V = \int_{V^0} \delta\overline{\Delta}^T\ [B_{NL}]^T\ [C_0]\ [B_{NL}]\ \left\{\overline{\Delta}\right\}\ d^0V \tag{4.44}$$

where B_L and B_{NL} are the strain-displacement transformation matrices.

$$\delta\left(R^1\right) = \int_{V_0} \delta\overline{\Delta}^T\ [B_L]^T\ \left\{S_0^1\right\}\ d^0V \tag{4.45}$$

$$\delta\left(R^2\right) = \int_{V_0} \delta\overline{\Delta}^T\ \{\Psi\}^T\ f^2\ d^0V + \int_{S_0} \delta\overline{\Delta}^T\ \{\Psi\}^T\ t^2\ d^0S \tag{4.46}$$

where

$$[B_L] = ([D] + [D_u])[\Psi]$$

$$[B_{NL}] = [\overline{D}][\Psi]$$

Using these equations along with the calculus of variations, the following finite element model for the nonlinear static analysis is obtained:

$$([K_L] + [K_{NL}])\left\{\overline{\Delta}\right\} = F^2 - F^1 \tag{4.47}$$

where K_L and K_{NL} are the linear and nonlinear (large-displacement) stiffness matrices. The stiffness matrix [K] = $[K_L]$ + $[K_{NL}]$ is symmetric since $[S^1]$ and $[C^0]$ are symmetric. The stiffness matrix is commonly known as the tangent stiffness matrix.

$$[K_L] = \int_{V^0} [B_L]^T\ [C_0]\ [B_L]\ d^0V \tag{4.48}$$

$$[K_{NL}] = \int_{V^0} [B_{NL}]^T \, [S_0^1] \, [B_{NL}] \, d^0V \tag{4.49}$$

$$F^1 = \int_{V^0} [B_L]^T \, [S_0^1] \, d^0V \tag{4.50}$$

$$F^2 = \int_{V^0} [\Psi]^T \, [f_0^2] \, d^0V + \int_{S^0} [\Psi]^T \, [t_0^2] \, d^1S \tag{4.51}$$

The equations of motion for the nonlinear dynamic analysis are of the same form as the equations for the nonlinear static analysis but include the effect of the inertia of the system. The dynamic equation in the finite element form can be written as

$$[M]_0^1 \left\{ \ddot{\Delta} \right\} + ([K_L] + [K_{NL}]) \left\{ \overline{\Delta} \right\} = F^2 - F^1 \tag{4.52}$$

The inertia effect renders the dynamic response more smooth than the static response and the convergence of the solution is more rapid. In general, the convergence is always obtained in the dynamic solutions provided that the time step is small enough. The numerical reasoning for this lies in the contribution of mass matrix and this contribution becomes dominant when the time step is small. Since the nonlinear dynamic response is highly path dependent, the analysis of nonlinear dynamic problems requires more iterations at each time step than the iterations required for each load step in the static analysis.

4.4.2 Updated Lagrangian Formulation

In the updated form, the previous known state becomes the reference state. The finite element model based on the updated Lagrangian formulation is presented below.

$$([K_L] + [K_{NL}]) \left\{\overline{\Delta}\right\} = F_1^2 - F_1^1 \tag{4.53}$$

where

$$[K_L] = \int_{V^0} [B_L]^T [C_1] [B_L] \, d^1V \tag{4.54}$$

$$[K_{NL}] = \int_{V^1} [B_{NL}]^T [\sigma^1] [B_{NL}] \, d^1V \tag{4.55}$$

$$F_1^1 = \int_{V^1} [B_L]^T [\sigma^1] \, d^1V \tag{4.56}$$

$$F_1^2 = \int_{V^1} [\Psi]^T [f_1^2] \, d^1V + \int_{S^1} [\Psi]^T [t_1^2] \, d^1S \tag{4.57}$$

The only theoretical difference between the two formulation is the choice of the refence condition. The choice of either formulation depends upon their relative numerical effectiveness which in turn depends upon the finite element and the constitutive laws.

4.5 Nonlinear Static Analysis

The static analysis is performed as a prerequisite for the dynamic analysis. As a step 1, a simplified model is analyzed under pressure loads. The analysis takes into account the large deformation behavior. For the nonlinear solution, the Newton-Raphson method with line search is used to obtain the converged solution. The stress stiffening effects are included while performing the analysis, which plays an important role in a thin structure's analysis. Stress stiffening (also called geometric stiffening) is the stiffening (or weakening) of a structure due to its stress state. This stiffening effect normally needs to be considered for thin structures with bending stiffness very

small compared to transverse stiffness resulting from inplane stresses, such as cables, thin beams, and shells, and couples the in-plane and transverse displacements. This effect also augments the regular nonlinear stiffness matrix produced by large strain or large deflection effects.

4.5.1 Case 1

Static analysis for a square plate under a simply supported conditions is performed. The t/a ratio is 0.00065 where t is the thickness of the plate and a is the width. The material model is elastic isotropic with E = 35 MPa and ν = 0.3. *Shell 63* (elastic shell element) and *Shell 41* have been used to simulate the static response. Nonlinear static analysis of a square plate under uniformly distributed pressure load of magnitude P_0 is performed. Figures 4.3 and 4.4 show the deformation profile for *Shell 63* for the pressure loads ranging between 5000 to 30000 Pa. Figure 4.5 shows the nonlinear response of very thin plate under pressure loading conditions. Figure 4.6 shows the deformation profile for *Shell 41* element for pressure loads 20000 Pa and 30000 Pa. It can be seen that as the pressure load is increased, deformation increases and structure carries load more and more in membrane action. The static analysis shows the membrane dominated characteristic of shell problem. Comparing elements, *Shell 63* and *Shell 41*, both the elements behave similarly. Figure 4.7 and 4.8 show the stress contours for *Shell 63* under increasing pressure loads. The stresses increase with the increasing pressure loads.

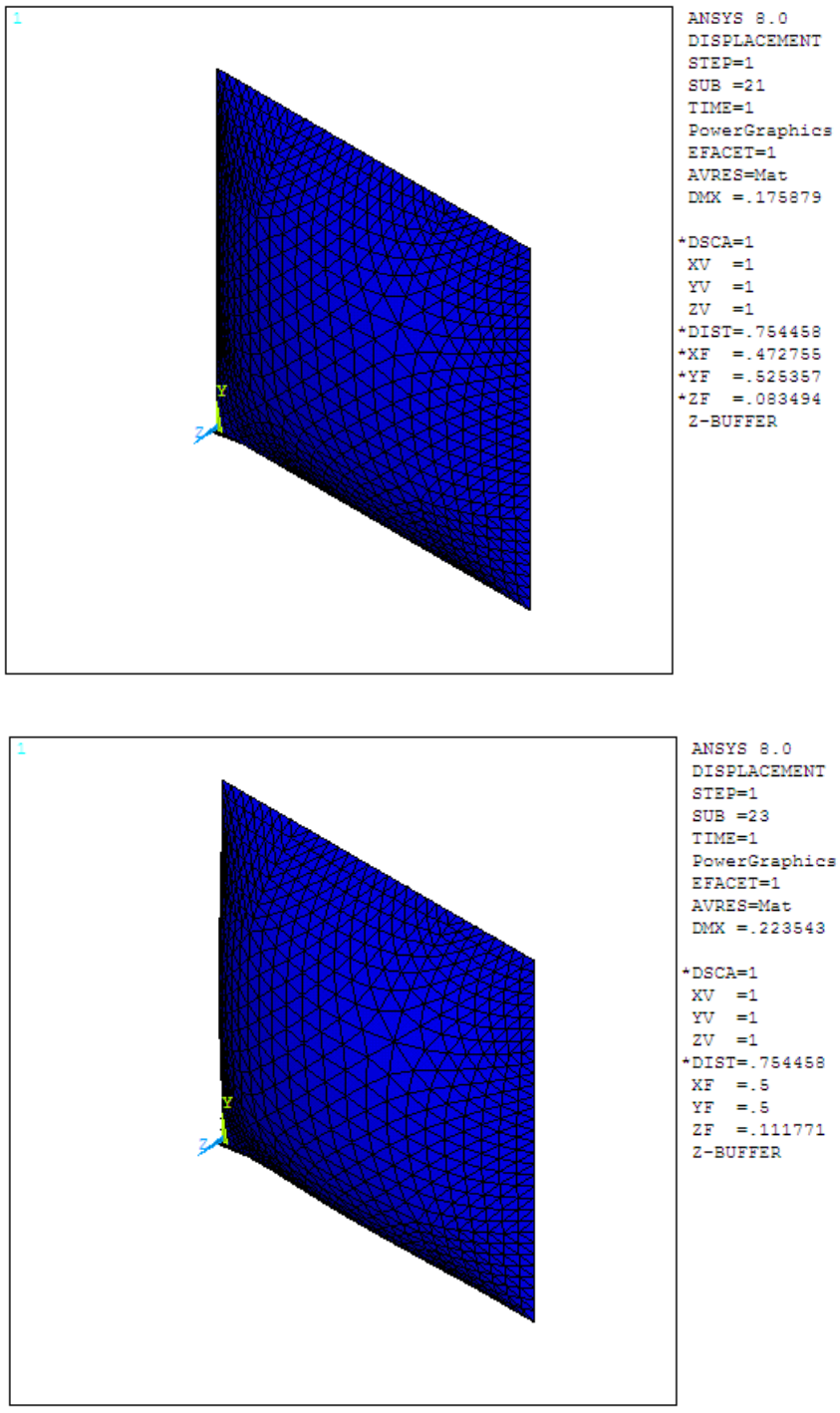

Figure 4.4: Displacement profile using Shell 63 under uniform pressure load

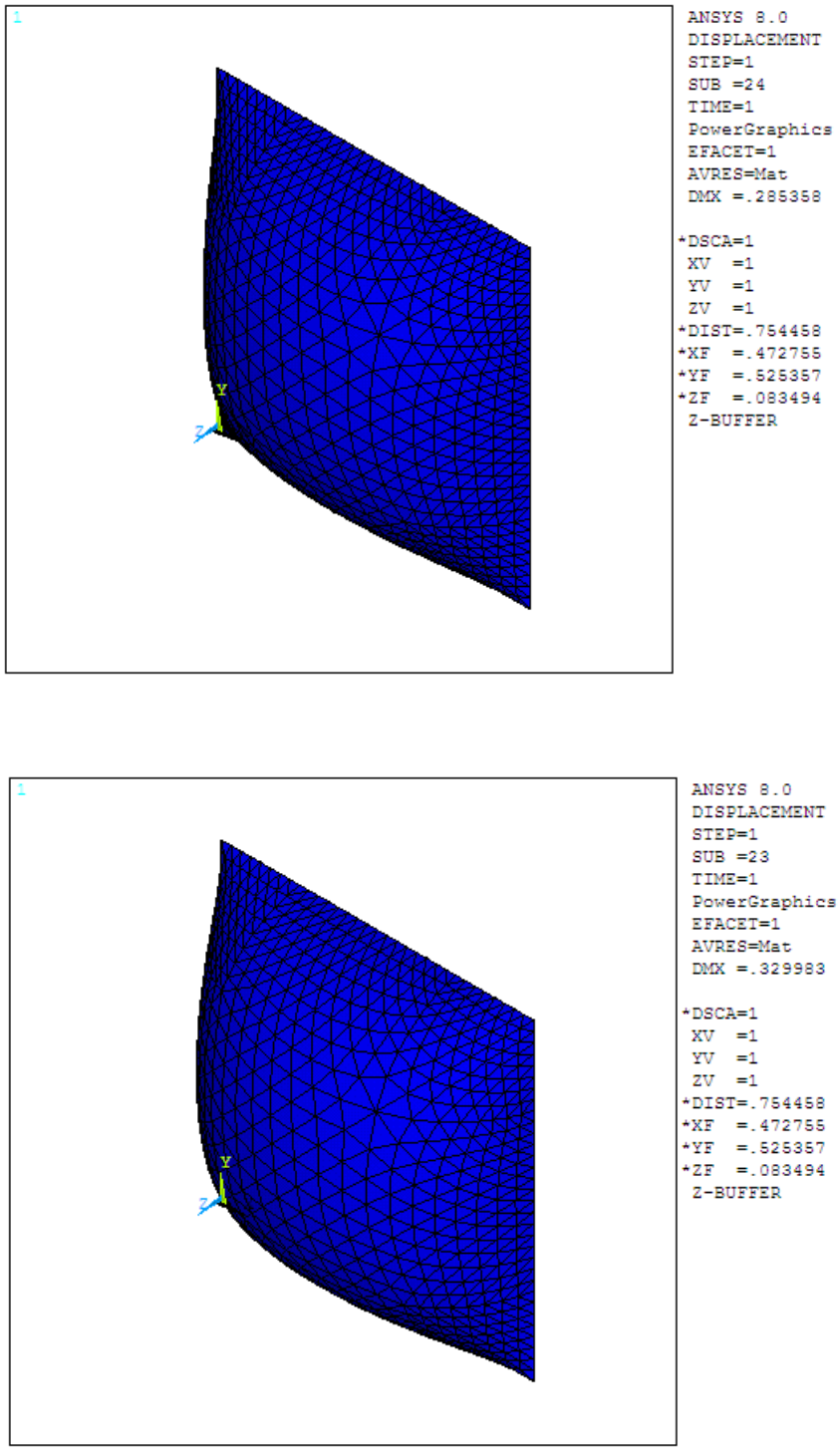

Figure 4.5: Displacement profile using Shell 63 under uniform pressure load

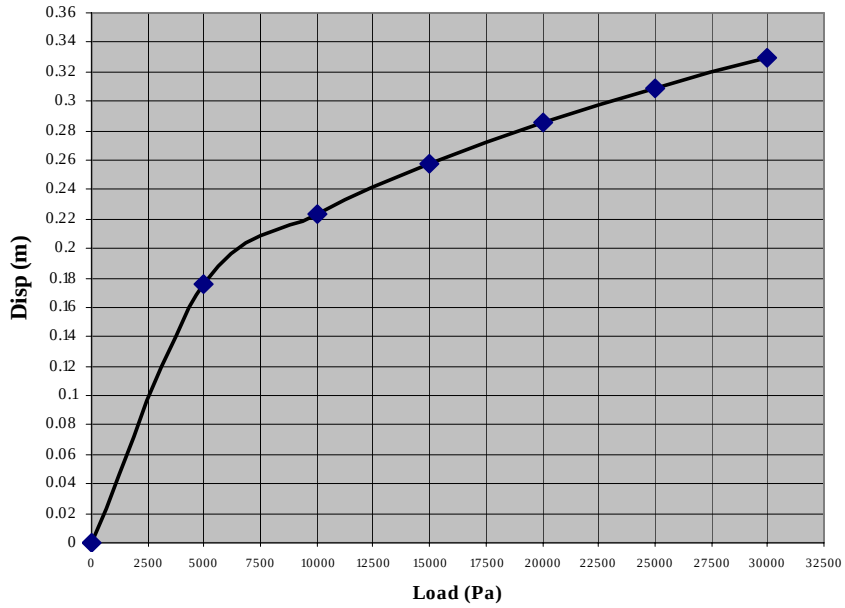

Figure 4.6: Nonlinear Response for plate structure showing transverse displacement under increasing pressure load

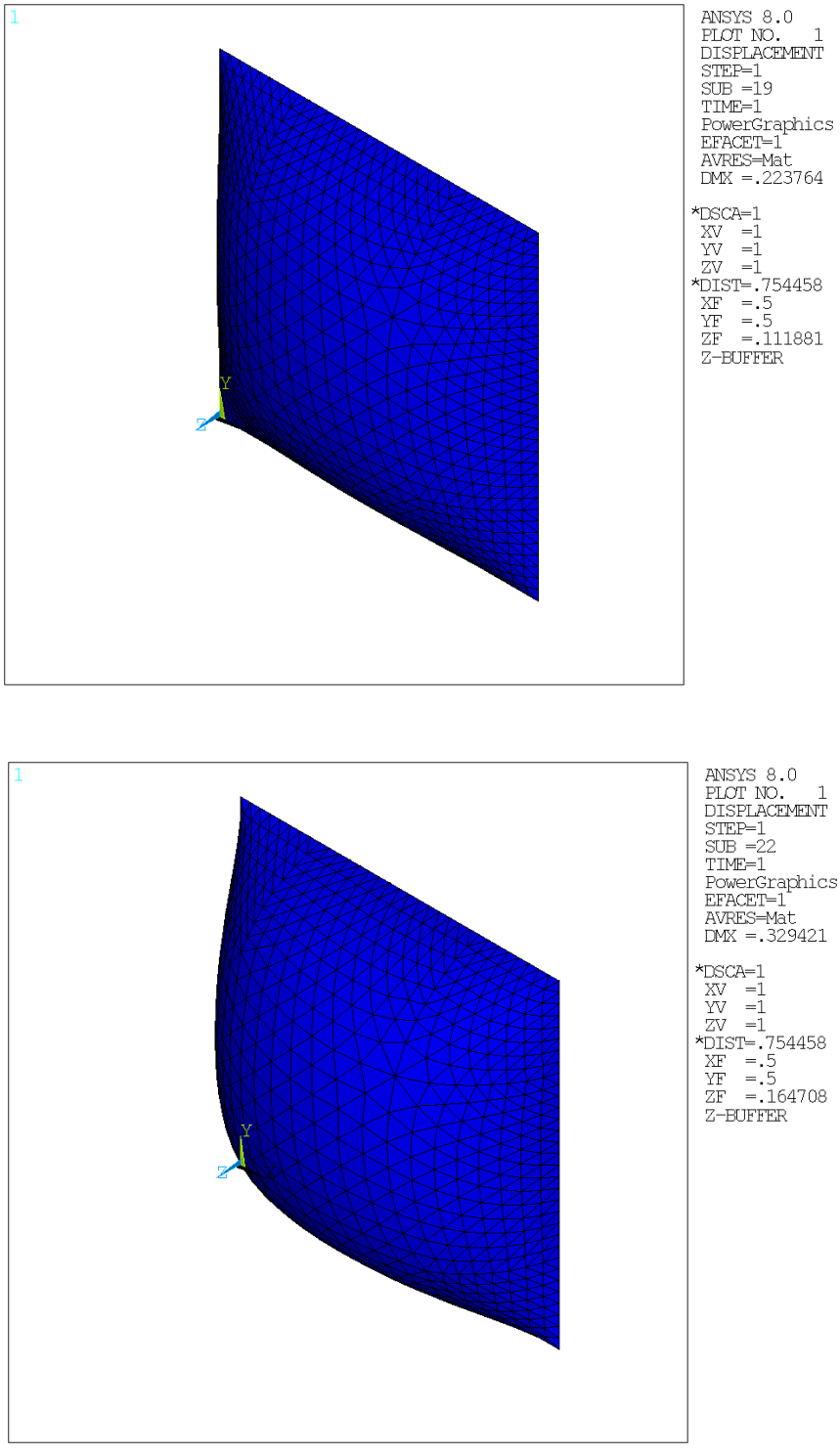

Figure 4.7: Displacement profile using Shell 41 under uniform pressure load

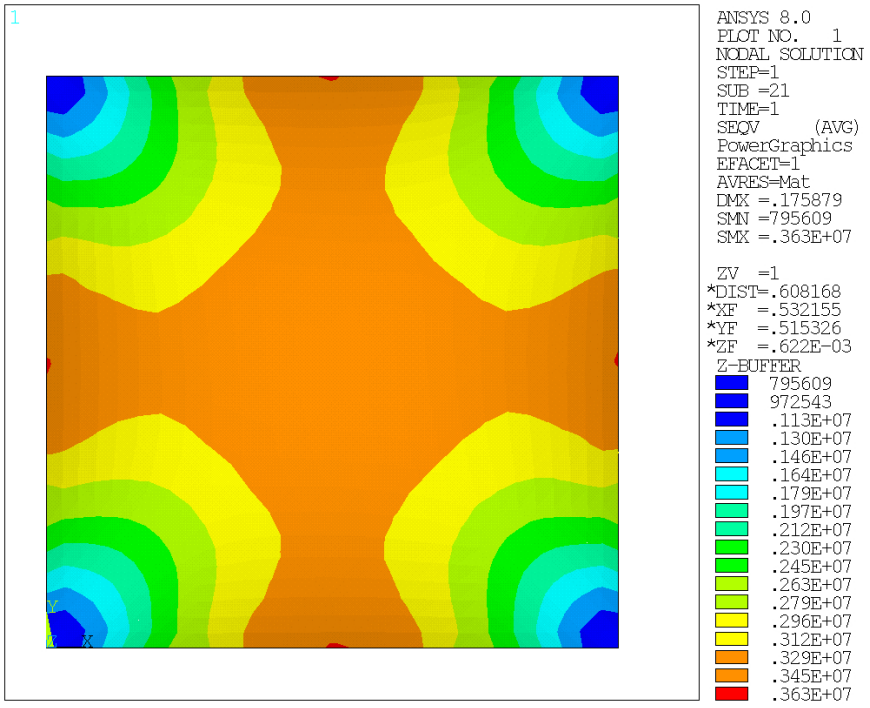

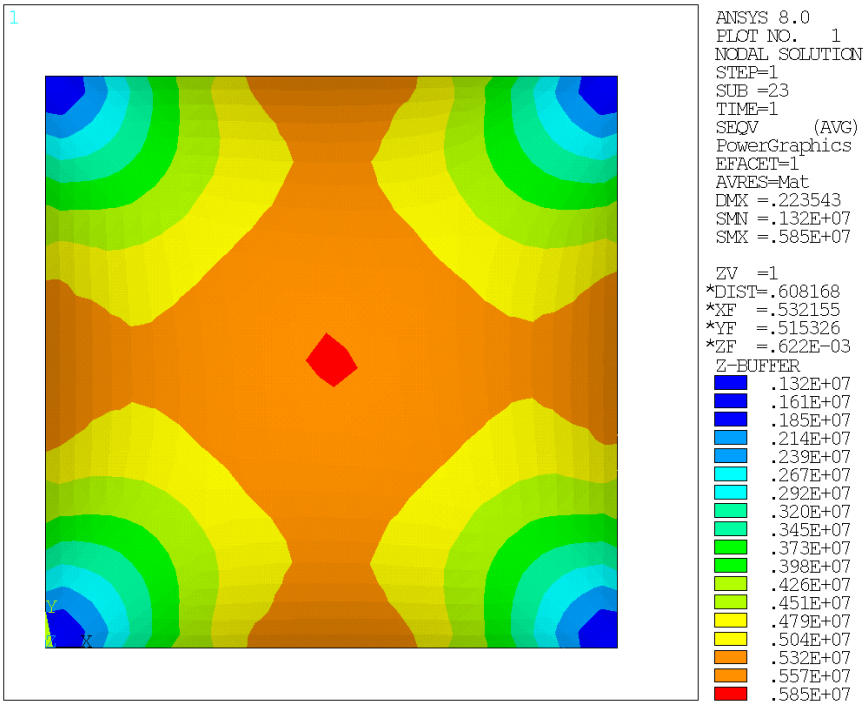

Figure 4.8: Stress Contours using Shell 63 under uniform pressure load

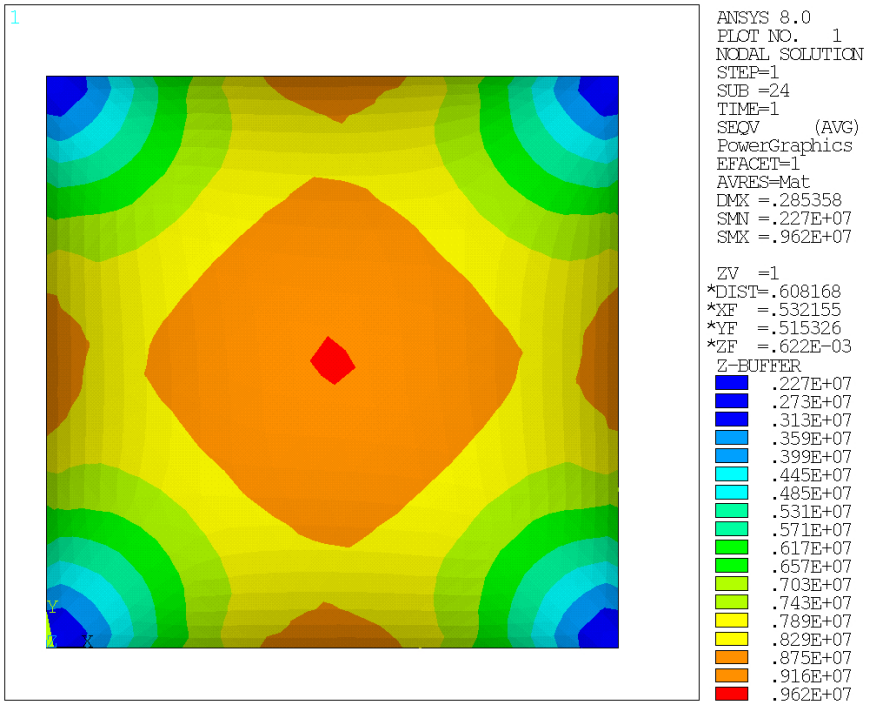

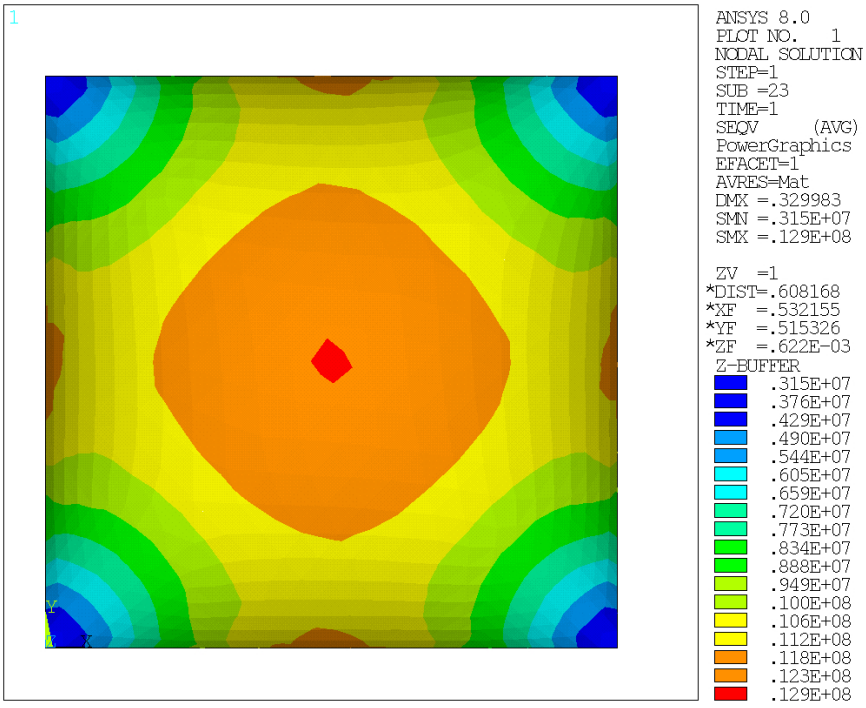

Figure 4.9: Stress Contours using Shell 63 under uniform pressure load

4.5.2 Case 2

Here, the static analysis for the liner material is performed. A simply supported square plate is considered. The t/a ratio is 0.00031 where t is the thickness of the plate and a is the width. The elastic isotropic material model with the properties, E = 250 Mpa and ν = 0.3 is used for the analysis. Nonlinear static analysis of the square plate under uniformly distributed pressure load of magnitude P_0 is performed. Figure 4.9 show the deformation profile at pressure load 20000 Pa. Comparing the deformation with that obtained in Case 1 for the given pressure load, deformation value is reduced due to transverse stiffening of the plate. Figure 4.10 shows the stress contour for the same pressure load. It can be observed that the stresses are increased significantly as compared to the Case 1.

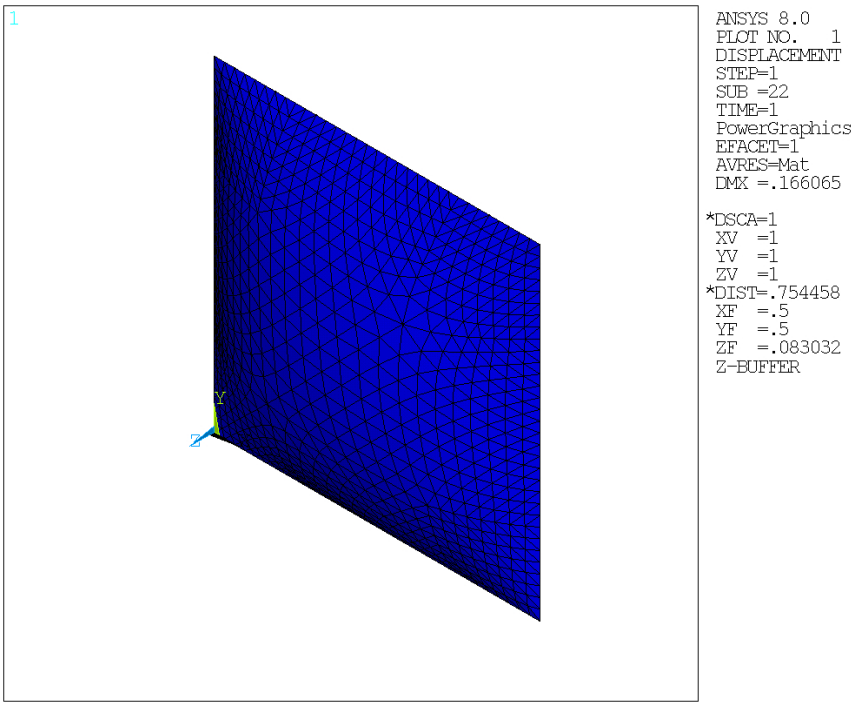

Figure 4.10: Displacement Profile using Shell 41 under uniform pressure load

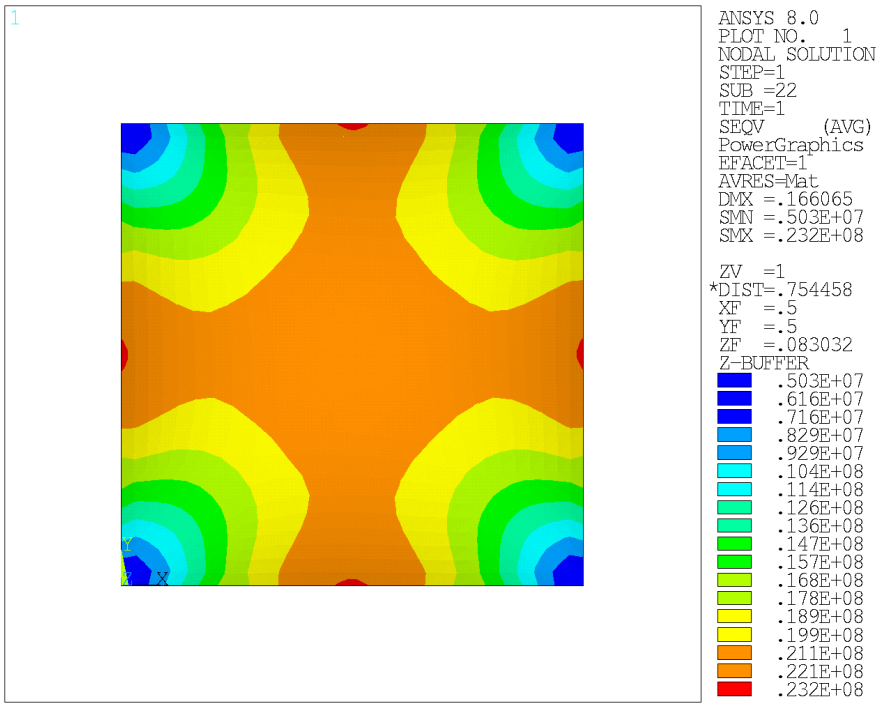

Figure 4.11: Stress Contours using Shell 41 under uniform pressure load

Chapter 5

NONLINEAR TRANSIENT ANALYSIS

5.1 Introduction

A ground vehicle, a jet flying through a thunderstorm and a tent subjected to the gusts have one thing in common, i.e., they all are subjected to dynamic loads. In dynamic problems, loading, structural response and the corresponding stresses/strains are function of time. A dynamic problem differs from the static problem on the account of the time-varying nature of the load, and due to the contribution of inertia.

The transient response of structures to dynamic loading is a subject which has generated a lot of interest from the design prospective in the recent past. In general, response of structures to dynamic loading is very difficult to predict due to their dependence on multiple factors like the duration of the loading, peak load, shape of the pulse, the impulse energy, boundary conditions

and material properties etc. And dynamic analysis of shell structures pose even much greater challenge. Obtaining solution analytically presents a very difficult preposition when nonlinearity is considered. Therefore, a numerical approach is sought which provide comparable accuracy and can be applied easily to complex problems.

This chapter provides a detailed understanding of the nonlinear dynamic analysis of flexible structures using a numerical approach. Section 2 presents the literature review on the structural response due to a blast, and transient analysis of various structural forms. Section 3 describes the numerical method used for the solution of the nonlinear dynamic equations. The Newmark-β method, the Newton-Raphson method, the line search method are explained. Section 4 presents the structural response of the flexible membrane structures, application being closed flexible shelters. The structural response comprising of displacement-time history and dynamic stresses have been obtained at a set of points.

5.2 Literature Review

The literature on the dynamic response of flexible structures to blast loads is limited. Through this literature review, an effort has been made to understand the transient response of various structures subjected to dynamic loads and thus, the literature on plates, folded plates, shells, membranes, composite structures and stiffened structures has been reviewed in this category. With the basic understanding developed through this review, the dynamic response of a closed flexible shelter has been modeled.

The response of elastic structure to blast constitutes a subject of great interest from the perspective of design of aerospace, naval, and automotive structures. The need for better understanding of structural damage due to the blast load has been of great interest in aerospace and defense related structures in recent times. Turkmen [27] studied the blast response of the isotropic plates theoretically and compared experimental and numerical results. He derived the equations of motion using the principle of virtual work in coordination with Love-Kirchoff's theory of thin elastic plates and obtained the solution of the dynamic equations using Runge-Kutta Verner method. Numerically, the transient response was obtained using ANSYS, a commercially available general purpose finite element program. The plate was modeled using shell elements and an implicit approach was used for the transient solution. Newmark's time integration method was used with the Newton-Raphson method for the nonlinear solution and the strain time history was obtained. It was observed that due to the presence of geometric nonlinearity, significant membrane strain occurs.

Aaron et al. [28] studied the elastoplastic dynamic response of rectangular plates due to blast loading. They developed the analytical model for the dynamic response of the plate using the Lagrangian formulation. Blast load calculations were done according to the methodology explained in Chapter 2 and the solution was obtained using a solution consisting of sine, cosine and exponential functions. A finite element solution was obtained using the implicit approach. Newmark's time integration method was used along with the Newton-Raphson method and the response was obtained for linear and models with geometric and material nonlinearities. Peak displacement value was observed for the nonlinear material model. The peak displacement value

for the nonlinear geometric model was found to be lowest among the other two due to the transverse stiffening of the plate. It was also observed that the peak displacement for the nonlinear geometric model was reached earlier in time than for the linear model.

Ambersoni et al. [29] investigated the response of explosively loaded clamped plate, experimentally and numerically. They measured overpressure generated due to the blast using pressure sensors and used this pressure time history as the dynamic loading over the shell finite element model for the plate. The modal superposition method (for linear analysis) and the direct integration method (for nonlinear analysis) were used and the acceleration time history was obtained. A good correlation was obtained between the experimental and numerical results in the forced vibration zone, while some discrepancy was observed in the free vibration zone due to the presence of higher frequencies. It was concluded that for dynamic analysis, the number of modes affect the accuracy of the response. Therefore, an adequate mesh size is needed in order to accurately capture the response at higher frequencies.

The analysis of shell structures is a very challenging task, both in terms of predicting as well as simulating the response. The prediction of behavior becomes more difficult due to the fact that shell characteristics change significantly as the thickness of the shell structures and boundary and loading condition change. Even simulating the behavior of shells is difficult as the dynamics of the shell involves a large deformation under transverse loading conditions, involving more computation effort. Koh et al. [30] studied the response of shell structures to blast loads through the applications like blast-resistant doors. The door consisted of two 9-mm mild-steel plates stiffened by four edge plates. The skin was modeled with shell element and the edge stiffeners were modeled

with beam element. The updated Lagrangian method was used for the large deformation analysis and the time integration for the dynamic solution was done using the central difference method. This approach is not only computationally less expensive as it does not require the stiffness matrix formulation and simultaneous equation solver but also does not encounter any convergence problems. The only limitation the method exhibits is that it is conditionally stable, thus require very small time steps to prevent numerical instability. The maximum displacement occurred over the skin away from the stiffeners. The response was compared with the implicit approach and the explicit code was found to be more efficient than the implicit one.

Louca and Pan [31] studied the dynamic response of stiffened and unstiffened plates under blast loads. They used the energy method based on the Lagrange formulation for the solution of the dynamically loaded plate where the equations of motion were solved using Runge-Kutta method using single mode and three moded shape functions. Under large deformation, the plate was assumed to behave as a shallow shell and had some initial imperfection where the imperfection had the same shape as the deformed plate. An initial out of plane, time independent imperfection is assumed in the analysis. Computationally, explicit codes DYNA-3D and ABAQUS Explicit codes were used for simulating the response of the plate modeled using the shell element. The deformed shape obtained over the response time showed a change in mode from an outward bulge containing three distinct peaks to that containing three half waves resulting in the stiffening of the plate. These stiffening effects are the consequence of membrane strains due to the increased nonlinear response. The effect of peak pressure on peak displacement was studied for various slenderness ratio (b/t) for the perfect plate. Peak displacement for a given pressure peak increased

for the more slender panels. The increase in the peak displacement was observed for imperfect plate as compared to the perfect plate and found to be increasing with the increase in the size of the imperfection. The positive (out of plane) imperfection had the stiffening effect on the plate while the negative imperfection resulted in the snap through behavior.

Lightweight barriers form an effective part of the protection system developed as guard against explosions. High ratios of allowable strain to stress, allowable stress to density and smaller spans are the most desired characteristics sought when considering a light barrier. Scherbatiuk [32] studied the effects of such barriers on the transmission of blast waves. He developed a model for the barrier consisting of lumped masses joined by springs housed in cylindrical tubes and rotational springs resisting bending, simulating membrane behavior. The barrier was modeled with the membrane and bending effects combined, membrane only, bending only, and moving rigid wall formulation to see their effects on the transmission of blast. The pressure, opposing the structural movemement, is applied on the opposite side of the membrane along with the blast load on the other side. The membrane and the moving rigid wall mid-span displacement response remained the same till the membrane reached the peak value and then abruptly changed the direction. The bending only and the membrane and bending combined showed the similar pattern. The transmitted pressure/impulse time response were plotted and similar trends were observed. A parametric study was done for different values of Young's modulus (E), density (ρ), initial thickness (H_0), and span (L) and transmitted peak overpressure, peak positive impulse and maximum strain and stress were plotted on the pressure-impulse plane for the membrane model. It was observed that the increased stiffness reduced the impulse transmitted and the maximum strain , but very high

stresses. Therefore, the use of a low modulus material was recommended.

The concept of lightweight portable barriers has been studied in recent times with the possible application of protecting equipments, structures and personnel from explosions. Crawford and Morrill [33] studied such barrier designs consisting of screen supported over the frames with cable anchorage to support the barrier. The main objective of designing such barriers is to reduce the transmitted blast pressure wave. The paper also discussed the response for such barriers against the blast loads.

Experimental testing faces a greater challenge in the dynamic characterization of structural systems with nonlinearities. Because of significant mass and stiffness, wiring, gauges, and limited measurement scale, it is very difficult to predict the response of flexible structures. Zhu [34] studied an optical technique for obtaining the dynamic response experimentally and compared the results with the numerical solution. He used the variational finite difference approach for the elastoplastic response of a clamped rectangular plate under impact condition and pressure loading, including the transverse deformation and material strain hardening effects. Experimental tests predicted that the plate initially took the shape of a flat plateau and with time, the plateau contracted toward the center and formed a pyramid-like permanently-deformed shape. Numerical analysis showed that the pyramid like permanent deformed shape was formed. Numerical and experimental results were found in good agreement with respect to the transient mode profile and permanent deflection.

Vendhan et al. [35] studied the transient response of rectangular plates due to underwater explosions. These structures find application in ship hulls. The paper discussed the underwater shock explosion considering the fluid-structure interaction phenomena by including the

water density effects. Elastoplastic analysis with and without strain effects was performed over the nonlinear shell finite element plate model and failure modes were predicted. Transient response of the plate was obtained over the linear and nonlinear ranges for the geometric and material models for the given shock factors. The material nonlinearity softened the structure and hardening was observed in the geometric nonlinear model due to membrane strains. The inclusion of the strain rate saw a reduction in the permanent displacement and a good correlation was observed with the experimental results, validating the requirement of inclusion of strain effect in the elastoplastic models.

The evaluation of technology of structural materials has been governed by the search for the material with minimum weight to strength ratio, lower cost, and ease of fabrication. The fiber reinforced composites fill this gap as they are light and flexible with the comparable or greater strength. Turkmen [36] studied the behavior of composite laminated structures to blast loads. Cylindrical laminated composite shells find application like aircraft structures, rockets, sports equipments etc. A theoretical solution was obtained based on the mathematical model derived using the classical shell theory and dynamically solved using the Runge-Kutta-Verner method. The solutions were obtained using 1,4,9 series solution. Finite element solution was obtained using a shell-based model. The strain time history and the response frequency were obtained. It was observed that larger moduli result in smaller peak values but higher frequency response.

Sinha et al. [37] studied vibration of laminated folded plate structures. These structures, due to their high strength, low weight, and high stiffness, are widely used for various engineering applications. The Mindlin assumptions that the mid plane deflections are small compared to the

thickness and that the normal to the mid plane before deformation remains straight after deformation but not necessarily normal, was used in formulating the finite element model for the folded composite plate structure. The vibration analysis was performed for different crank angles (angle that the ridge line make), fiber angles, number of plies and number of folds. It was observed that the fundamental frequency decreased with the increase in the fiber angle and showed the reverse trend with the increase in the number of layers. The ridge line in the folded structure imparts additional stiffness as compared to the flat plate and has higher fundamental frequency vibrations.

Chen et al. [38] developed the finite strip method for the nonlinear transient analysis of composite laminated plate. In finite strip method, the plate is divided into finite number of strips with degrees of freedom located along the lines of the strip using cubic crosswise interpolation form. The Newmark method was used for the dynamic solution and extended to the nonlinear range with the Newton-Raphson method. The transient analysis for isotropic, orthotropic and laminated plate model was performed against the blast loads and the center plate deflections and stress time histories were plotted.

The drawback composite structures have is that they have low shear modulus and thus are prone to high transverse deformation. Hsi-Yung and Chang [39] studied the impact response of the laminated plate due to aluminum sphere and evaluated the stress-strain distribution through the thickness. They used the 8-noded brick element for modeling of the plate and added the incompatible modes to it to improve the in-plane deformations and to minimize the computer time. The contact forces due to impact were based on loading and unloading processes and were calculated using the Newton-Raphson method. The Newmark method was used for the transient

analysis. The transient response of the plate was obtained for three different impactor velocities and for clamped and simply-supported boundary conditions. It was observed that the simply supported plate was more flexible in resisting the impact. All the components of stress and strain were measured as the function of time and showed significant variation with time and the initial velocity of the impactor. The stress and strain variation through the thickness can help in predicting for the failure mode of the laminated plate, thus impact damage can be predicted.

Impact is accompanied by propagation of stress wave that travel outward from the point of impact and this energy may result in structural vibration. Abrate [40] studied the impact response of composite structures. The contact mechanics was based on the laws of loading and unloading processes. Numerical study of impact response of graphite-epoxy laminate plate against the steel sphere was conducted. It was observed that the motion of the plate was accompanied by oscillations.

Geers and Sobel [41] presented the dynamics shell response analysis and studied the practical aspect of solutions by numerical methods. Linear response of the shell structure was studied and transient response of the cylindrical shell was obtained. It was observed that the severe dispersions characterizes the propagation of the flexture wave and response was dominated by oscillations. It was also observed that the convergence difficulties associated with the flexture shell response are more severe than with membrane response.

5.3 Nonlinear Dynamic Solution

The most general approach to determining the structural response is direct integration of the dynamic equilibrium equations. The term direct here implies that prior to the numerical integration, transformation of equations into a different form (modal coordinates) does not take place. Direct integration methods are based on two fundamental principles. Firstly, the equilibrium including the inertia and the damping forces is sought at discrete time steps with in the interval of the solution and secondly, variation of displacement, velocity, and the acceleration are assumed within each time interval, Δt.

In general, direct integration approaches are catagorised into explicit and implicit methods. The explicit methods are used for the problems like involving, high speed dynamic events which require many small increments to obtain high-resolution solution like simulation of short duration blast loads on steel plate, complex contact problems like analysing response of surfaces subjected to impact, complex postbuckling analysis and highly nonlinear quasi-static analysis etc. Explicit algorithm, commonly, uses the central difference method to integrate the equations of motion explicitly through time, using kinematic conditions at each increment to calculate the conditions at the next iteration. Explicit methods do not require formulation of global tangent stiffness matrix, thus avoid iteration and convergence problems. Therefore, these methods are more useful for the problems with high degree of nonlinearity and events where the duration of time of loading is very short. But explicit methods show limitation in the sense that they are conditionally stable i.e. solution holds only if the Δt/T is smaller than some critical value, called the stability limit.

Violation of the above condition could lead to numerical instability which may result in a solution which can grow exponentially with time.

Implicit methods are unconditionally stable i.e. upper bound on the time step size does not exist, relative to the accuracy considerations. The implicit method uses the Newmark method. The method require the formulation of stiffness matrix at each iteration and seek convergence of solution of equation with respect to some tolerance value. The implicit approach gives acceptable solution with the higher order of time step than the explicit method but the response deteriorates as the step size is increased relative to time period. The computational cost is very high as large number of iterations are required. Explicit method can provide a cost effective solution with careful choice of time step size. Thus, the choice of integration approach should be made in such a way so as to ensure the efficiency and robustness of the numerical simulation. Here, transient response is obtained using an implicit approach.

5.3.1 Newmark Method

In 1959, Newmark introduced an implicit method of computation for the solution of problems in structural dynamics. The algorithm assumed that the average acceleration is constant over an integration time step. Since then, this method has been used in many structural dynamics problems. The linear dynamic equilibrium equation is written as

$$M\ddot{U}_t + C\dot{U}_t + KU_t = F_t \tag{5.1}$$

where M, C, K and F_t have the usual meaning.

Using Taylor series expansion, we can write the displacement and velocity at time t as

$$U_t = U_{t-\Delta t} + \dot{U}_{t-\Delta t}\Delta t + 1/2\ddot{U}_{t-\Delta t}\Delta t^2 + 1/6\dddot{U}_{t-\Delta t}\Delta t^3 + ... \tag{5.2}$$

$$\dot{U}_t = \dot{U}_{t-\Delta t} + \ddot{U}_{t-\Delta t}\Delta t + 1/2\dddot{U}_{t-\Delta t}\Delta t^2 + ... \tag{5.3}$$

Newmark truncated these equations and expressed them into the following form

$$U_t = U_{t-\Delta t} + \dot{U}_{t-\Delta t}\Delta t + 1/2\Delta t^2\ddot{U}_{t-\Delta t} + \alpha\Delta t^3\dddot{U}_{t-\Delta t} \tag{5.4}$$

$$\dot{U}_t = \dot{U}_{t-\Delta t} + \ddot{U}_{t-\Delta t}\Delta t + \delta\Delta t^2\dddot{U}_{t-\Delta t} \tag{5.5}$$

Assuming linear acceleration within the time step,

$$\dddot{U} = (\ddot{U}_t - \ddot{U}_{t-\Delta t})/\Delta t \tag{5.6}$$

Substituting $\dddot{U}$ in Eq. 5.4 and 5.5, we get Newmark equations in the standard form.

$$U_t = U_{t-\Delta t} + \dot{U}_{t-\Delta t}\Delta t + [(1/2-\alpha)\ddot{U}_{t-\Delta t} + \alpha\ddot{U}_t]\Delta t^2 \tag{5.7}$$

$$\dot{U}_t = \dot{U}_{t-\Delta t} + [(1-\delta)\ddot{U}_{t-\Delta t} + \delta\ddot{U}_t]\Delta t \tag{5.8}$$

where α and δ are the integration parameters. Solving from Eq. 5.7 for $\ddot{U}_t$ in terms of U_t and substituting in the equation 5.8, we get $\dot{U}_t$,and $\ddot{U}_t$ in terms of U_t. Using the relations for $\dot{U}_t$ and $\ddot{U}_t$ in Eq. 5.1, the solution (U_t) at time t is obtained and thus the velocity and acceleration are obtained at time t.

The aim of any numerical integration scheme is to obtain a solution close to the actual response of the dynamic system. The selection of an appropriate time step is vital as the cost and reliability of the method depends on the length of the time step. The time step should be

small enough to obtain the desired accuracy and should not be unneccesarily small as that would lead to a more costly solution. The analysis of stability and accuracy characteristics of integration methods provide an important guideline for the appropriate time step selection.

Newmark's integration scheme, for integration parameters α = 1/4 and δ = 1/2, is unconditionally stable. If the solution for any initial condition does not grow out of bounds at any time step Δt, numerical scheme is termed as unconditionally stable. This method is known as constant average acceleration method (more commonly as trapezoidal rule). In general, α and δ are governed by the following relations.

$$\alpha = 1/4(1+\gamma)^2 \tag{5.9}$$

$$\delta = 1/2 + \gamma \tag{5.10}$$

γ is the amplitude decay factor. For γ = 0, the method becomes the constant average acceleration method. Figure 5.1 shows the constant average acceleration method.

The algorithm for the solution of the dynamic equations, using Newmark integration scheme, requires the formulation of mass, damping and stiffness matrices for the given system with the starting time t=0. The displacement, velocity and acceleration are initialized as U_0, $\dot{U}_0$, $\ddot{U}_0$. The time step length and time integration parameters are selected depending on the stability and accuracy criteria and the integration constants are calculated. The effective stiffness matrix is calculated and then triangularized. For each time step, effective load and the displacement (solution) are calculated. Once the solution is obtained, acceleration and velocity are updated. Step by step solution for the above procedure is presented in the following.

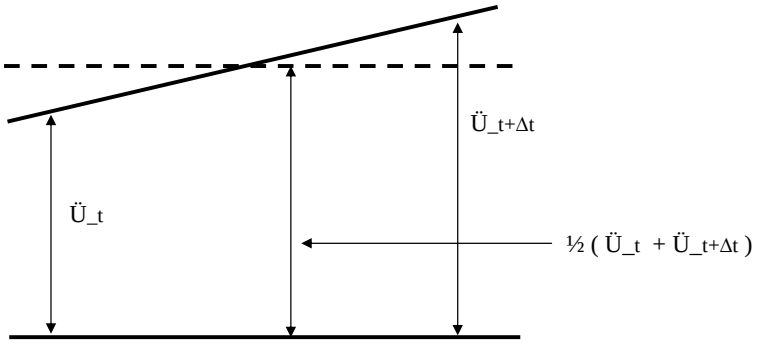

Figure 5.1: Newmark's Constant Average Acceleration Method

Integration constants are

$$a_0 = \Delta t^2/\alpha \; ; \quad a_1 = \delta/\alpha \; \Delta t; \quad a_3 = \Delta t/\alpha$$

$$a_4 = \delta/\alpha - 1; \quad a_5 = \Delta t/2(\delta/\alpha - 2); \quad a_6 = \Delta t(1 - \alpha); \quad a_7 = \Delta t \; \alpha$$

Calculating effective stiffness matrix and triangularizing,

$$\hat{K} = K + a_0 M + a_1 C \tag{5.11}$$

$$\hat{K} = LDL^T \quad (Triangularized \;\; form) \tag{5.12}$$

At each time step, the effective load is

$$\hat{R}_t = R_t + M(a_0 U_{t-\Delta t} + a_2 \dot{U}_{t-\Delta t} + a_3 \ddot{U}_{t-\Delta t}) + C(a_1 U_{t-\Delta t} + a_4 \dot{U}_{t-\Delta t} + a_5 \ddot{U}_{t-\Delta t}) \tag{5.13}$$

The displacement, acceleration, and velocity at time t are

$$LDL^T U_t = \hat{R}_t \tag{5.14}$$

$$\ddot{U}_t = a_0(U_t - U_{t-\Delta t}) - a_2\dot{U}_t - a_3\ddot{U}_t \tag{5.15}$$

$$\dot{U}_t = \dot{U}_{t-\Delta t} + a_6 U_{t-\Delta t} + a_7 U_t \tag{5.16}$$

The procedure is repeated for the next time step. This implicit time integration method can be applied to nonlinear problems. The extension to nonlinear analysis require that iterations be performed at each time step and the stiffness matrix be formulated and triangularized at each iteration or at some selective points in time. Most commonly, the nonlinear solution is obtained using the Newton-Raphson method.

5.3.2 Newton-Raphson Method

The Newton-Raphson method is one of the most rapidly convergent processes for the solution of the nonlinear equations. The Newton-Raphson formula consists geometrically of extending the tangent line at a current point until it crosses zero, then setting the next guess to the abscissa of that zero-crossing.

Consider the nonlinear equation

$$R(U) = 0 \tag{5.17}$$

where $R(U) = F - K(U)$, is the residual vector, also known as the out of balance force vector since it gives a measure of the lack of equilibrium in the structure. When the norm

of the residual vector is small, the equilibrium is attained approximately. Assuming $R(u)$ satisfied equilibrium at the rth iteration, the method seeks the solution at the $(r+1)^{st}$ iteration. Expanding Eq. 5.17, using Taylor series expansion, we get

$$R(U) = R(U^r) + (\partial R/\partial U)_r \delta U + 1/2(\partial^2 R/\partial U^2)_r \delta U^2 + higher\ \ order\ \ terms = 0 \quad (5.18)$$

where $(\partial R/\partial U)_r$ and $(\partial^2 R/\partial U^2)_r$ are the Jacobian and Hessian matrices respectively. In structural mechanics, the Jacobian is called the tangent stiffness matrix (K_T). The tangent stiffness is the slope of the curve R versus U and is assumed to be non-singular. Since it is assumed that the approximate solution is close to the exact solution, second order and other higher order terms are neglected, resulting in the linearized form.

$$K_T(U^r).\delta(U) = R(U^r) \quad (5.19)$$

The solution of the above equation gives the increment in displacement at the rth iteration. Using this the incremental displacement, the solution at the next iteration is obtained as

$$U^{r+1} = U^{(r)} + \delta U \quad (5.20)$$

The above two equations give the Newton-Raphson method for one iteration. In most analyses, more than one iteration is invariably required to obtain the solution. Thus, the above procedure is repeated until convergence is achieved within the specified tolerance. The solution is said to be converged when the restoring load vector equals the applied load vector within the specified tolerance. Convergence is defined as follows

$$\|R\| \leq \epsilon_r \ R_{ref}$$

where ϵ_R is the tolerance, R_{ref} is the reference value, and $\| \ \|$ is the norm used. Generally, a tolerance 0.001 is considered appropriate. L_2 norm has been used.

Newton Raphson method requires the calculation and factorisation of the stiffness matrix after each iteration within a time step. Since major cost/iteration lies in the formulation of the stiffness matrix, the Newton-Raphson method is considered computationally expensive. An alternative procedure, the Modified Newton method, uses the same algorithm as the Newton-Raphson method but require the updating of the stiffness matrix less frequently, thus making it computationally less expensive. But it has a slower convergence rate due to its linear asymptotic convergence. Newton-Raphson method converges quadratically. This strong convergence property makes it the method of choice for any function whose derivative is continuous and the initial conditions are close enough to the desired solution.

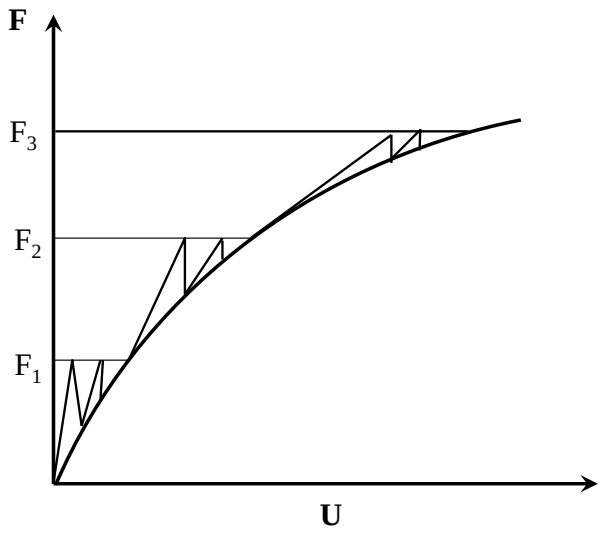

Figure 5.2: Incremental Newton Raphson Procedure

Figure 5.2 shows step by step how the Newton-Raphson method moves toward the converged solution for more than one iteration. The method starts with initial value U_0, where U_0 is the initial converged solution. For this given solution, the tangent stiffness matrix (K_T) and the force vector F are computed. Using these values, the increment in the solution vector is calculated. Thus, the addition to the previous step gives the solution. This whole process is repeated till the convergence is obtained.

5.3.3 Line Search

For highly nonlinear problems, the Newton-Raphson method does not always lead to a converged solution, if the approximate solution is far from the radius of convergence, the method fails. For such cases, a converged solution is obtained with the help of the line search algorithm. The line search algorithm tries to improve the solution by scaling the solution vector by a scalar parameter called the line search parameter. Consider the equation

$$U^r = U^{r-1} + \delta U \tag{5.21}$$

After modifying the equation by line search algorithm, the equation becomes

$$U^r = U^{r-1} + s.\delta U \tag{5.22}$$

where s is the line search parameter varying on the scale of 0.5 to 1. The value of s is automatically determined using the minimum potential energy principle

$$\partial\Pi/\partial s = \Delta_{U^T}[F - R(s.(\Delta U_i)] \tag{5.23}$$

where $\partial\Pi/\partial s$ is the gradient of the potential energy with respect to s.

5.3.4 Equation Solver

The system of simultaneous linear equations generated by the finite element procedure is solved either using a direct elimination process or an iterative method. A direct elimination process is primarily a Gaussian elimination approach that involves solving for the unknown vector of variables u in the equation

$$[K]\{u\} = \{F\} \tag{5.24}$$

where [K] = global stiffness

$\{u\}$ = global vector of nodal unknown solution

$\{F\}$ = global applied load vector

The direct elimination process involves decomposition (factorization) of the matrix [K] into lower and upper triangular matrices, [K] = [L][U]. Then, the forward and back substitutions using [L] and [U] are made to compute the solution vector u. A typical iterative method involves an initial guess of the solution vector $\{u\}$ and then, a successive steps of iteration leading to a sequence of vectors u_2, u_3, ... such that, in the limit, u_n = $\{u\}$ as n tends to infinity. The calculation of u_{n+1} involves [K], $\{F\}$, and the $\{u\}$ vectors from one or two of the previous iterations. Typically, the solution converges to a value within the specified tolerance after a finite number of iterations. A sparse solver has been used here due to its efficiency and robustness for the nonlinear solutions. The Sparse solver make use of the fact that the finite element matrices are sparsely populated and this helps in solving the system of equations efficiently by minimizing the operation count.

5.4 Transient Response

5.4.1 Transient Analysis

The dynamic response of shelters against external blast loads is obtained using transient analysis option using ANSYS. As seen for the static analysis, geometric nonlinearity plays a major role in determining the response of the structure. Therefore, a nonlinear dynamic analysis is sought in order to determine the response of the flexible structure against the blast. ANSYS provides the option of transient analysis for the structural response under dynamic conditions.

Transient analysis is a means of determining the structural response due to time dependent loading conditions. It provides time-varying displacement, stress, strain, and force response due to the combination of static, dynamic, and harmonic loads. The transient analysis provide three methods to approach the solution. The modal superposition method calculates the structural response by adding the factored mode shapes (eigenvectors) from the modal analysis. This method is fast and efficient but fails to provide a meaningful solution when a structural nonlinearity is involved. The reduced method condenses the problem size by using master degrees-of -freedom and thus the reduced system matrices. This reduces the computational time significantly and once the solution is obtained, the expansion pass expands the solution to the full model. But this method does not work for the nonlinear analysis. The full method satisfies all the criteria for performing the nonlinear transient analysis. It is more expensive than the other two methods but it takes into account all types of nonlinearities such as plasticity, large deflection and large strain etc. It uses the full system matrices to calculate the structural response. No mass approximation is required.

The flow chart in Fig. 5.3 shows complete working of the full method.

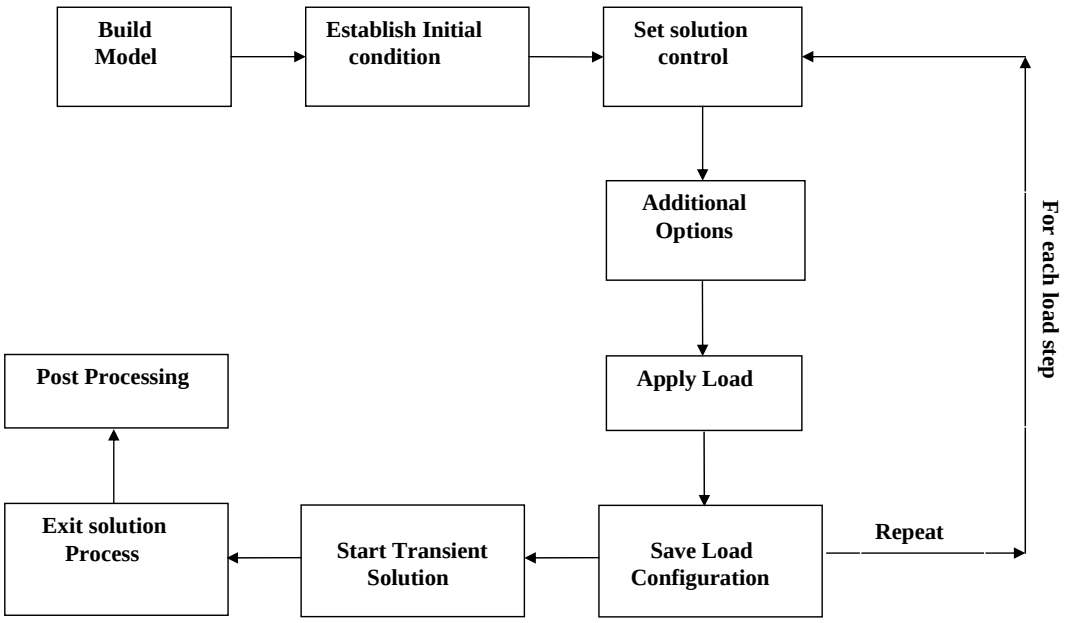

Figure 5.3: Flowchart showing algorithm for Full Method for the Transient Analysis

5.4.2 Modeling Blast Loads

The air blast creates a compression wave that moves outward in all direction. As this pressure wave hits an obstacle in its path, the part of the pressure wave is transmitted and part is reflected back, being a function of the rigidity of the reflecting surface and orientation of the surface

to the wave. The reflected pressure is the pressure imposed on the structure immediately after the reflection of pressure wave and is greater than the incident pressure. The pressure profile consists of positive and negative phase where positive phase is characterized by the initial sudden rise in the pressure and then decaying exponentially with time till reaching the reference pressure. While the negative phase is characterised by under pressure i.e. pressure below the reference pressure and increasing to reference pressure. The overpressure generated by air blast surrounds the whole tent-liner system with time delay over the other surfaces relative to the surface facing the blast. During the field test conducted by Air Force Research Laboratory, pressure outside and inside of the tent are estimated using the pressure gauges. This pressure data has been used over the finite element model. Figure 5.4 shows the pressure versus time plots for the front and back sides.

The blast load is modeled as the time varying element pressure load over the finite element model for the tent. The uniform pressure loading is assumed over each side of tent at a given time instant, varying with sides. The high overpressure causes a sudden and fast structural movement and this sudden movement generates a transmitted pressure wave inside the closed structure. This pressure opposes the structural movement caused by the external loading, changing the overall pressure distribution over each side. This effect is taken into account and the reduced pressure loading is applied over the structural system. Reduced pressure load is calculated by subtracting the inside pressure from the external pressure. In Fig. 5.4, the reduced pressure distribution is shown by yellow line. The reduced pressure loading applied over the back wall consists of negative pressure profile i.e. pressure acting from inside is higher than the external loads and this plays a significant role in the dynamics of the structure. Figure 5.5 shows the varying pressure loading

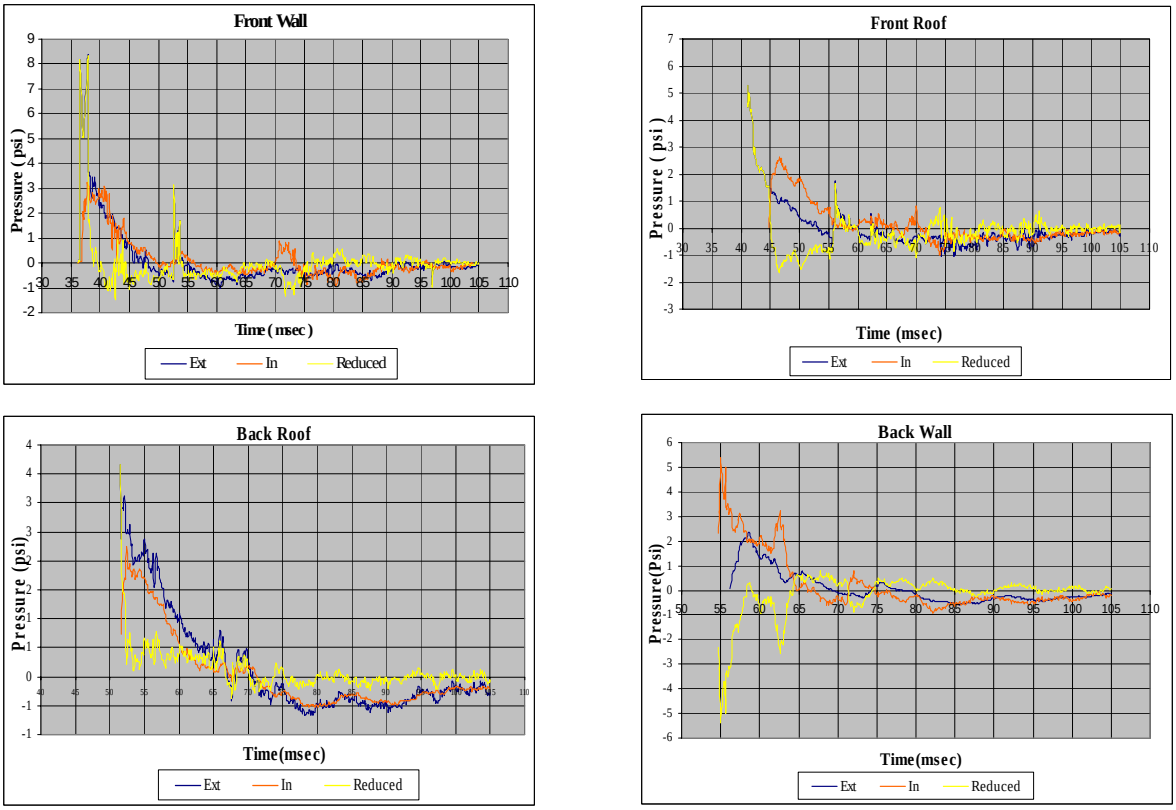

Figure 5.4: Blast load profile showing external, internal and reduced pressure Variation woth respect to time

over the finite element model for tent at a given time step where the color arrows demonstrates the magnitude and variation. More than 100 time step functions are used to simulate the blast load over the whole structure with smallest time step size of 0.5 msec.

Conservative and Non-Conservative Loading

When the load acting on the structure maintains a constant direction irrespective of the deflection of the surface, the loading is conservative. In case of a nonconservative loading, the load changes direction following the structural deflection and is known as a follower load. *S*hell 63 and *S*hell 41 support only conservative loading. *S*hell 181 incorporates the follower effects of distributed pressure loads. Inclusion of follower force effects enhances the rate of convergence.

5.4.3 Transient Solution

An implicit approach, the Newmark method combined with the Newton-Raphson method, is used for the nonlinear solution. The Newmark method provide an unconditionally stable solution. Geometric nonlinearity is included. The out-of-plane stiffness of a structure can be significantly affected by the state of in-plane stress in the given structure. This coupling between in-plane stress and transverse stiffness, known as the stress stiffening, is most pronounced in thin structures like the ones being modeled here. The damping effects are not considered. The sparse direct solver is used for the solution due to its robustness and speed as desired in the nonlinear analysis and for large models.

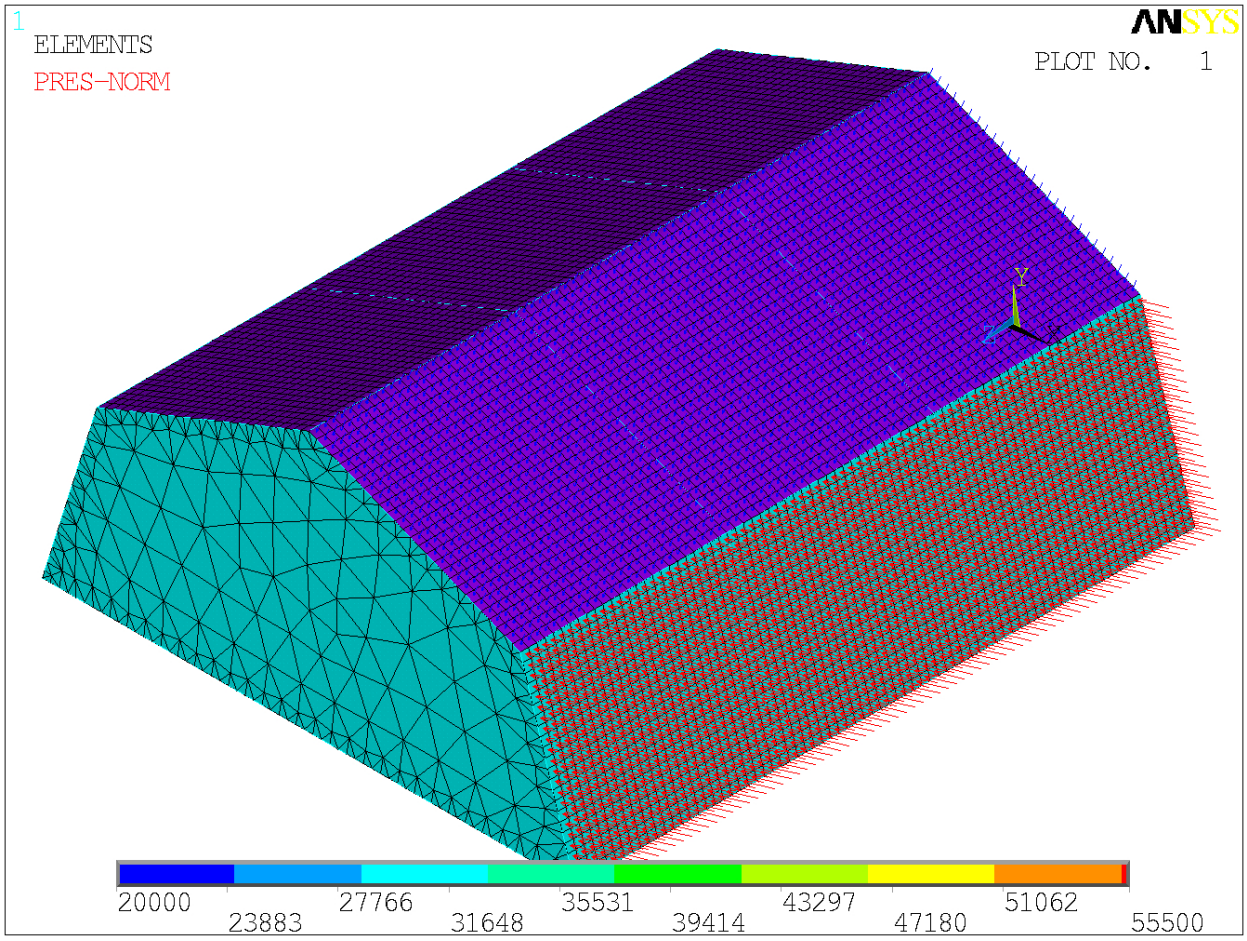

Figure 5.5: Element pressure load over the Front sides varying with time, colored arrows showing the magnitude and the variation

5.4.4 Dynamic Characteristics

Structural response due to time varying loads, generally consists of displacement, stresses and strain time histories. These dynamic parameters provide greater insight into the damage detection and characterisation of dynamic systems.

Displacement Response

Displacement response over each side of the shelter are obtained and the deflection at the center of each side is computed. Figures 5.6-5.8 show the displacement versus time histories for each sides of the tent using *Shell 63*, *Shell 181* and *Shell 41.* The negative profile denotes inward (into tent) movement and positive profile gives the outward (out of tent) movement.

Discussion

The first movement of the front wall, front roof and back roof are into the tent (inwards) while the back wall moves outward. Displacement profiles for the three shell models show similar pattern. The response is accompanied by oscillation in the forced and free vibration zone, resembling an impact response like behavior. This kind of behavior is seen for all the sides. It is also observed that in the free vibration zone, back wall response oscillates about a mean displacement value before moving toward the equilibrium position. Peak values for *Shell 41* and *Shell 63* are almost the same for all sides, with small difference being due to the finer mesh *Shell 63* model. *Shell 181* with default drill stiffness show a slow convergence behavior. The scaling of drilling degree of

freedom along with the follower load effects accelerates the convergence. This element uses the penalty approach to relate the rotational freedom to the in-plane displacements by choosing the appropriate penalty stiffness. And this value can be changed by changing the scaling parameter provided to fine tune the value of the rotational stiffness. Peak values obtained using *Shell 181* are higher for all the sides in comparison to the response histories obtained using the two other element types.

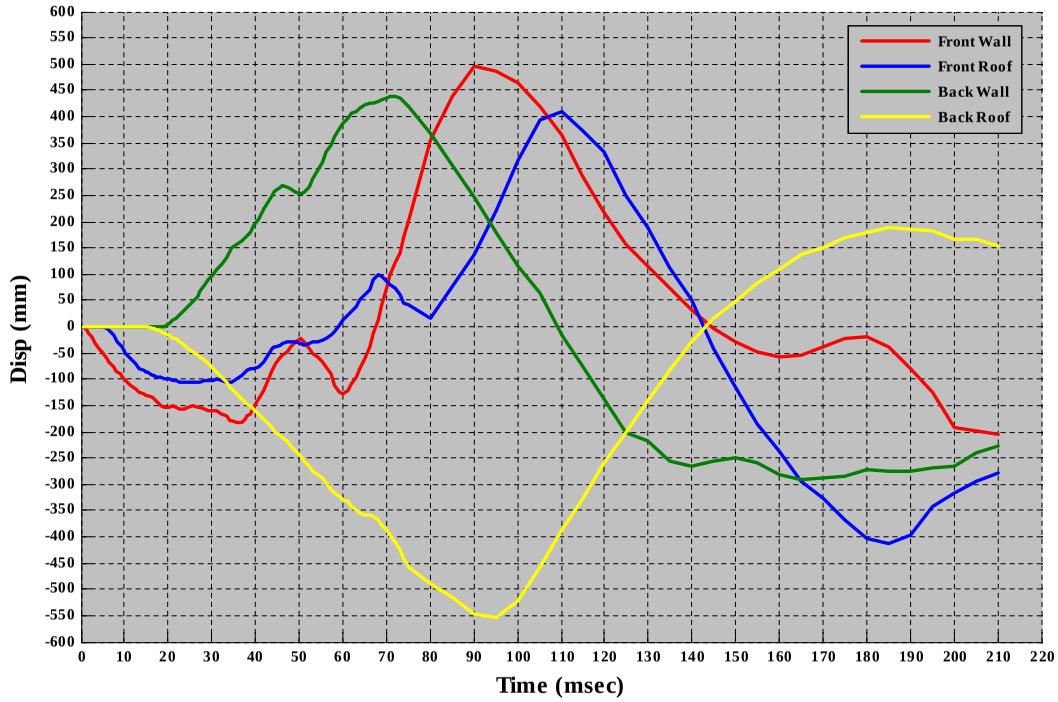

Figure 5.6: Displacement versus time profile, using Shell 63 for modeling the fabric skin

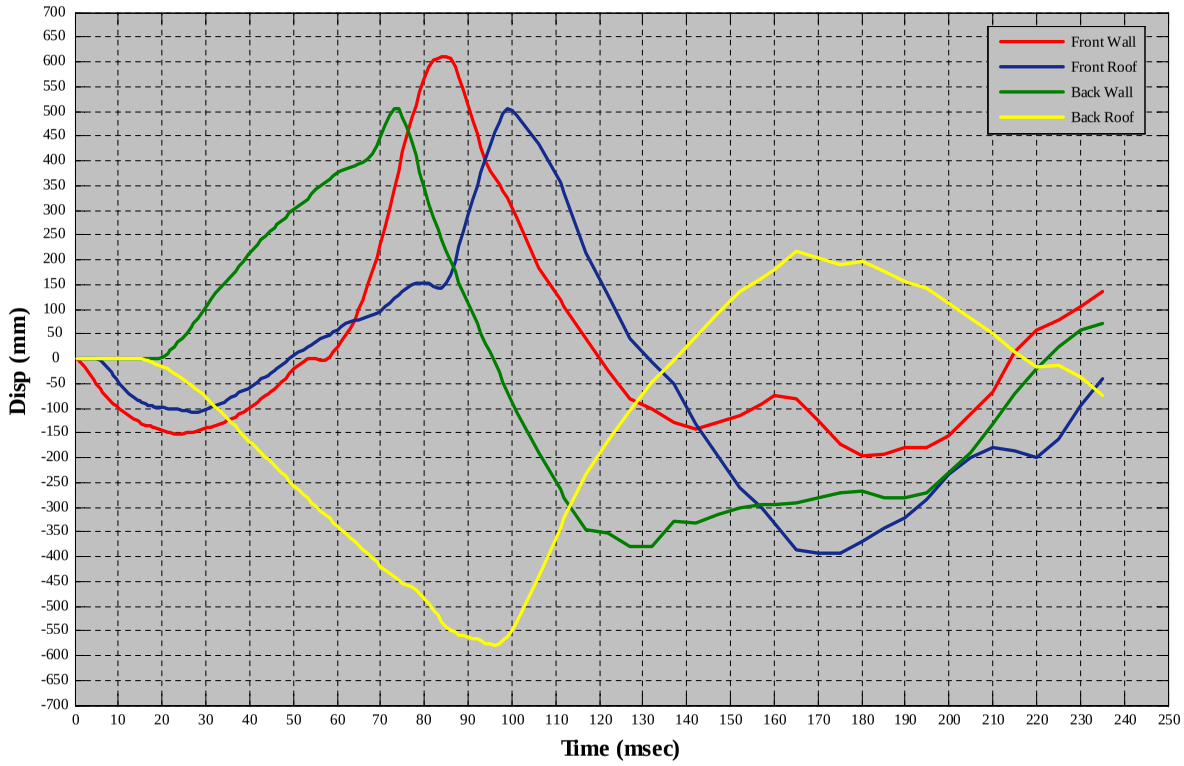

Figure 5.7: Displacement versus time profile, using Shell 181 for modeling the fabric skin

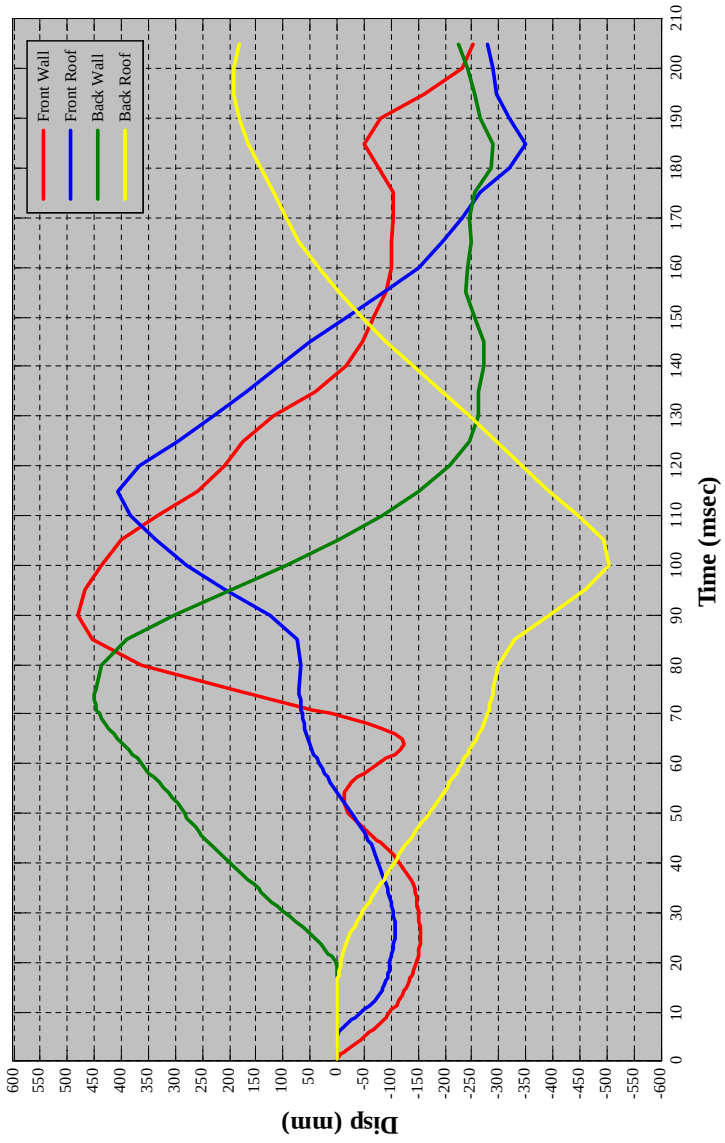

Figure 5.8: Displacement versus time profile, using Shell 41 for modeling the fabric skin

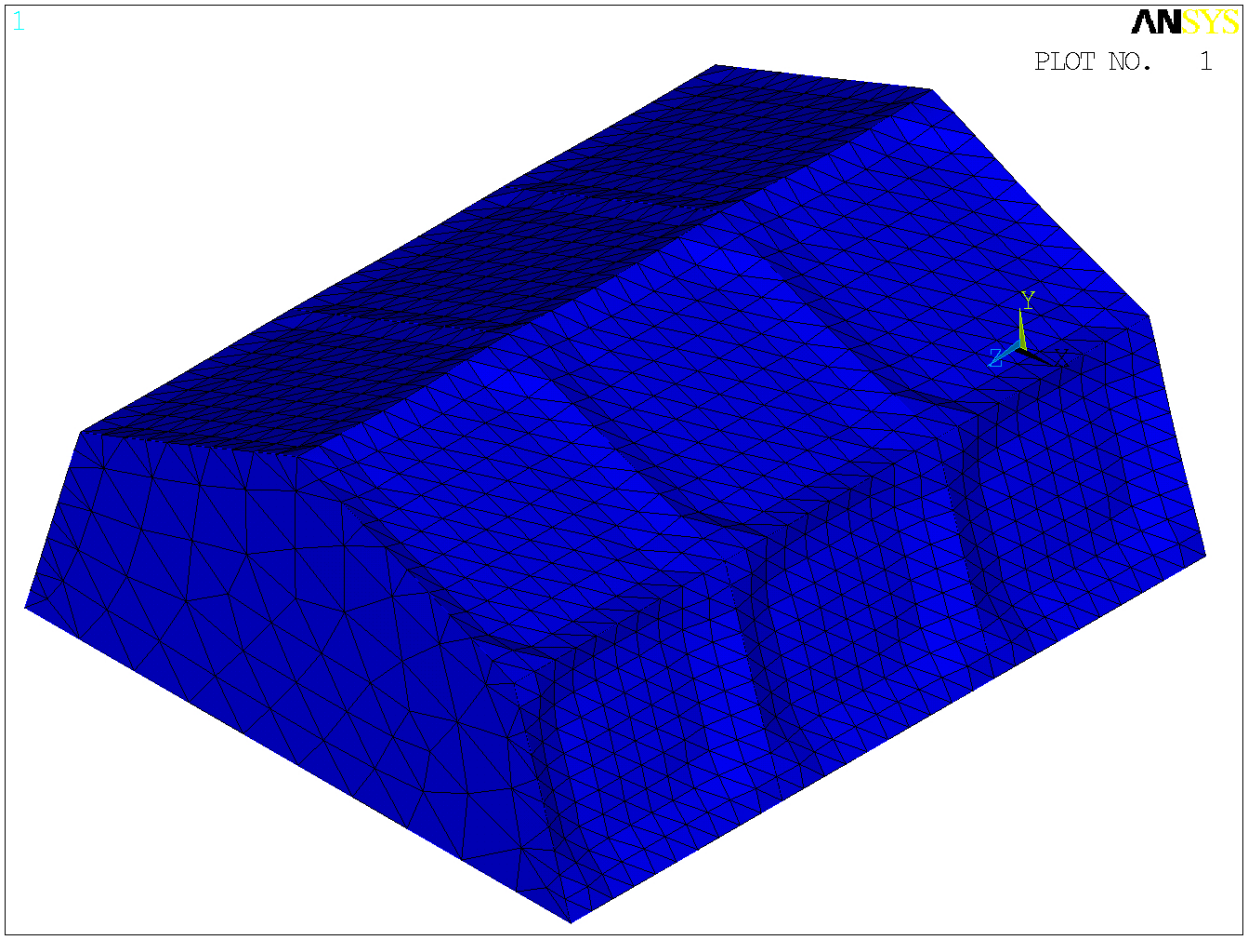

Figure 5.9: Response snap shot showing Front side movement when blast load is acting

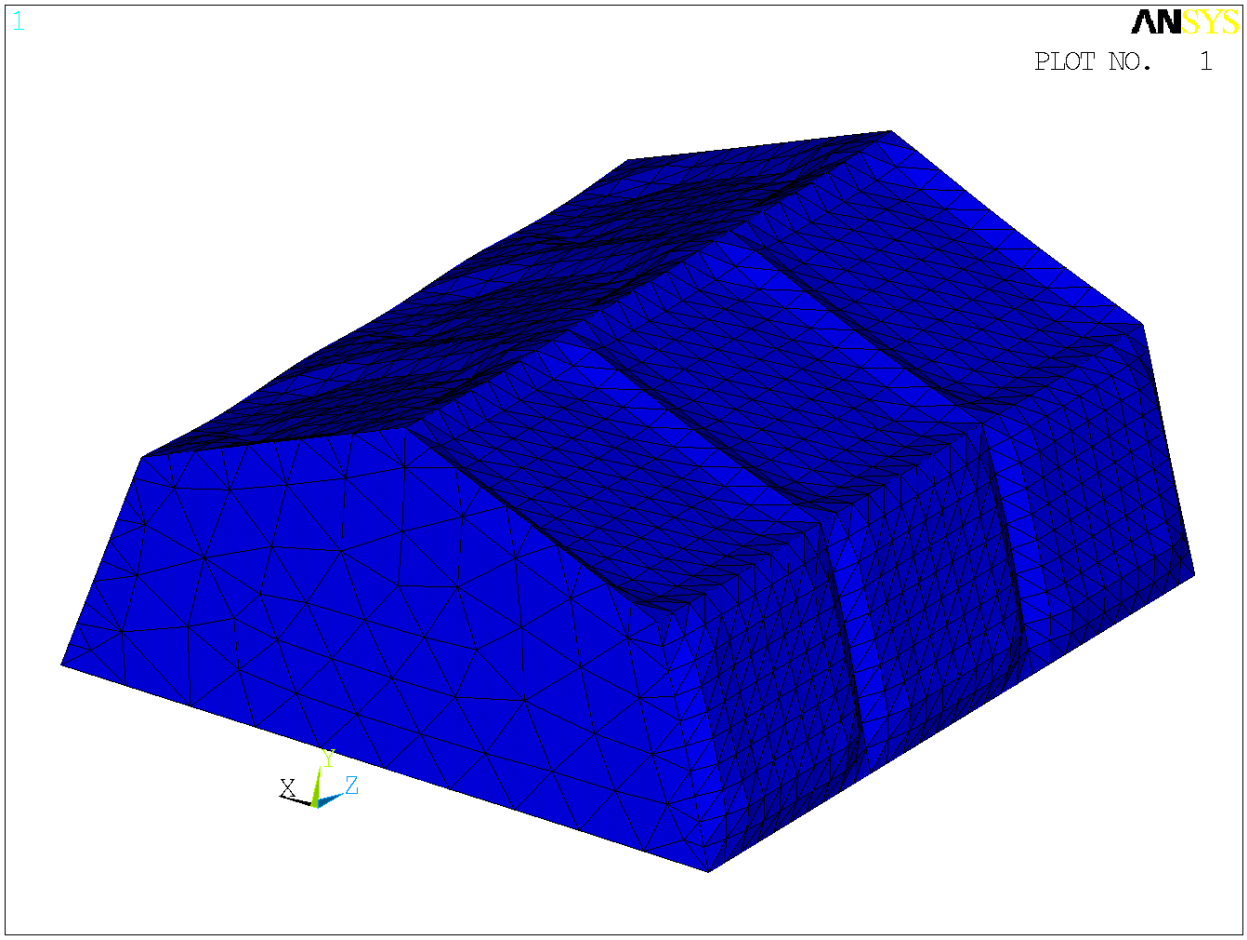

Figure 5.10: Response snap shot showing Back side movement when blast load is acting

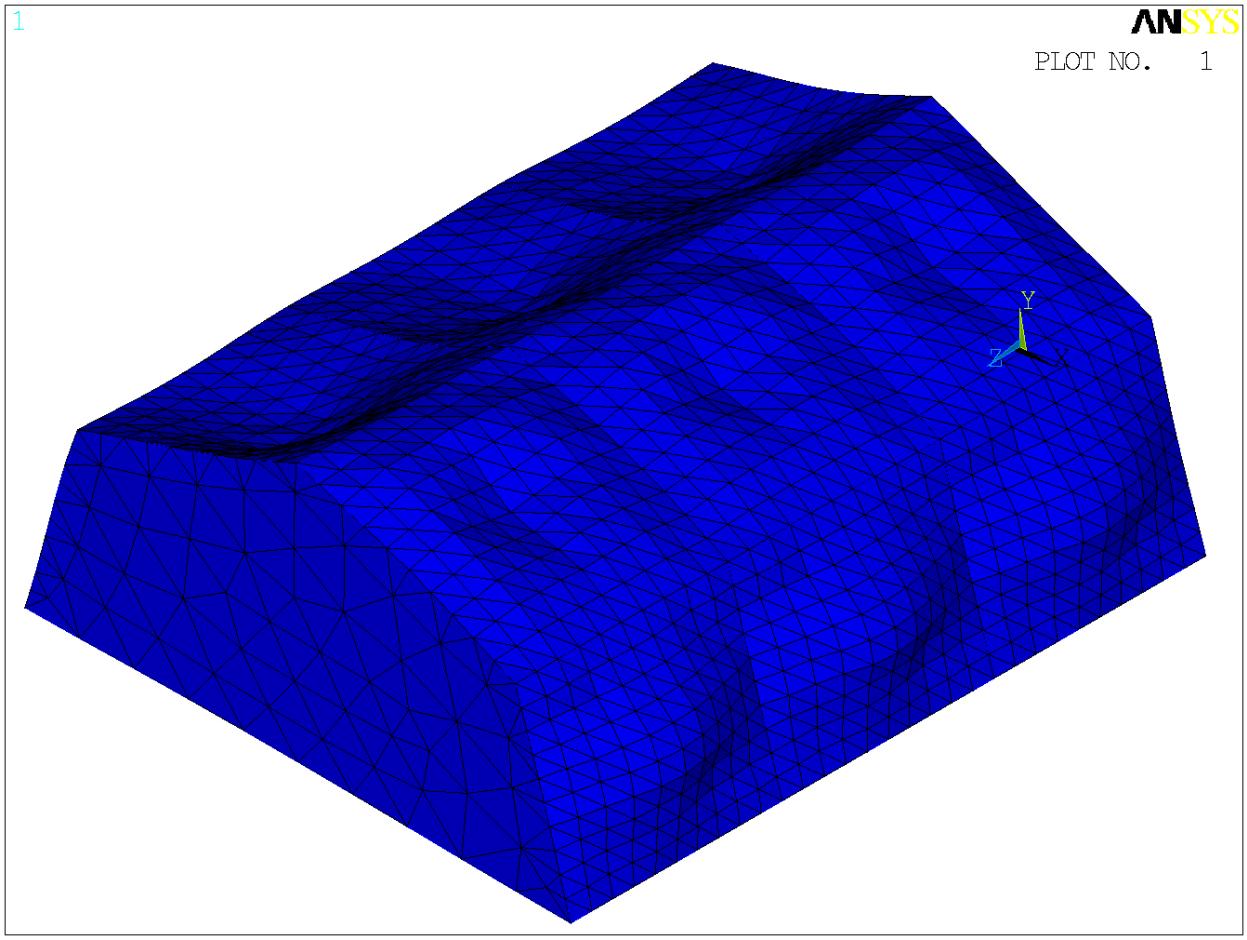

Figure 5.11: Response snap shot showing Front side movement, in the free vibration zone

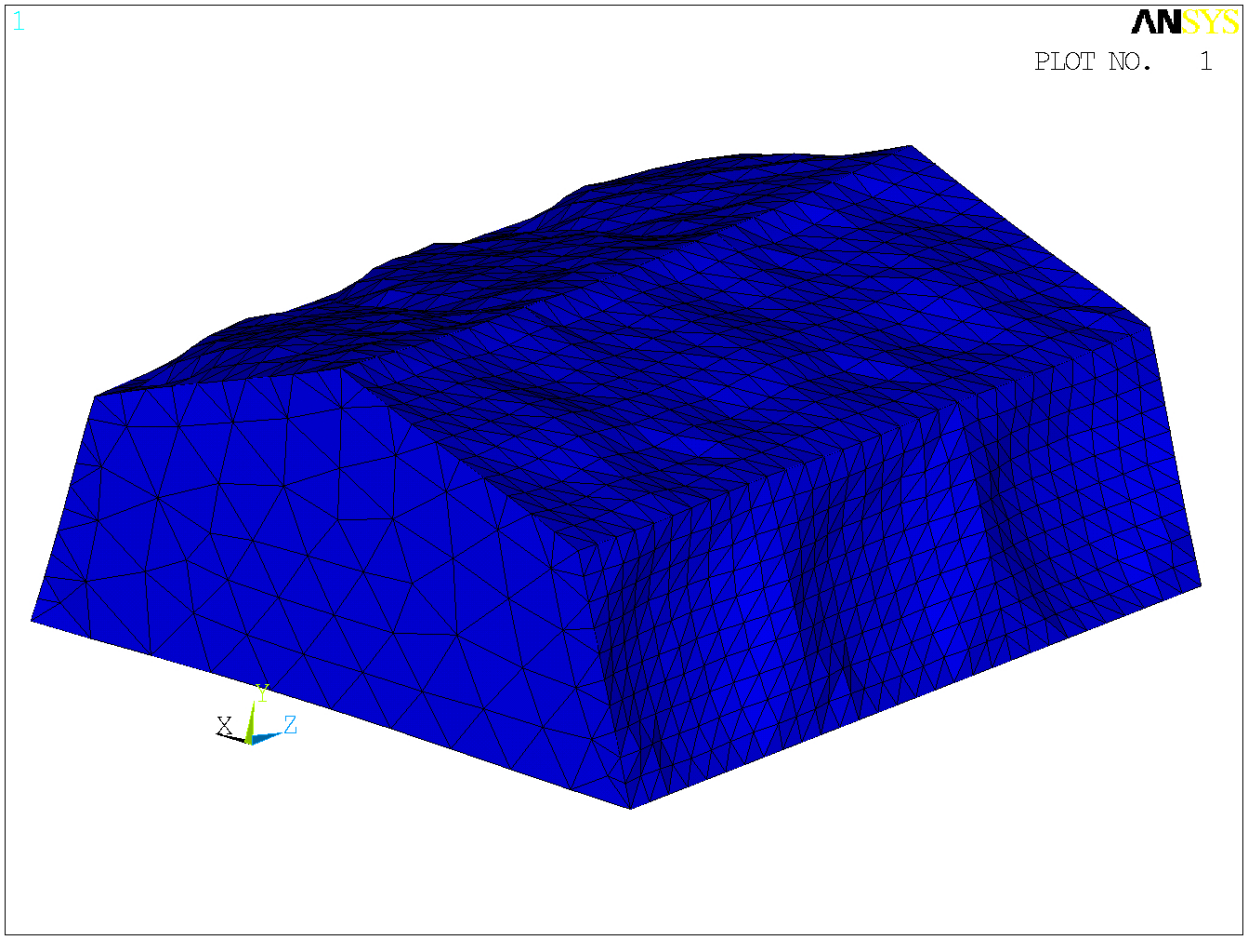

Figure 5.12: Response snap shot showing Back side movement in the free vibration zone

Dynamic Stress Behavior

The dynamic stresses for all the sides are computed. Figures 5.9 and 5.10 show the stress variation with time in the x and y directions, plotted at center of each side. The stress varies signficantly with time, during the time the blast acts on the shelter and in the initial stages of the free vibration period. The dynamic stress behavior follows similar pattern for all the sides. The maximum stress value is observed for the back wall and occurs between 70-80 msec, coinciding with the maximum displacement observed during this period from the displacement-time history. This is due to transmitted pressure waves from other sides hitting the back wall. The magnitude of stresses for the front wall are also large as being the blast facing side, those magnitude are next to those for the back wall.

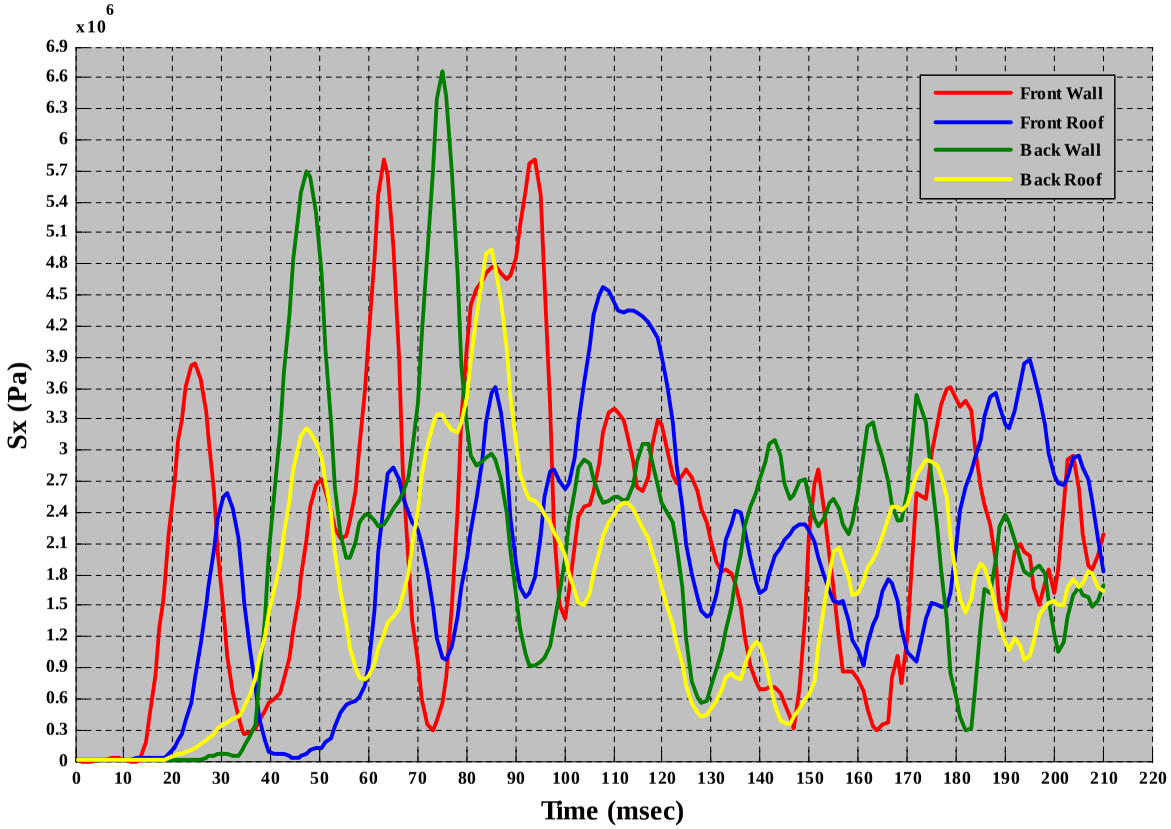

Figure 5.13: Variation of stress in the x-direction with time

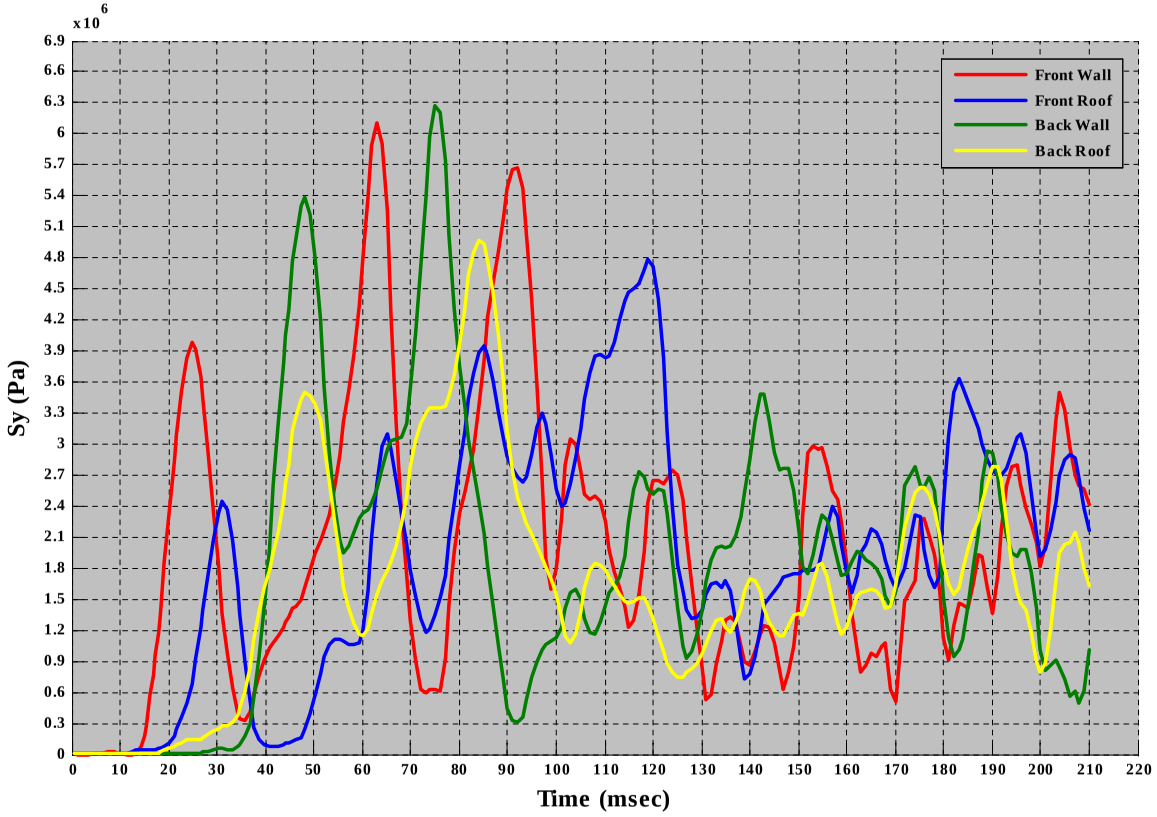

Figure 5.14: Variation of stress in the y-direction with time

5.5 Parametric Study / Analysis

The parametric study plays an important role in setting the design guideline for a given system. Parameterization consists of simulating the behavior for number of design variation and capturing response as a function of design variables. A parametric study for different values of Young's modulus and density is performed.

The analysis is performed for two sets of values, where in each set, for a given value of density, dynamic response of structural system has been sought for increasing values of modulus. In Case 1, for the given density (ρ) = 9215 Kg/m^3, shelter response is analyzed for different values of Young's modulus. In Case 2, the material model has density (ρ) = 6910 Kg/m^3 and the tent's response is obtained for different E values. The value of poisson's ratio ν = 0.3 is same for both the cases. The transient analysis is carried out for all the subcases and displacement response are compared and based on that some design guidelines are made.

5.5.1 Dynamic Response of Shelter for increased E with original Density

The material model consists of density (ρ) = 9215 Kg/m^3 and Young's modulud (E) = 100 Mpa. The displacement-time history has been plotted. Figure 5.15 shows the response history for all the sides. The peak displacement value for all the sides are reduced and required less time to reach the peak value as compared to the displacement profile in Fig. 5.6. Also a higher frequency response is observed.

5.5.2 Dynamic Response of Shelter for increased E with original Density

The material model consists of density (ρ) = 9215 Kg/m^3 and Young's modulus (E) = 170 Mpa. The responses follow a similar trend to that followed by the previous case. Figure 5.16 shows displacement plot for all the sides. The peak displacement value for all the sides are reduced and the solution required less time to reach the peak value as compared to Fig. 5.6. The response frequency of the dynamic system has increased resulting in higher oscillations, for all the sides.

5.5.3 Dynamic Response of Shelter for original E and decreased Density

The material model consists of density (ρ) = 6910 Kg/m^3 and Young's modulus (E) = 35 Mpa. Figure 5.17 shows displacement time history for all the sides. The peak displacement value for all the sides are have increased significantly as compared to Fig. 5.6, showing that inertia significantly affects the response of the shelter. Also, peak values are reached in less time as compared to in the Fig. 5.6. The response of the dynamic system is accompanied by large oscillations due to the presence of higher frequencies.

5.5.4 Dynamic Response of Shelter for increased E and decreased Density

The material model consists of density (ρ) = 6910 Kg/m^3 and Young's modulus (E) = 100 Mpa. Figure 5.18 shows displacement time history for all the sides. The peak displacement value for all the sides have reduced as compared to results shown in the Fig. 5.15, due to higher value of E. The response has become faster in comparison to case 2(a), i.e, time period is shorter. The response of

the dynamic system is accompanied by large oscillations.

5.5.5 Dynamic Response of Shelter for increased E and decreased Density

The material model consists of density (ρ) = 6910 Kg/m^3 and Young's modulus (E) = 170 Mpa. Figure 5.19 shows displacement time history for all the sides. The peak displacement value for all the sides have reduced as compared to the response shown in Fig. 5.16, due to higher E value used here. The response has become faster in comparison to case 2(a) and 2(b), i.e, the time period of the response is shorter. The response frequency of the system has increased in comparison to the 2(b) as can be seen in the figure.

5.5.6 Discussion

The density of material and Young's modulus plays significant role in response of the system. Higher the value of E, higher the resistance of the system against the blast. The peak values are reduced as the Young's modulus is increased, resulting from the increase in stiffness. The increased stiffness leads to reduced transmitted impuse and pressure [32] and reduced value of maximum strains. But disproportionate increase in stiffness value could lead to very high stresses which could result in the failure.

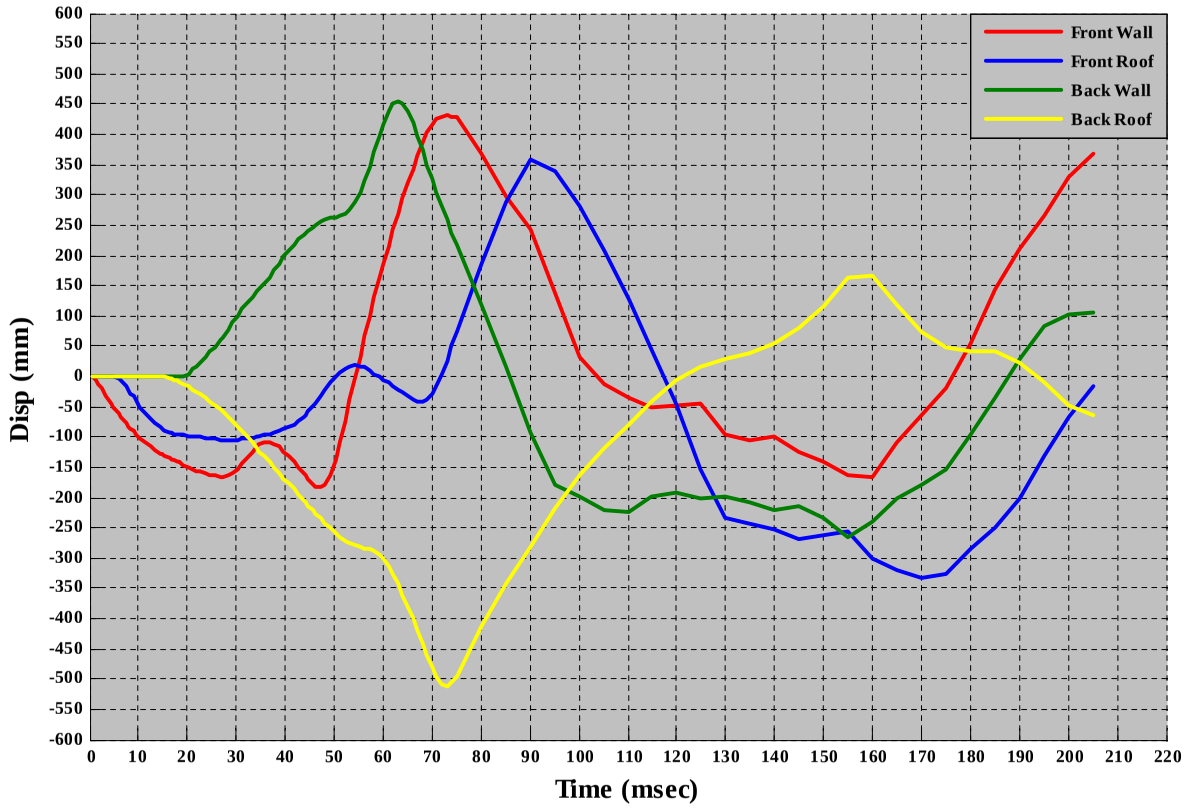

Figure 5.15: Displacement Response at the center of each side of the tent, for the Shell 41 model

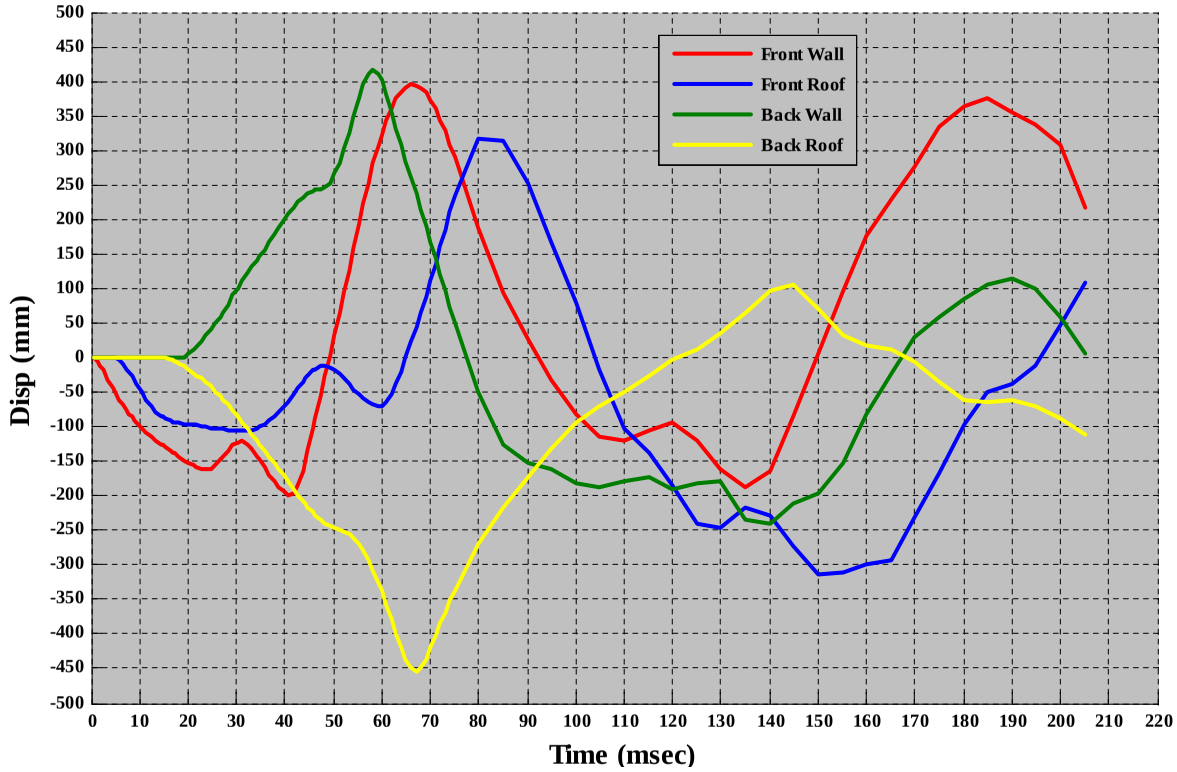

Figure 5.16: Displacement Response at the center of each side of the tent, for the Shell 41 model

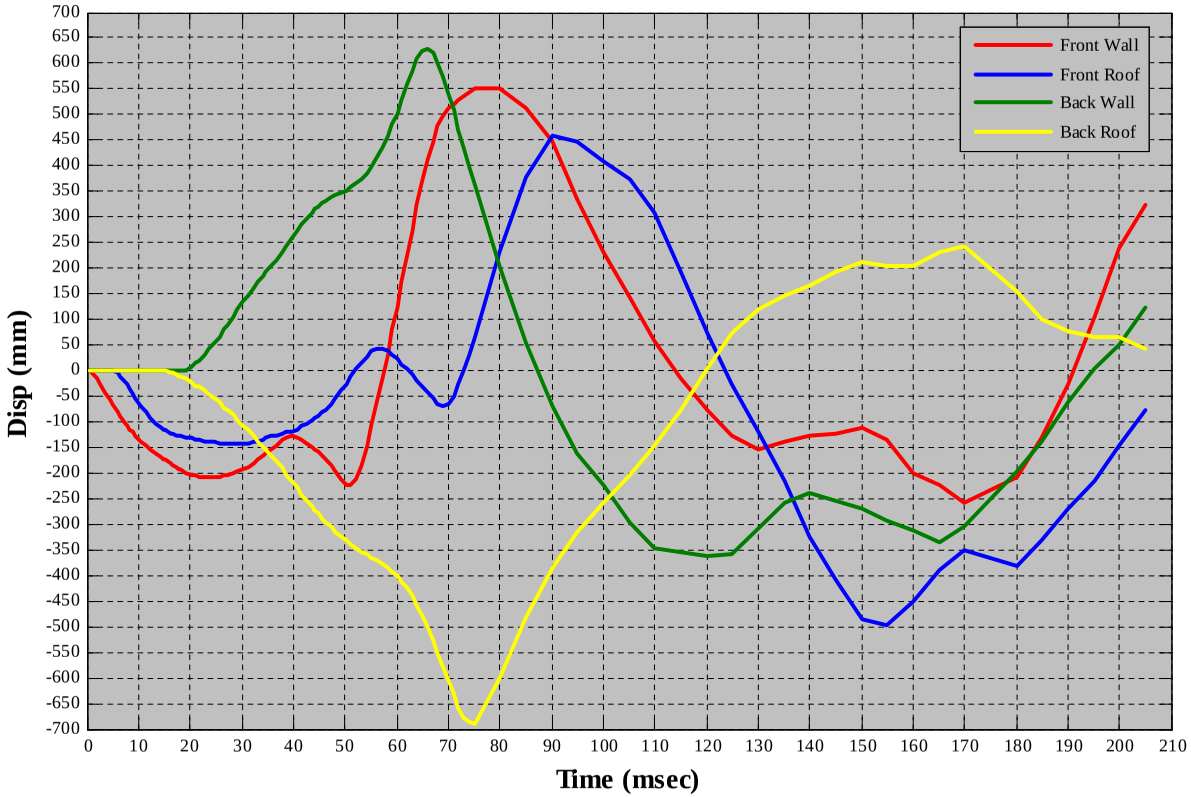

Figure 5.17: Displacement Response at the center of each side of the tent, for the Shell 41 model

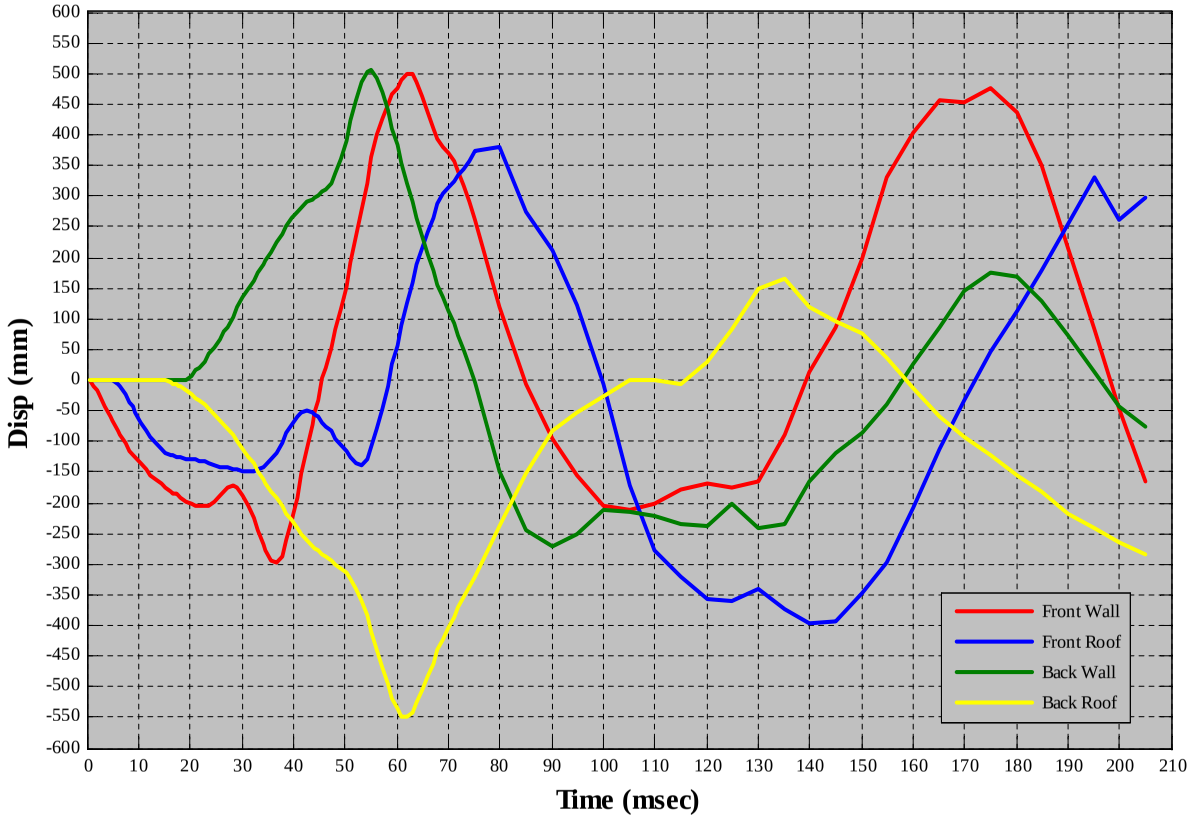

Figure 5.18: Displacement Response at the center of each side of the tent, for the Shell 41 model

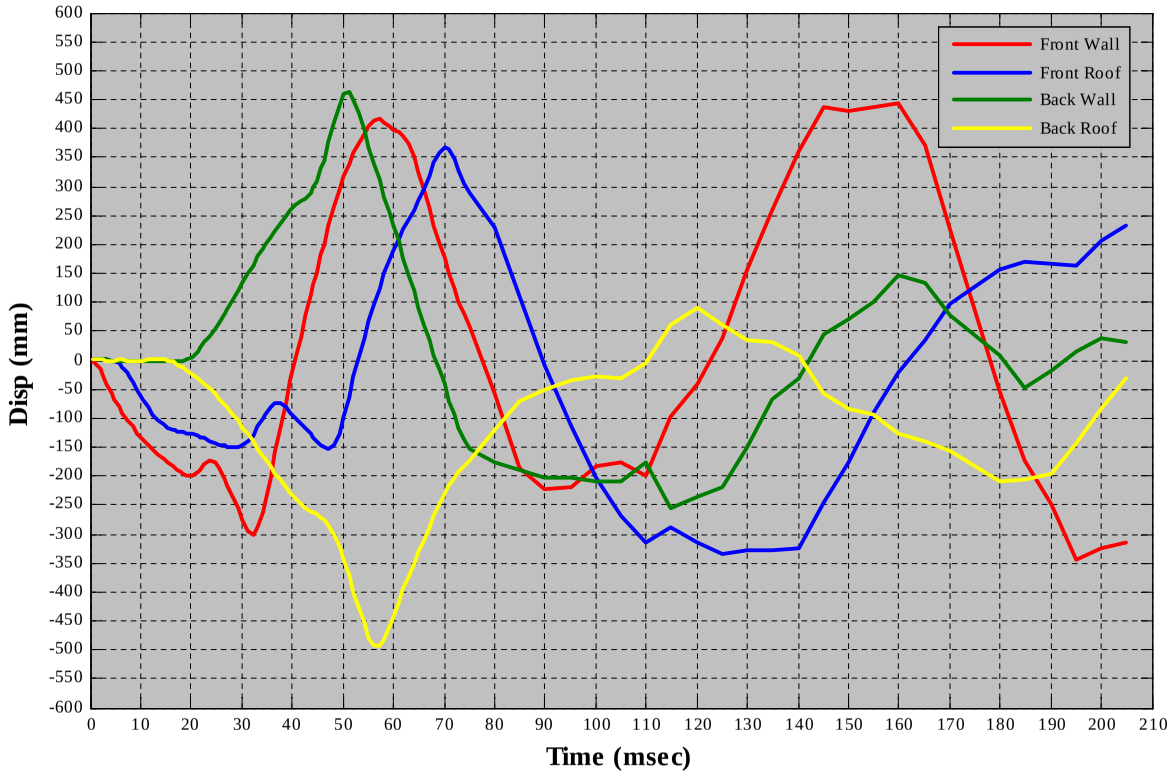

Figure 5.19: Displacement Response at the center of each side of the tent, for the Shell 41 model

Chapter 6

SUMMARY AND CONCLUSIONS

Highly flexible structures have been widely used in various industries, and find numerous applications due to their many advantages like lightweight, low cost etc. Flexible shelters, one of the flexible structure application, have been used as temporary storage places for housing equipments, vehicles etc. TEMPER Tents have been widely used by Air Force and Army, for various field applications and presently, are being tested for the force protection standards against explosions like air-blast. These shelters have pressurized Collective Protection System (CPS), liner, fitted to the frame structure, which can provide protection against explosives and other harmful agents. Field tests were carried out by Air Force Research Laboratory and it was found that the liner was damaged, with major failure being on the aft side of the tent. The present research focused on the computational modeling and response of TEMPER Tent against the air blast. A comprehensive 3-D finite element model has been developed using ANSYS and dynamic response of shelter was obtained against the blast loads.

A simplified finite element model has been developed, consisting of fabric skin supported over the frames based on two approaches. In the first model, the shell is considered as a membrane away from its boundaries, in which the stress couple is neglected in its interior region. In the second approach, stress coupling is neglected over the whole region. Based on these approaches, two basic finite element models are built. In the first model, a shell element (including both bending and membrane action), is used for modeling the fabric skin and beam elements are used for the frames. In the second model, the skin is modeled with a membrane-only element and the frames are modeled with beam elements. Using a direct approach, two shell models (for fabric skin) have been built using *Shell 63* and *Shell 181*. *Shell 63* element supports both the membrane only and membrane-bending combined option and include stress stiffening and large deflection capabilities. *Shell 181* include all these options as for *Shell 63* and in addition, accounts for the follower loads. Using second approach, shell model for skin was developed using *Shell 41* element. *Shell 41* is a membrane element and does not include any bending stiffness. This element also include stress stiffening and large deflection capabilities.

A shell is a three dimensional structure, with thickness being small compared to the other two dimensions and have a high load carrying capacity. This characteristic make them a challenging problem from analysis and simulation point of view. A brief study was done to learn about their asymptotic behavior. A flat shell element formulation for shells is now being widely used due to its simplicity, yet an effective modeling of shell structures. But this pose rank deficiency problem for the folded plate structures. Due to the existence of coplanarity, surface normals are identical, resulting in singularity in the global matrix. This issue has been addressed

to some extent.

In general, response of any structural forms to dynamic loading is very difficult to predict due to structural response dependent on multiple factors like the duration of the loading, peak load, shape of the pulse, the impulse energy, boundary conditions and material properties etc. And dynamic analysis of shell structures pose even a much greater challenge. Obtaining solution analytically presents a very difficult problem when nonlinearity is considered. Therefore, a numerical approach is sought. ANSYS has been used for obtaining the dynamic response of shelters against the blast loads.

Blast loading is a dynamic phenomenon, generating a pressure wave in air with a rapid release of energy. The high overpressure causes a sudden and fast structural movement and this sudden movement generates a transmitted pressure wave inside the closed structure. This pressure opposes the structural movement caused by the external loading, changing the overall pressure distribution over each side. The effect of this opposing pressure is taken into account and the reduced pressure loading is applied over the structural system. During the field test conducted by Air Force Research Laboratory, pressure generated due to blast, outside and inside the tent, are estimated using the pressure gauges. And, this blast data has been used for modeling the load over the finite element model and is modeled as the time varying element pressure load.

Transient analysis is a method of determining the structural response due to time dependent loading conditions. The full method has been used for performing the nonlinear transient analysis. It is more expensive in terms of computation involved but it takes into account all types of nonlinearities such as plasticity, large deflection and large strain etc. Implicit approach

has been used where Newmark method along with the Newton-Raphson method has been used for the nonlinear analysis. The dynamic response consisted of displacement-time history and dynamic stresses has been obtained. Displacement time history provided the dynamic movement of the tent structure. Dynamic stresses showed large fluctuations with time in the forced and initial free vibration zone. The tearing of the liner could have been triggered due to its sudden impact on the 45^0 brace, attached to frame structure to provide the additional support. From the displacement response, the first movement of the back wall is outward, in contrast to the other sides whose first movement is into the tent. This movement results in sudden impact of the part of liner with the 45^0 brace. The impact happens in the forced zone and during this period, the dynamic stresses are also high. The sudden impact could trigger the tearing of the liner.

On the computational side, The *Shell 41* and *Shell 63* showed the similar response behavior, with small difference due to the finer mesh for *Shell 63.* While *Shell 181* model showed slow convergence behavior while using the default drill stiffness. But scaling of drill freedom (with respect to number of elements) along with follower force effect (with respect to load) accelerated the convergence.

A parametric study was performed with different values of the density and Young's Modulus. It was observed that the mass could be an effective means of reducing the peak responses. As the value of the Young's Modulus (E) is increased, the peak displacements were reduced resulting from the increase in stiffness. The increased stiffness leads to reduced transmitted peak pressure and reduced value of maximum strain. But a disproportionate increase leads to higher stresses which could result in failure. Therefore, a high modulus value should be avoided. Also, smaller

span for the skin should be considered. It was observed that the first movement of the back wall is outward, in contrast to the other sides whose first movement is into the tent.

At present, a comprehensive 3D model for the shelters has been developed. A more complex model would include a 3D shell model for the frames, for the analysis against the larger loads where the frames would be susceptible to damage. A nonlinear material model could be developed. ANSYS includes the capability of modeling material nonlinearity. The present analysis does not include any damping effects. Structural damping may be intersting in the aspect of the dynamic response. An explicit approach can be used for the dynamic analysis. The explicit methods are used for highly dynamic events which require very small increments in time to obtain a high-resolution solution like a short duration blast event. For an explicit analysis, LSDYNA (a nonlinear dynamics commercial code) can be used.

Bibliography

[1] Young L. G., Ramanathan, S., Jiazhu, H., and Pai, F., "Numerical and experimental dynamic characteristics of thin-film membranes", *International Journal of solids and structures*, vol. 42, 2005, pp. 3001-3025.

[2] Hammons, M. I., "Anti terrorism / Force Protection Criteria Validation Test", *Quick Look Report for Air Force Civil Engineer Support Agency*, March 2000.

[3] http://www.army-technology.com/contractors/field/index.html.

[4] Donahue, K. L., "Chemical and Biological Barrier Materials for Collective Protection Shelters", *Soldier and Biological Chemical Command, Natick, MA-01760*

[5] Goh, J. K. S., *Analysis of pressurized Arch-Shell*, MS Thesis, Civil Engineering, Virginia Tech, Dec 1998.

[6] Carradine, D. M., *Experiments on the Response of Arch-Supported Membrane Shelters to Snow and Wind loading*, MS Thesis, Civil Engineering, April 1998.

[7] Porter, J. R., Hawk, J. R., and Hammons, M. I., "Survivability of Collective Protection Systems Subjected to Air Blast Loads", *Air Force Research Laboratory, Tyndall AFB, FL 32403*, 2003.

[8] Baker, W. E., *Explosions in Air*, University of Texas Press, 1973.

[9] Smith, P. D. and Hetherington, J. G., *Blast and Ballistic Loading of Structures*, Butterworth-Heinemann Oxford, 1994.

[10] Bulson, P. S., *Explosive Loading of Engineering Structures*, E and FN Spon, London, 1997.

[11] Beshara, F. B. A., "Model of Blast Loading on Aboveground Structures-I. General Phenomenology and External Blast. Internal Blast and Ground Shock" , *Computers and Structures*, vol. 51, no. 5, 1994, pp. 585-596.

[12] Zienkiewicz, O. C., *The Finite Element Method in Engineering Science*, McGraw-Hill, London, 1971

[13] Knight, Jr., N. F., "The Raasch Challenge for Shell Element", *AIAA*, Paper no. 96-1369, 1996

[14] Allman, D. J., "Evaluation of the Constant Strain Triangle with Drilling Rotations", *International Journal for Numerical Methods in Engineering*, Vol. 26, 1988, pp. 2645-2655.

[15] Allman, D. J., "A Basic Flat Facet Finite Element for the Analysis of General Shell", *International Journal for Numerical Methods in Engineering*, vol. 37, 1994, pp. 19-35.

[16] Mohan, P., *Development and applications of flat triangular element for thin laminated shells*, Ph.D. Dissertation, Aerospace Engineering, Virginia Tech, 1997.

[17] Dhatt, G., Morcotte, L., and Matte, Y., “A New Triangular discrete Kirchhoff Plate/Shell Element”, *International Journal for Numerical Methods in Engineering*, vol. 23, 1986, pp. 453-470.

[18] Jenkins, C. H., and Leonard, J. W., “Nonlinear dynamics response of membranes: State of the art”, *Applied Mechanics Review*, vol. 44, no. 7, 1991, pp. 319-328.

[19] Smalley, K. B., Tinker, M. L., and Taylor, W. S., “Structural Modeling of a Five-Meter Thin-Film Inflatable Antenna / Concentrator : Engineering Notes”, Journal of Spacecraft, vol. 40, no. 1, 2002, pp. 27-29.

[20] Quadrelli, M. and Sirlin, S., “Modeling and Control of Membranes for Gossamer spacecraft”, Part 1: Theory”, *42nd AIAA/ASME/ASCE/AHS/ASC Structures, Structural Dynamics, and Material Conference and Exhibit*, A01-25018, 16-19 April 2001.

[21] Bonet, J., Wood, R. D., Mahaney, J., and Heywood, P., “Finite Element analysis of air supported membrane structures”, *Computer Methods in applied mechanics engineering*, vol. 190, 2000, pp. 579-595.

[22] Stanuszek, M., “FE analysis of large deformation of membranes with wrinkling”, *Finite Elements in Analysis and design*, vol. 39, 2003, pp. 599-618.

[23] *ANSYS Release 8.0 Documentation*

[24] Chappelle, D. And Bathe, K. J., *The Finite Element Analysis of Shells - Fundamentals*, Springer-Verlag Heidelberg New York, 2003.

[25] Lee, P. S., and Bathe, K. J., “On the asymptotic behavior of shell structures and the evaluation in finite element solutions”, *Computers and Structures*, vol. 80, 2002, pp. 235-255.

[26] Reddy, J.N., *An introduction to nonlinear finite element analysis*, Oxford University Press, 2004.

[27] Turkmen, H. S., “Structural Response of Isotropic Plates Subject to Blast Loading”, *Advances in Computational Structural Mechanics, Civil-Comp Press, Edinburgh*, 1998, pp. 101-107.

[28] Gupta, A. D., Gregory, F. H., Bitting, R. L., and Bhatacharya, S., “Dynamic Analysis of an Explosively Loaded Hinged Rectangular Plate”, *Computers and Structures*, vol. 26, 1987, pp. 339-344.

[29] Jacinto, A. C., Ambrosini, R. D., and Danesi, R. F., “Experimental and Computational Analysis of Plates under Air Blast Loading”, *International Journal of Impact Engineering*, vol. 25, 2001, pp. 927-947.

[30] Koh, C. G., Ang, K. K., and Chan, P. F., “Dynamic Analysis of Shell Structures with Application to Blast Resistant Doors”, *Shock and Vibration*, vol. 10, 2003, pp. 269-279.

[31] Louca, L. A. and Pan, Y. G., “Response of Stiffened and Unstiffened Plates Subjected to Blast Loading”, *Engineering Structures*, vol. 20, no. 12, 1998, pp. 1079-1086.

[32] Scherbatiuk, K.D., “Effect of a Flexural Membrane on Blast Transmission and Mitigation”, *Proceedings of Response of Structures to Extreme Loading Conference, Toronto, Canada*, August 3-6, 2003.

[33] Crawford, J. E. and Morrill, B., “Development of a Lightweight, Portable Airblast Barrier”, *MABS16 Conference*, 2000.

[34] Zhu, L., “Transient Deformation Modes of Square Plate Subjected to Explosive Loading”, *International Journal of Solids and Structures*, vol. 33, no. 3, 1996, pp. 301-314.

[35] Vendhan, C. P., Rmajeyathilagam, K., and Rao, V.B., “Non-linear transient dynamic response of rectangular plates under shock loading”, *International Journal of Impact Engineering*, vol. 24, 2000, pp. 999-1015.

[36] Turkmen, H.S., ” Structurtal Response of Laminated Composite Shells subjected to Blast Loading: Comparison of Experimental and Theoretical methods”,*Journal of Sound and Vibration*, vol. 249 (4), 2002, pp. 663-678.

[37] Sinha,P. K., Niyogi, A.G., and Laha, M. K., “Finite element vibration analysis of laminated composite folded plate structures”, *Shock and Vibration*, vol. 6, 1999, pp. 273-283.

[38] Chen, J., Dawe, D. J., Wang, S., “Nonlinear transient analysis of rectangular composite laminated plates”, *Composite Structures*, vol. 49, 2000, pp. 129-139.

[39] Yung, H. T., and Chang, F. K., “Transient Dynamics of Laminated composite Plates Subjected to Transverse Impact”, *Computers and structures*, vol. 31, no. 3, pp. 453-466.

[40] Abrate, S., “Modeling of impact on composite structures”, *Composite Structures*, vol. 51, 2001, pp. 129-138.

[41] Geers, T. L. and Sobel, L. H., “Analysis of the transient response of shell structures by numerical methods”, *Lockheed Palo Alto research Laboratory*.

[42] Bathe, K. J., *Finite Element Procedures in Engineering Analysis*, Prantice Hall Inc., New Jersey, 1982.

[43] Goyal, V. K., *Analytical Modeling of the Mechanics of Nucleation and Growth of Cracks*, Ph.D Dissertation, Aerospace Engineering, Dec., 2002.

Vita

Hitesh Kapoor was born in Simla on a snowy evening, on January 14, 1979. He received his bachelor's degree in Aeronautical Engineering from Punjab Engineering College, Chandigarh. During the 4 years, he won 5 gold medals in various sports activities. He then enrolled at Virginia Tech and received Master's degree in Aerospace Engineering. During the program, he worked on the dynamics of flexible membrane structures. In future, he would like to pursue a challenging career in the field of computational mechanics.